A

Presented to
the faculty of the School of Engineering and Applied Science
University of Virginia

in partial fulfillment
of the requirements for the degree

by

APPROVAL SHEET

This

is submitted in partial fulfillment of the requirements
for the degree of

Author:

Advisor:

Advisor:

Committee Member:

Committee Member:

Committee Member:

Committee Member:

Committee Member:

Committee Member:

Accepted for the School of Engineering and Applied Science:

Jennifer L. West, School of Engineering and Applied Science

ABSTRACT

Behind armor blunt trauma (BABT) refers to non-penetrating injuries incurred when body armor deforms into the body of the wearer in the action of stopping a projectile. BABT is relevant in both the military and civilian security populations, and ranges in severity from mild skin laceration to death due to cardiac or pulmonary complications. Considering pulmonary contusion (PC), or bruising in the lungs due to trauma, is estimated to occur in up to 75% of cases of blunt thoracic trauma, PC is estimated to be a major complication in events of BABT. PC is diagnosable by radiological scans, and severity is determined through the percentage of portions containing blood throughout the whole lung. It is estimated that up to 20% of PC injuries are undiagnosed, and severity of PC is often underdiagnosed. Paired with a morbidity rate of up to 82% and an increased likelihood of intubation and ventilation, PC causes a large threat to military and civilian personnel experiencing BABT without reliable access to medical care. This necessitates a predictive measure of PC so that injuries due to BABT may be better mitigated to improve military readiness and expedite return to duty.

The main objective of this study is to create a model for lung tissue that includes a damage threshold, and then utilize the model to predict volume of PC in the case of BABT. This starts with the development of a validated material model for lung. Small sample shear testing of porcine lung parenchyma is performed and then fit to a constitutive model derived for shear loading. The fitted parameters are implemented into a finite element material model for lung, and the model is validated by matching kinematic response to experimentally performed indentation testing on lung tissue. Once the material model for lung is achieved, it is included into a human body model that has been validated for use in BABT loading events. Through experimental testing in shear, a failure threshold for lung tissue is determined and included within the human body model so that lung damage resulting from BABT can be output from simulations. With an output of lung damage volume resulting from lung tissue failure, methods are determined for predicting the physiological injury of PC. This is done by correlating the damage volume output from the model to reports of PC volume from live-porcine BABT testing found in the literature. As a result, PC volume can be determined directly from BABT simulations with the human body model, eliminating the need for costly experimental testing on human surrogates. The major contribution of this study towards the protection of first responders and warfighters is the ability to predict PC injury in BABT events. This will help in the diagnosis and mitigation of blunt pulmonary trauma in relation to wearers of body armor.

ACKNOWLEDGEMENTS

First and foremost I would like to thank my husband, Miller Eaton. Without him, I'm not sure I would have had the strength and perseverance to see this through to the end. He has been my constant support through the literal blood, sweat, and tears that it took to be where I am today – which, consequently, happens to be finishing up a PhD while taking care of a newborn in a new apartment in a state I never thought I'd live. Our future is bright, and I never would have gotten here without you, Miller.

I also, very much, owe this accomplishment to my family. To my mom, Melissa, for always being there on the other line of the phone when the stress became too much. To my dad, Ray, for always having just the advice I needed and making the world seem like a more manageable place. And, to my brother, Nolan, for being a good sport every time I asked for advice on my work or future job, even though he is in a different field of engineering. Thank you all so much, I love you, and I'll always watch for deer.

Next, I would like to thank all the students and employees I have worked with during my time at the Center for Applied Biomechanics (CAB). I never expected to go to grad school and find such support, companionship, and lifelong friends among my fellow coworkers. There's too many people to list here and still have a reasonably sized acknowledgements section, but I want to give a special thanks to Brandon Perry. Without his friendship and constant guidance, I truly believe I would have failed or quit long ago. It's been a rocky road, but I think that at the end, our lives are better for having gone through it. Thanks Brandon, we Midwesterners will always stick together.

Finally, I would like to thank my son, Jack. I've cherished the constant companionship while doing my simulations, writing, and defending. I'm one of few people who can say that without a doubt I was never alone through the creation of this dissertation. I was so excited to meet you, and I hope that one day you will be proud of me like I'm already so proud of you.

Thanks to everyone I have met, talked to, or thought about during my time at CAB. You have all, in some way, helped me achieve this.

CONTENTS

LIST OF FIGURES

LIST OF TABLES

ABBREVIATIONS

$\triangle$ Constant

AIS   Abbreviated Injury Score

ALI   Acute Lung Injury

ARDS   Acute Respiratory Distress Syndrome

BABT   Behind Armor Blunt Trauma

BFD   Back-Face Deformation

b_j Constants

BMI   Body Mass Index

BOOP   Bronchiolitis Obliterans Organizing Pneumonia

C Constant

C_1, C_2 Constants

CIREN   Crash Injury Research and Engineering Network

CT   Computed Tomography

DRAGun   Differential Rate Air Gun

E Young's Modulus

$\boldsymbol{F}$ Deformation Gradient

FE	Finite Element
G(t)	Reduced Relaxation Function
G_0	Short term shear modulus
G_∞	Long term shear modulus
GHBMC	Global Human Body Model Consortium
G_j	Constants
HBM	Human Body Models
I_1	First strain invariant
I_2	Second strain invariant
ICU	Intensive Care Unit
J	Jacobian
K	Bulk Modulus
m	Constant
MAP	Mean Arterial Pressure
MPAP	Mean Pulmonary Arterial Pressure
MVC	Motor Vehicle Crashes
n	Sample Number/Material Constant (v)
N	Specimen Number
NIJ	National Institute of Justice

PaO$_2$	Partial Pressure of Oxygen (arterial)
PC	Pulmonary Contusion
PMHS	Postmortem Human Specimen
QLV	Quasi-linear Viscoelastic
R	Rotation Matrix
RLL	Right Lower Lobe
SaO$_2$	Arterial Oxygen Saturation
SD	Standard Deviation
SED	Strain Energy Density
SSE	Sum Squared Error
t	Time
U	Stretch Tensor
VC	Viscous Criterion
W	Strain energy per unit mass
WALT	Waterloo Thorax Model
x$_1$	Deformed Displacement
X$_2$	Undeformed Displacement
α	Constant
β	Constant

ε	Strain
λ_i	Stretches
v	Poisson's ratio
ρ_o	Density of lung
σ	Stress
τ	Time Constant

CHAPTER 1: Introduction

1.1 STATEMENT OF PROBLEM

Pulmonary contusion (PC) is a potentially life-threatening injury that is estimated to occur in up to 75% of blunt thoracic trauma cases. (C. Miller et al., 2019) PC is problematic in that contusion in the lungs peaks 24-48 hours after initial injury with respiratory distress peaking at 72 hours. (Cohn, 1997; Cohn & DuBose, 2010) X-ray imaging can fail to diagnose 21% of PC cases, and severe PC is linked with increased morbidity and mortality. (Jin et al., 2014; P. R. Miller et al., 2001; Schild et al., 1989) Due to these factors, PC often goes undiagnosed or underdiagnosed. (Clark et al., 1988) The lack of identification of PC within the medical field causes a lack of understanding within the biomechanical field. It is difficult to determine the relationship between mechanical lung tissue failure and physiological injury if cases of PC remain unknown. This propels the need to determine better ways of predicting lung tissue damage and its connection to PC for the improvement of diagnostic measures.

The need for diagnosis of PC is especially relevant within the military population where combat readiness is crucial, and there is little to no access to specialized imaging equipment. Behind armor blunt trauma (BABT) has been identified as an injury mechanism having a great risk of PC, due to the blunt, non-penetrating nature of body armor stopping a projectile but deforming into the body of the wearer. (Carroll, 1978; Drobin et al., 2007; Gryth et al., 2008; Hanlon & Gillich, 2012) BABT has more localized energy impact conditions than those commonly seen in motor vehicle crashes. (Prat, Rongieras, Sarron, et al., 2012) Therefore, methodologies in place for predicting thoracic injury in automotive crashes may not fully encompass the specific injury mechanisms of BABT. There is also no consistent predictive measure of pulmonary injuries within the literature, and nothing thus far definitively correlates physical lung injury with PC. (Eaton et al., 2022)

More specified lung material models are needed to mitigate this threat. Lung material models are widely varied throughout the literature, and the source of individual lung parameter values is somewhat unclear. (Nsiampa, 2011; Rater, 2013; Roberts et al., 2005) This in part stems from the use of surrogates with no correlation to human, and the use of differing surrogates for the same model. (Shen et al., 2012; Vawter et al., 1979) Further, there has only been lung tissue testing performed in tension or biaxial tension, and no kind of material validation has occurred to determine if the material model accurately represents different testing mechanisms. (Eaton et al., 2022) To move forward in lung injury

prediction, an accurate material model for lung is needed to correctly model lung response in thoracic impacts. Only then can any connection to injury be established.

It is evident that PC is a serious issue within the civilian community, and it is expected to be a greater problem in the wearers of body armor from the incidence of BABT. (Cannon, 2001; P. R. Miller et al., 2001) A possible method to improve the diagnoses of PC, and subsequently injury mitigation, is to understand the specific injurious mechanisms through use of a lung material model. However, such an incorporating lung model does not exist within preexisting literature. In general, for the case of BABT, there is no established method of modeling thoracic impacts that differ from those seen in motor vehicle crashes. This directly effects the ability to determine lung injury criteria from BABT events, causing a disconnect in possible PC prediction. A better understanding of the material properties of lung tissue and when pulmonary damage occurs during BABT needs to be gained for the prediction of incidence and severity of PC injuries.

1.2 MOTIVATION

The biggest limiting factor in the development of a concise material model for lung is the lack of diversified component testing to feed into a mathematical model. All previous small-component testing on lung tissue was in the form of tensile testing, save for one study in compression that proved the isotropic nature of lung. (Weed et al., 2015) While tensile testing is useful for the creation of lung models, the testing available is very limited. Not only is there no other test setup to ensure the applicability of a developed model, but the data present in the literature is also performed at a limited range of velocities. There is no usable quasi-static data for fitting material parameters before the onset of nonlinearity at dynamic strain rates, and there is no testing velocity above 0.1 m/s. (Gao et al., 2006; Rausch et al., 2011; Vawter et al., 1979) Increased testing velocity is important in conjunction with thoracic impacts, as internal organs including the lungs are estimated to reach velocities of 1 – 3 m/s. (Lau & Viano, 1981; Prat, Rongieras, de Freminville, et al., 2012; Rater, 2013) It has also been hypothesized that compressive forces on the lungs, such as those from a thoracic impact, result in lung failure from shearing of the tissue, not failure in tension. Testing setups such as shear testing or forms of compression in which the material is allowed localized shearing would be more beneficial to a future addition of a failure threshold. This way, a material model and failure criteria would be achieved via the same manner of mechanical testing. Likewise, all testing for a material model should be done with the same surrogate – one that is comparable to human lung by way of a known correlation or scaling. There have been strides in the testing and

successive modeling of murine lung material, but no transfer to human currently exists, making this data unusable for human body models. (Gayzik et al., 2007, 2011; Rausch et al., 2011; Stitzel et al., 2005) All other material models for human lung developed in the last two decades have used canine lung as the experimental basis. (D. S. Cronin, 2012; Danelson & Stitzel, 2015; Rater, 2013; Roberts et al., 2005; Shen et al., 2008a) This is a major problem within the field since the dog data, from Vawter et al., was considered to have significant differences from cadaveric (PMHS) lung during matched testing. (Vawter et al., 1979; Zeng et al., 1987) The field of lung biomechanics is limited by the use of surrogates uncorrelated to human.

A model for lung material is useful within a finite element human body model for investigating the response of thoracic impacts such as BABT. However, most widely used human body models have been developed for use in motor vehicle crashes, and the accuracy of the kinematic response during BABT or other localized blunt thoracic loading has not been evaluated. This is evident in Cronin et al.'s study on BABT impacts and comparison to reported cases in which the human body model used in the study was developed for automotive uses. (D. S. Cronin et al., 2021a) There is a level of uncertainty present when using a model that has never been utilized for BABT-like events in that there is no comparison of experimental kinematic data. Still, the study does set a precedent for modeling the specific interaction between the body armor and the human body. Using both a dynamic impactor modeled after the shape of deforming body armor at different time points, and a static impactor that did not change shape, it was shown that there was no statistical difference in simulations of the same impact energy. (D. S. Cronin et al., 2021a) This allows for simplification in future modeling of the BABT interaction, making it easier to focus on the response of the lung during impact.

Even if the limitations in the modeling of lung material and BABT interactions did not exist, PC still could not be predicted due to the lack of any form of failure criteria on lung tissue itself. There has been no testing of mechanical lung tissue failure. The closest study involves the impact of live-murine lungs from which a volume of PC is obtained. (Gayzik et al., 2011; Stitzel et al., 2005) Problems arise in going directly from impact conditions to PC, which has been known to change over time. This skips the determination of lung damage due to mechanical failure, which is an unchanging value dependent only upon impact conditions. Other forms of injurious thresholds for the lungs include bronchial pressure-based criteria. This idea of lung failure comes from studies on blast lung, which have strain rates well above the levels seen in blunt impact, and for which lung and other organs must be treated with different mechanical models. (Bass et al., 2008) For blunt impacts, it has been assumed that pressure levels in the bronchi correspond to AIS 3 rib fractures, which correspond to AIS 3 lung injuries. The first problem with

this lung injury threshold is that it relies on number of rib fractures, even though studies have disproven a relationship between number of rib fractures and severity of PC. (C. Miller et al., 2019) Another issue lies in the AIS measures for lung injuries not directly referring to PC or even solely blunt lung injuries – pneumothorax and laceration from ribs is also included. This shows that the lung injury criteria in use is a severe limitation when requiring a correlation between BABT and PC.

In summary, the defined problems in the previous section have arisen due to the limitations in understanding lung biomechanics, modeling BABT-type interactions, and connecting these topics of research to incidence and severity of PC. To achieve prediction of PC in BABT events, additional research beyond the preexisting studies is needed. For the end goal of PC prediction in BABT, there must first be an updated lung material model with a relevant surrogate, a methodology for evaluating the use of human body models in localized blunt trauma, and a quantitative method of determining the amount of PC from lung tissue failure.

1.3 SCOPE OF RESEARCH

The **objective** of this dissertation is to **create a model for lung tissue that includes a damage threshold, and then utilize the model to predict volume of PC in the case of BABT**. The model and damage threshold are based in fresh porcine lung data. This is the first study to have both a validated material model and failure threshold based in the same human surrogate, and to have that surrogate be a large mammal. Cases of BABT will be simulated as an example of the applicability of this lung material model. Within this example application, a methodology is created to assess BABT impacts using a finite element human body model. Finally, a connection between lung damage, through the failure threshold, and PC, through reported studies of live-porcine testing, is made in order to predict the volume of PC for BABT events.

Through background research conducted in Chapter 2, three aims for achieving the objective of this dissertation were realized. The aims are listed below, along with an outline of tasks through the corresponding chapters. A summary of these goals can be seen in Figure 1.3.1 in the form of a flow chart.

AIM 1: Develop a validated material model for lung

A material model for lung must first be created to properly model the pulmonary response during BABT. This is initiated by small-sample testing of lung parenchyma described in Chapter 3. Chapter 3 results in shear datasets containing both quasi-static and step-hold testing of porcine lung tissue, and a dataset of

step-hold indentation tests to be used for material model validation. Chapter 4 consists of the development of a shear-based constitutive model with the experimental basis in Chapter 3. Material parameters gained from Chapter 4 are used in Chapter 5 for the development of a finite element lung material model. This lung material model incorporates the shear testing and fitting from Chapters 3 and 4, and is validated by the indentation dataset from Chapter 3. Once the finite element model is fitted to all three forms of experimental testing, the aim has been achieved and a validated material model for lung is developed.

AIM 2: Determine how to model lung damage in BABT

Creating a usable model for lung material only satisfies part of the goal to be able to predict PC. A methodology needs to be established in which BABT interactions with the human body, and therefore lung, can be represented. When paired with an updated lung material, the model can act as a tool in the determination of injury prediction. This process starts in Chapter 6 with the validation of whole body GHBMC (Global Human Body Model Consortium) response to BABT. The GHBMC has been compared with human body response during motor vehicle crashes, and a comparison needs to be made during the response of BABT. This is done by comparison of PMHS kinematics during a BABT event. Once the GHBMC is evaluated for use during BABT, a method of determining amount of lung damage is addressed. Chapter 7 determines a threshold for failure in lung tissue by small sample shear tests to failure. An established mechanical failure threshold can be incorporated into the GHBMC to detect amount of lung damage during BABT. However, a model for BABT is only applicable if it can be matched to experimental BABT testing in the literature. Within the field, live-porcine BABT tests give one consistent metric by which to determine the impact energy into the body. That metric is the depth into ballistics clay of the back-face deformation of the body armor used in the testing. Therefore, Chapter 8 determines the relationship between clay displacements and BABT so that the tool created to model BABT with the GHBMC can be utilized to reconstruct BABT with different known hard armors. This allows for the GHBMC, validated for BABT response in Chapter 6, paired with the lung damage threshold found in Chapter 7 to be versatile enough to represent different experimental BABT testing through the relationship found in Chapter 8. All of this together establishes a methodology for recreating BABT interactions to include the volume of lung damage seen in these events, which is necessary for any prediction of PC.

AIM 3: Determine methods for predicting PC

Only once a lung material model has been created, and a damage threshold found to implement into a methodology for recreating BABT with the GHBMC, can a method for predicting PC be determined. PC can only be measured in live specimens, since PC corresponds to a volume of blood that only occurs through exsanguination via an active heart. Therefore, BABT simulations must be connected to live-porcine BABT testing to establish a method for predicting PC. There are two paths that are explored for the prediction of PC using reported live testing: using studies in which PC is reported and connecting PC volume with modeled damage volume, and using studies in which blood oxygen saturation levels are reported and connecting the physiological readings with modeled damage volume. Chapter 9 involves the prediction of PC from lung damage. By using the information gained in Chapters 8 and 7 to recreate the impacts unto live-porcine with the GHBMC and find a lung damage volume, a connection can be made to PC through the reported PC volumes in studies involving two separate test setups. This connection between PC and damage allows for the investigation into the relationship of PC and SaO_2 in Chapter 10. The purpose of Chapter 10 is to consider the possibility of determining incidence and severity of PC using a physiological reading. This is achieved through the known connection between PC and damage from the model in Chapter 9, though if a relationship is established to SaO_2, future prediction of PC can rely solely on information gained from blood tests or medical devices such as a pulse oximeter. Both results of Chapters 9 and 10 explore methods for predicting PC from BABT events, and thus achieve the overarching objective.

Chapter 11 consists of the conclusions of this work. This includes major contributions to the field, assumptions and limitations of the research performed, and future work needed to improve upon the topic. A summary concisely details how the objective was met, and a model for lung tissue that includes a damage threshold was created, and then utilized to predict volume of PC in the case of BABT.

Figure 1.3.1
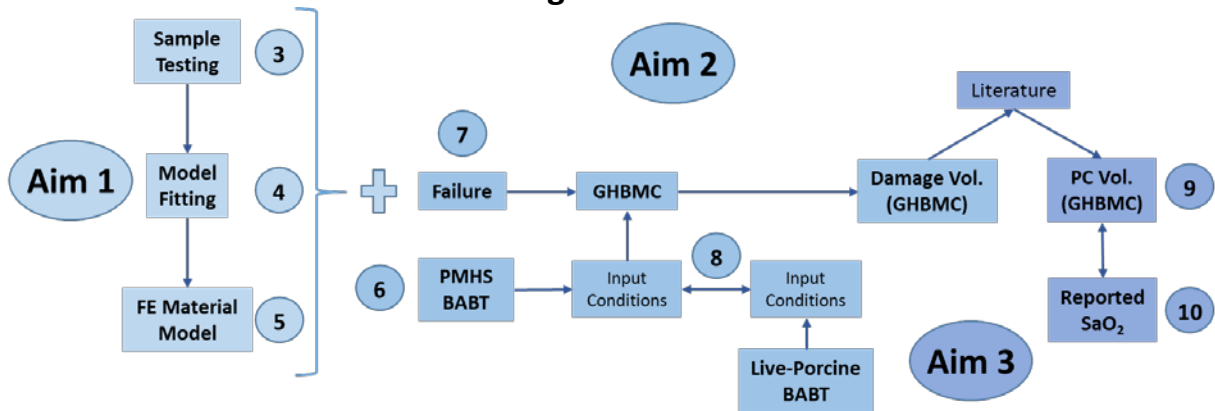
Fig. 1.3.1 – A summary of the dissertation through a flow chart. Aims are indicated in ovals color-coded to match the respective elements that fall under that aim. Chapter numbers appear in circles and are positioned next to their corresponding contents.

CHAPTER 2: Background

2.1 ANATOMY AND INJURY

To determine the gaps in knowledge regarding the relationship between lung biomechanics and blunt injury, the function and importance of lungs from an anatomical standpoint must be properly understood. Lungs are instrumental in the exchange of oxygen and carbon dioxide within the blood. Air flows into the trachea and then the bronchi, flows down the bronchioles, and finally into the alveoli. The alveolar sacs are covered in capillaries where oxygen diffuses into the bloodstream and carbon dioxide diffuses out of the bloodstream to be exhaled. The alveoli size for humans and various other mammals is known, so that future comparison between species may be readily available.(Lum & Mitzner, 1987) The main structure of the lung is made up of these alveoli from which whole lung deflation and inflation are produced. These different air volumes for both humans and other mammals is also known to the scientific community.(Crosfill & Widdicombe, 1961; Millar & Denison, 1989) This overall structure can be seen in Figure 2.1.1 which provides an image of porcine lung through micro-CT. For this current work, it is important to define the magnitude of scale with respect to the structures of the lung, for mechanical and mathematical purposes. Micro-scale will be thus defined as pertaining to the structure of the alveoli themselves or looking at the whole of the tissue as being made up of individual alveoli. Macro-scale will be defined as treating the tissue of the lung as the sum of the smaller structures, i.e. a continuum approximation. In the scope of this paper and in reference to injury, testing, and modeling, the macro-scale ideal will be the focus and the lung tissue will be treated like a continuous solid organ.

Knowing the function and configuration of the lungs can lead the way in determining the mechanism of injury and how injury affects structure and function. Pulmonary contusion (PC), otherwise described as hemorrhaging or edema in the lungs, is defined as the disruption of capillaries causing bleeding into the various spaces of the lung.(Ganie et al., 2013) This bleeding can cause a multitude of symptoms including hypoxemia, hypoxia, dyspnea, coughing, chest pain, hypercarbia, and pulmonary shunting, and intubation and mechanical ventilation may be necessary.(Cohn, 1997; Ganie et al., 2013; Yamamoto et al., 2005) Since PC is defined solely as bruising within the lungs, the diagnosis is nonspecific to the many injury mechanisms that may cause PC. This work will focus on PC caused by blunt impacts, therefore blunt lung injury will be the first injury mechanism to be detailed. Blunt injuries to the lung are characterized by high energy impact events without penetration, usually in the form of high velocity impacts that cause quick acceleration or deceleration.(Ganie et al., 2013; Yamamoto et al., 2005) In these

events, lung tissue failure is due to the tearing of the alveolar structures in shear. As the thorax is compressed, alveolar structures are ripped from places of higher density due to the differences in acceleration within the lung tissue itself.(Ganie et al., 2013; D. L. Miller & Mansour, 2007; Wagner et al., 1988; Yamamoto et al., 2005) The shearing of lung tissue due to the compression of the thoracic wall is the leading cause for injurious PC, and has been reported as early as 1761.(Fallon, 1940; Grimal et al., 2005; D. L. Miller & Mansour, 2007; Wagner et al., 1988) While other injuries besides PC are often present with blunt thoracic trauma, blunt-caused PC can occur within an intact rib cage.(Fallon, 1940; D. L. Miller & Mansour, 2007; Ross, 1941) This has led some to theorize about the possibility of 'contre-coup' PC from blunt impact. Contre-coup injuries are commonly referred to only within the context of brain, and are used to describe the phenomenon of impact on one side of an organ causing damage on the opposite side.(Rashid, 2000) While an early finite element model of impact to the lungs predicted the possibility of contre-coup injuries, there has not been much evidence in the literature for it to be considered a threat in blunt impacts.(Bush & Challener, 1988) Four reported cases of contre-coup in lung were found, all detailing a side impact with the contralateral lung being affected. However, in all cases there were comorbidities such as intra-abdominal blood or hemothorax which makes the exact injury mechanism of the lung tissue unclear.(Nema et al., 2013; Rashid, 2000) Further, in studies of blunt thoracic impact on live animals, no contre-coup injuries were achieved.(Drobin et al., 2007; Gayzik et al., 2011; Gryth et al., 2007; Raghavendran, Davidson, Helinski, et al., 2005) For this work, contre-coup injuries will not be considered further for lack of sufficient mechanism of injury, and the focus will be on blunt PC from the blunt impacts to lung tissue causing a shear tearing injury.

An injury that causes PC and commonly occurs in conjunction with blunt thoracic trauma is that of lacerations. Lacerations are penetrative injuries into the lung tissue from foreign objects that have penetrated the thoracic wall and pleura or, most frequently, displaced rib fractures.(Wagner et al., 1988) In instances where blunt PC is also present, lacerative areas may exacerbate the volume of blood found in the lungs. This is especially true with any combinations of flail chest, pneumothorax, hemothorax, or the like.(Ganie et al., 2013; D. L. Miller & Mansour, 2007; Wagner et al., 1988) Diagnosis of PC volume through imaging is not dependent upon injury mechanism, so if looking explicitly at blunt PC, other injuries that could cause blood in the lungs must be taken into account.

Figure 2.1.1   **Figure 2.1.2**
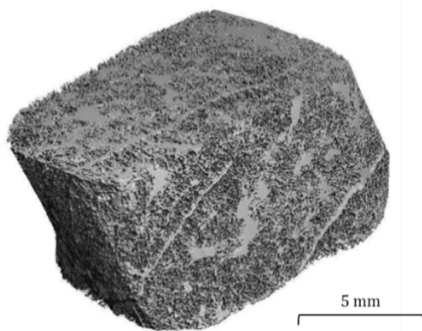
Fig. 2.1.1 - Section of porcine lung imaged using micro-CT
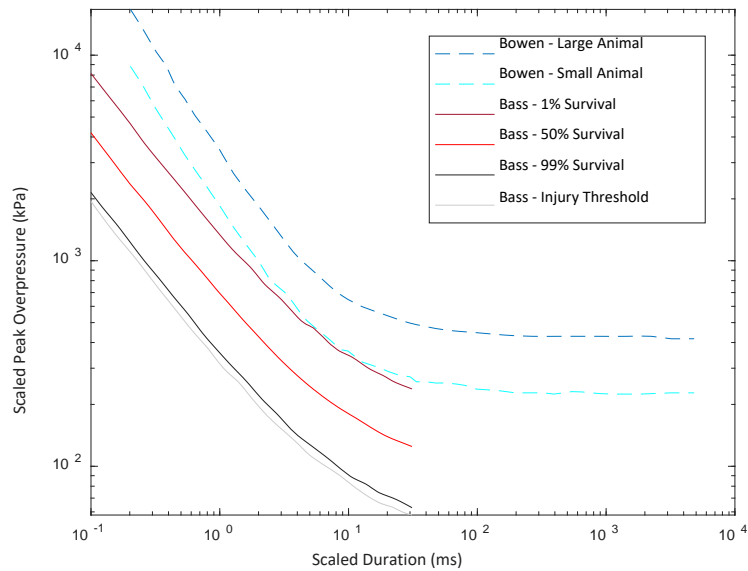
Fig. 2.1.2 - Compiled data from Bowen et al. and Bass et al. on blast lung thresholds in scaled peak overpressure versus scaled duration. Bowen's curves are dashed and Bass et al.'s curves are solid.

Another injury mechanism that is commonly associated and/or attributed to blunt lung injuries, especially in militant or other combatant scenarios, is blast lung. However, through the course of history it has become clear that blast and blunt lung injury have separate onsets and means of mechanical failure. 'Blast lung' refers to injuries received from close proximity to high pressure shock waves resulting from an explosion or blast. (Cohn, 1997; Rafaels et al., 2010; Ross, 1941) These blast lung injuries sparked interest in the research of blast in various mammals and development of an injury and mortality threshold for the lungs. The most prolific of these injury risk curves comes from Bowen et al. and are referred to as 'Bowen's curves' or 'the Bowen curves.'(Bowen et al., 1968) Attributed with the first injury risk information for lung, Bowen et al. compiles lethality data from high explosion and shock tube testing on both large animals (burro, monkey, sheep, swine, goat, dog, cat, steer) and small animals (rat, hamster, rabbit, mouse, guinea pig) in terms of peak overpressure and phase duration.(Bowen et al., 1968) Bowen's curves have been used frequently throughout the literature, seemingly unquestionably, as the understood threshold for all lung injury. However, in 2008 Bass et al. redeveloped blast lung thresholds using reviewed literature.(Bass et al., 2008) While Bowen et al. used a Probit analysis with the original 12 mammal experiments, Bass et al. included more than 50 experiments on blast with over 1,100 large animals and utilized a nonlinear logistic regression to arrive at injury risk curves comparable to Bowen's.(Bass et al., 2008; Bowen et al., 1968) Figure 2.1.2 is a reproduction of Bowen's original large

and small animal lethality curves along with Bass et al.'s curves for 1%, 50%, and 99% survivability and an injury threshold. The mechanism of injury due to blast is the same for lung as for the other air-filled organs of the body – pressure and volume based due to the compressibility of air. Blasts can cause a 'bursting' effect in the alveolar structures from the expansion of gases when a shock wave passes.(Cohn, 1997) This pressure-induced bursting mechanism is distinctly different from the compression-induced shearing mechanism found in blunt injury, but blast injury thresholds are still, somewhat erroneously, applied to blunt trauma. This is attributed to a historical assumption that lung had only one injury predictor, pressure, rather than behaving like other solid organs with stress/strain concentrations.(Cohn, 1997; Grimal et al., 2005; Ross, 1941) Blast and blunt injuries not only have different mechanisms, but also distinct impact conditions, it having been shown that the velocity of deformation in blunt scenarios is much less than in blast scenarios (3 – 20 m/s versus 40 – 90 m/s).(Viano, 1991)

Mechanisms of injury that will not be detailed within this work include lung injury from gastric aspiration or other types of fluid inhalation as well as any injuries caused by non-blast pressure differences such as mechanical ventilation. This is to narrow the scope to blunt lung injuries from ex vivo sources that have clearly defined mechanical properties. It is important to remember, however, that these types of injuries can occur concurrently with other lung injuries, possibly making prognoses worse. A common measure associated with these kinds of injuries is acute lung injury (ALI). ALI is not mutually exclusive to all forms of lung injury, e.g. PC can occur with or without ALI and ALI can occur with or without PC. Rather, where PC is both physical (mechanical failure) and physiological (associated symptoms), ALI is more physiological, defined as an oxygenation ratio (PaO_2/FiO_2) at or below 300 mmHg, and any presence of edema in the lungs. ALI can lead to acute respiratory distress syndrome (ARDS), defined as ALI but with PaO_2/FiO_2 at or below 200 mmHg, which indicates a patient's decline into hypoxemic respiratory failure.(Matute-Bello et al., 2008; Raghavendran et al., 2009) Both ALI and ARDS are important components for the understanding of the effect of blunt lung injury and its progression.

2.1.1 Recommendations

The trouble in defining blunt PC may arise from the extent, or lack thereof, of lung damage that can be seen through imaging techniques. A clinical diagnosis of PC seems to involve observation of a large quantity of blood within the lungs, but that pooling of blood is nonspecific to an exact methodology of injury. While it may be right to assume that PC indicates regions of gross lung failure, further study is needed to be able to determine injury mechanism within the tissue. For instance, gross tissue failure is most likely caused by smaller micro-tears. It is unknown how many smaller structure failures are required

for the diagnosis of blunt PC. This may also depend on type of lung injury: it needs to be determined if the threshold for finding PC in blunt versus lacerative cases contains the same number of smaller structural failures. Further research is needed to properly define PC in order to relate extent of failure within the tissue with what can be found at diagnoses.

2.2 CAUSES OF BLUNT THORACIC TRAUMA

Just as there are multiple injury mechanisms in the lungs, there are likewise many outward causes for these injuries. These causes can be roughly split into two categories: civilian thoracic trauma and military or law enforcement thoracic trauma. As the former contains more of the populace than the latter, civilian thoracic trauma incidence will be discussed first. From the invention of the automobile, the greatest cause of blunt PC in the civilian population was revealed as motor vehicle crashes (MVC).(Alfano & Hale, 1965; Clark et al., 1988; Fallon, 1940; Ross, 1941) As a way to compile information from MVC in a useful network for research, the National Highway Traffic and Safety Administration (NHTSA) established the CIREN (Crash Injury Research and Engineering Network) database. PC occurs in nearly 22% of all CIREN MVC, and occupants who die before discharge are more likely to have had PC.(Gayzik et al., 2009; O'Connor et al., 2009) There are a greater number of PC incidences in frontal crashes, with the number of incidences from lateral crashes not far behind. Considering that frontal crashes are more than two times more likely than lateral crashes, lateral crashes therefore have the largest proportion of PC – near-side impacts accounting for more PC cases than far-side impacts.(Danelson & Stitzel, 2015; Gaewsky et al., 2017; Gayzik et al., 2009; O'Connor et al., 2009; Weaver et al., 2013) In frontal crashes, the most frequent mode of injury consists of impact with the instrument panel, steering wheel, seatbelt, airbag, seatback (for backseat passengers), or any combination thereof. For lateral crashes, impacts are most frequently with the near-side door, center console, seatback, or any combination thereof.(Weaver et al., 2013) Left, right, or bilateral lung contusions are highly contingent on the side of the impact, and the impact's proximity to the occupant.(Gayzik et al., 2009; O'Connor et al., 2009) Looking at all CIREN cases including CT, regardless of crash type – in occupants with no other chest injuries, PC volume in the lungs was as high as 21% of total lung volume, and in occupants with other chest injuries the PC volume was as high as 70%,(Weaver et al., 2013) suggesting that a compromised thoracic wall or presence of other injuries may have an effect on the severity of PC.(Danelson et al., 2011; Danelson & Stitzel, 2015; Weaver et al., 2013) However, the assumption cannot be made that any PC listed is PC from blunt impacts, since the CIREN database only lists medical diagnoses and not specific mechanisms of PC such as blunt impact

or laceration from displaced ribs.   Further studies on impact type and inclusion of other thoracic injuries should be a future focus to determine the influence on PC.   Other databases such as the National Automotive Sampling System should also be included in retrospective studies and compared with the CIREN cases previously examined.

While MVC account for the vast majority of PC cases within the civilian population, there are other causes of blunt thoracic trauma that result in PC. For instance, in a study of 75 patients found to have PC, 50 were injured by MVC, 9 by motorcycle crashes, 5 by being hit as a pedestrian, 4 by a fall, 2 by assault, 4 by crush injuries, and 1 by a kick from a horse.(Wagner et al., 1988) This shows that blunt PC may be caused by any kind of high-energy blunt impact to the thorax including thoracic crush and assault to the chest. The first reported case of PC in English was in 1840 when a man died with an intact ribcage after a wagon wheel had passed over his chest. At autopsy, massive PC was found without any tear in the pleura.(Fallon, 1940) Also in early report of PC, Fallon presents a case from 1939 in which a patient took place in a boxing contest and later developed PC. He goes on to list possible causes of PC such as a vehicle passing over the body, a fall from a height, blows to the chest, and lifting a child by the arms.(Fallon, 1940) Fallon's case mirrors more modern cases of PC such as a case report from 2015 detailing a 30 year old man who died after a recent bar fight. At exhumation and autopsy, severe PC in the right lung was realized as cause of death.(Kishorkumar et al., 2015) Another noteworthy case report of non-MVC induced PC followed a 19 year old collegiate football player. After a left-side tackle, the player later complained of left-side chest pain, but upon examination no visible external injuries were found. Chest radiographs were ordered and PC in the lower lung was discovered.(Meese & Sebastianelli, 1997) These cases, and cases similar, show that PC can be caused by any kind of blunt impact and are not solely reserved for cases of more extreme trauma such as high-speed MVC.

Even though military and law enforcement personnel are just as at-risk for PC due to the aforementioned civilian causes, the military population has another major cause of PC that has little to no relevance to the average civilian: behind armor blunt trauma. Behind armor blunt trauma, or BABT, refers to non-penetrating injuries resulting from body armor stopping a bullet or piece of shrapnel.(Cannon, 2001) In stopping a projectile, the body armor deforms into the wearer in a localized blunt impact, and injuries to the lungs are considered one of the most severe types of damage from BABT.(Grimal et al., 2005) It is necessary to note here that 'penciling' is an occurrence where body armor stops a bullet but fails in a distinct way that results in shards of body armor penetrating the body.(Carr et al., 2016) While related to BABT, this injury mechanism is penetrative and this case will be disregarded in future discussions of blunt injury. BABT can occur in both soft (aramid fabric layers) and hard (aramid layers with

13

a ceramic plate) armors, and the problem was first reported in the 1970s and has been since characterized as an emerging problem.(Cannon, 2001; Carroll, 1978) The major distinguisher between BABT-type events and MVC-type events comes in the form of velocity versus mass of impact. BABT events, and other blunt ballistic events such as non-lethal weaponry, see local velocities between 10-80 m/s with impact masses between 100-1000 g while automotive events see local velocities between 4-15 m/s with impact masses between 4000-100000 g.(Bir et al., 2004; Nsiampa, 2011; Prat, Rongieras, Sarron, et al., 2012) External injuries from BABT are almost always present and consist of skin lesions and contusion, while internal injuries are not always present but the most commonly seen include rib fracture and PC. All fatal BABT case reports accessible in the open literature contain the diagnosis of PC.(Bustamante et al., 2019; Cannon, 2001; Carr et al., 2016; Carroll, 1978; D. S. Cronin et al., 2021a)

Research into blast lung has given way to the theory that the wave created from impacts into body armor may have some injurious effect on the lungs; some go as far to say that pressure peaks are the only injurious mechanism in BABT. There have been studies on measuring exact pressures in the lungs from BABT events, however, there has not been any conclusive evidence that the pressures are directly causing injury, or if there is a direct correlation to severity of injury.(Prat et al., 2010; Prat, Rongieras, Sarron, et al., 2012; Wen et al., 2015) It is still unclear if these pressure peaks from BABT events are a cause of PC-inducing injury within the lung, or if the blunt effect is a greater injury mechanism.

2.2.1 Recommendations

A wider range of cases including automotive-caused PC should be explored to correlate different crash scenarios with lung injury. More databases like CIREN should be included for study, especially if other databases offer more thorough information or information not included in CIREN cases. Future studies should include more insight into crash type and severity of PC, along with a distinction between blunt PC and lacerative PC. There should also be future studies addressing the question of injurious wave propagation within the lungs during a blunt trauma event. There is not enough evidence in the literature to provide a causation between internal pressure differences and blunt-type lung injury. Even if there exists pressure-based injury in blunt trauma events, it may be on a much smaller scale than compression and shear-type injuries, and thus negligible when looking at PC as a whole. Nevertheless, more data is needed to determine the significance of impact pressure to structural lung injury.

2.3 RETROSPECTIVE STUDIES

The methods of clinical diagnosis and reported short and long term impacts of PC cases need to be understood so that the severity of PC and how PC effects quality of life can be determined. PC has been reported to peak within 24-48 hours after initial injury, with respiratory distress and other symptoms peaking as much as 72 hours later.(Cohn, 1997; Cohn & DuBose, 2010; P. R. Miller et al., 2001) This provides an immediate problem for ease of diagnosis considering most patients are imaged only upon admission to hospital. In a study performed by Erickson et al., PC was induced in rhesus monkeys and the specimens were monitored for 48 hours. Chest radiographs (X-rays) were performed on the specimens at 4 hours, 24 hours, and 48 hours after impact. Nearly 80% of the specimens' volume of PC increased significantly from 4 hours to 48 hours after impact.(Erickson et al., 1971) Not only is the timeframe of imaging essential, but also the imaging modality. Computed tomography (CT) has long been known to be the best method for diagnosing PC, although many cases rely on X-rays at initial visit.(Cohn & DuBose, 2010; Gayzik et al., 2007; Schild et al., 1989) In the study performed by Schild et al. on live canine, all specimens with PC could be diagnosed using CT immediately after injury yet only 37% were immediately diagnosable through X-ray. After six hours post-injury, 21% of PC occurrence was missed with X-ray, and at necropsy it was found that even CT scans underestimated the volume of contusion.(Schild et al., 1989) In Erickson et al.'s study, specimen necropsy revealed that X-ray underestimated volume of PC in 62% of the specimens.(Erickson et al., 1971) Cases of PC being missed on initial X-rays have also been reported among patients at hospital.(Alfano & Hale, 1965; Fallon, 1940; Tyburski et al., 1999; Wagner et al., 1988) In a retrospective study performed by Wagner et al., 151 lung abnormalities where identified using chest radiography in 85 different patients while CT identified 423 lung abnormalities.(Wagner et al., 1988)

The danger of this delay in diagnosing PC is that usually only severe cases are later realized. Clark et al.'s retrospective study looked into patients with PC, flail chest, or both to determine any connection to mortality. A "significant percentage" of patients originally thought to only be in the flail chest category were determined to have both flail chest and PC upon autopsy.(Clark et al., 1988) Missed cases of PC can sometimes be attributed to no boney fractures since the necessity for imaging may seem purposeless.(Alfano & Hale, 1965; Kishorkumar et al., 2015; Meese & Sebastianelli, 1997) Alfano and Hale warn that, in especially younger patients without boney fracture, PC may appear in its most severe form.(Alfano & Hale, 1965) The reported cases of PC found in literature may only be representative of more severe cases, since severity of PC may be underdiagnosed or missed altogether.

Despite discrepancies in diagnosis and severity of PC, studies on the mortality of patients with PC can help determine PC's effect through knowledge gained at autopsy. In Clark et al.'s study, PC alone had

a mortality rate of 16%, but when PC was observed with flail chest mortality was 42%. Of the 16% that died as a result of PC, 30% received their injuries from motorcycle accidents, 23% from a vehicle striking a pedestrian, 20% from falls, and 4% from MVC. Requirement of intubation was skewed towards the death group, with 35 (n=36) patients versus 44 (n=108) patients from the surviving group.(Clark et al., 1988) Jin et al. also concurred that pre-hospital intubation and mechanical ventilation were predictors for mortality in patients with PC, as well as presence of shock, gastrointestinal bleeding, and need for emergency surgery on admission. However, it was found that rib fractures, hemothorax, pneumothorax, and hemopneumothorax were not predictors of mortality in patients with PC.(Alisha, 2015; Jin et al., 2014) This seems to be somewhat at odds with the increased mortality rate for patients with PC and flail chest reported by Clark et al., but could be explained by other possibly fatal injuries also associated with flail chest and not necessarily contributing to PC.(Clark et al., 1988; Jin et al., 2014) The discrepancy could also be explained by the lack of separation in severity of PC cases. C. Miller et al. performed a retrospective study on patients with PC by separating them into two categories: severe, where ≥20% of the total lung volume was contused, or moderate, where anything less than 20% of the lung was contused. In patients with no PC, 2.75% had flail chest (n=31) and in patients with moderate PC, 5% had flail chest (n=12); though, in patients with severe PC, 16.5% had flail chest (n=14), indicating a higher correlation between PC and flail chest for more severe cases.(C. Miller et al., 2019) It appears that the separation of moderate and severe PC is likewise relevant in risk of mortality. The non-PC group and the moderate PC group had mortality rates of 4.97% and 4.24% respectively, while the severe PC group had a mortality rate of 9.41%, revealing another possible connection between severity of PC and other associated injuries and comorbities.(Clark et al., 1988; C. Miller et al., 2019) It has been suggested that PaO_2/FiO_2 at admission to hospital could have value in the predicted outcome of a patient with PC.(Alfano & Hale, 1965; Alisha, 2015; Cohn & DuBose, 2010; Fallon, 1940) Although, P. Miller et al. concluded that in patients with PC there was no relationship between PaO_2/FiO_2 readings at admission and extent of contusion in the lungs.(P. R. Miller et al., 2001)

There may be tenuous connections to mortality in patients with PC, though on the other hand, PC's connection to morbidity seems anything but tenuous. Although not a predictor of mortality, the proportion of patients with PC spending time in the ICU is significantly greater than patients without PC, possibly indicating the increase in morbidity due to PC.(Alisha, 2015; C. Miller et al., 2019) This can be attributed to the fact that blood in the alveolar spaces creates an excellent medium for bacteria growth.(Ganie et al., 2013) In one study, in the survival group of 108 patients, there were 102 pulmonary-related complications, with pneumonia affecting 26% of the survivors.(Clark et al., 1988)   Another study

found that PC is an independent risk factor for pneumonia; in patients with PC, 31% developed early-onset pneumonia.(Antonelli et al., 1994) Pneumonia rates in patients with PC are known to be double than in patients without PC.(Antonelli et al., 1994; C. Miller et al., 2019) There also appears to be a correlation with PC and bronchiolitis obliterans organizing pneumonia (BOOP) in rats, but the exact correlation, if any, between PC and BOOP in humans remains unclear.(Ganie et al., 2013; Raghavendran, Davidson, Woytash, et al., 2005) An additional risk factor associated with PC is ARDS; ARDS preceded pneumonia in up to 82% of patients with PC.(P. R. Miller et al., 2001) P. Miller et al. reports that ARDS increased likelihood of pneumonia, occurring 52% (n=21) in PC patients with ARDS and 21% (n=28) in PC patients without ARDS, and also the likelihood of mortality, 24% in PC patients with ARDS and 3% in PC patients without ARDS.(P. R. Miller et al., 2001) In a separate study, patients with PC that develop ARDS not only had an increased probability of death, but also required longer stays in the ICU, on average 28 days versus 8 days for PC patients with no ARDS.(Jin et al., 2014) Risk factors for developing ARDS included pre-hospital intubation, the need for drainage, and severity of PC.(Jin et al., 2014; P. R. Miller et al., 2001) The separation of PC into severe (≥20% of lung volume contused) and moderate (<20%) actually stems from incidence of ARDS versus contusion severity. For those with PC in the 0 – 20% range of whole lung contusion, the incidence of ARDS averaged 23%. Yet for the 20-30% range the incidence was 78%, for 30-40% incidence was 84%, and greater than or equal to 40% gave an 100% incidence of ARDS. The jump in ARDS incidence from 23% to 78% when 20% of lung volume is contused is the justification for the split of PC into severe and moderate at the 20% total lung volume contused mark.(P. R. Miller et al., 2001) Between severe PC, moderate PC, and no PC groups, significant differences were seen in ICU admittance, need for a ventilator, and age. The mean age for patients with thoracic trauma but no PC was 58 years, for moderate PC patients 49 years, and for severe PC patients 39 years, possibly indicating that a younger population is more at risk for severe PC.(C. Miller et al., 2019)

Differences in age may be related to severity of PC, as well as the question of number of rib fractures. It has been theorized that younger patients develop more severe PC due to a more compliant ribcage that allows for bending without fracture, while in older populations there are more rib fractures and less severe PC due to the energy disbursement of ribs failing.(Alfano & Hale, 1965; Bulger et al., 2000) While there has not been direct correlation between the factors of age, rib fractures, and PC severity altogether, retrospective studies have a possibility of supporting the connection, although nothing is significantly definitive. The elderly population has a higher risk of rib fractures in blunt thoracic trauma, and with increased number of rib fractures comes a higher incidence of pneumonia.(Bulger et al., 2000; Kent et al., 2008) While there are many causes for pneumonia, it nevertheless remains a possibility that

the higher likelihood of pneumonia with greater number of rib fractures stems from an increased development of PC. This is especially relevant with the evidence that PC is often missed on X-ray imaging, leading to a speculated lower number of diagnoses than actual cases.(Erickson et al., 1971; Schild et al., 1989) In a study on rib fractures in the elderly (≥65 years), for a similar number of rib fractures, pneumonia and mortality rates were 31% and 22% respectively for the elderly population, and 17% and 10% respectively for the younger population.(Bulger et al., 2000) Another study found that the percentage of patients over 60 years of age who died having no worse of an injury than rib fractures was an overwhelming 76.5% where the younger population was substantially lower.(Kent et al., 2008) One study found that patients with severe PC were statistically younger than patients with moderate or no PC, and a younger population is more likely to have severe PC without the presence of severe rib fractures. However, in the same study, the severe PC group is also the most likely group to receive 7+ rib fractures. When determining a threshold of PC both age and number of rib fractures may need to be considered in conjunction rather than as separate predictors.(C. Miller et al., 2019) This could be interpreted as the appearance of a threshold somewhere in between ribcage stability and definite chance of severe PC, but there may be other likely explanations. Weaver et al. correlated PC with the predictors of weight and BMI (body mass index kg/m^2) for occupants in MVC, with the predictor of age being "mildly significant" (0.05< p-value <0.10). Interestingly, the significant and mildly significant predictors for rib fracture were, in order of significance, age, weight, bilateral PC, and BMI.(Weaver et al., 2013) Diagnostic practices in hospital may also have an effect in the detection and mitigation of PC. For instance, imaging practices may be different among a younger population versus the elderly, leading to increased PC diagnoses for a certain group. The types of comorbidities and other injuries may also lead to either missing PC diagnosis or earlier detection. Further studies on the correlation between PC and age or number of rib fractures may shed some light on this relatively unexplored pathway into insights on the causes and effects of PC.

In summary, retrospective studies may lead to possible clinical predictors of mortality and morbidity, as well as insight into certain at-risk populations. There is a trend of younger patients being more affected by PC and having more severe PC.(Alfano & Hale, 1965; Fallon, 1940; Kishorkumar et al., 2015; Kollmorgen et al., 1994; Meese & Sebastianelli, 1997) Yet, pneumonia rates in elderly populations receiving blunt thoracic trauma may hint at more sinister lung issues.(Bulger et al., 2000; Kent et al., 2008; C. Miller et al., 2019) There seems to be a discrepancy within the literature involving the insight of oxygenation ratio (PaO$_2$/FiO$_2$) into severity of PC and as a predictor of mortality. One study lists the ratio as a significant predictor,(Alisha, 2015) while another finds no statistical significance between PaO$_2$/FiO$_2$ and patient outcome.(P. R. Miller et al., 2001) Still another specifies that PaO$_2$/FiO$_2$ readings taken at 24

hours after admission into hospital is a predictor of mortality, with readings taken at admission and at 48 hours much less significant a predictor.(Kollmorgen et al., 1994) It is important to remember that the cause of these types of inconsistencies in retrospective studies could arise from other injuries, comorbidities, and further complications that are not highlighted within the study. Studies on PC and mortality may also have disagreements with one study providing evidence that PC itself may not be an independent predictor of mortality.(O'Connor et al., 2009)

2.3.1 Recommendations

Retrospective studies offer great insight into the injury and morbidity progression of those with diagnosed PC. However, future studies should aim to detail any differences in diagnostic practices between different age populations so that the possible reasoning of missed or late diagnoses can be addressed. Further, a more detailed review of the significance of age and number of rib fracture on PC should be performed. A review of this nature could answer important questions about potential predictors of severe PC and lead to an understanding of why PC may be missed altogether. Research is also needed in the effect of comorbidities on PC severity.

2.4 ANIMAL SURROGATES AND EXPERIMENTAL TESTING

The need for animal surrogates in biological testing rises from availability of tissue, cost, and expendability of life. The specific animal surrogate utilized depends on the objectives of the study and how well the surrogate can mimic human responses within those objectives. There will always be a trade-off in animal surrogate testing; for instance, a porcine surrogate mimics the size of lungs within humans, however rats offer a larger specimen size (n) for a much lower cost. For lungs, matching micro-scale properties is often attempted so that scaling between species solely consists of a multiplicative ratio. Tenney and Remmers amassed a large comparison of lung parameters between various mammalian species.(Tenney & Remmers, 1963) A summary of their work, given in percent difference from the value for man, can be seen in Table 2.4.1.

Small animal surrogates are preferred in studies requiring a large sample size for significant results or theory validation. Small animals have been used in numerous lung studies for the clinical entity, however; this work will focus on small animal studies centered around blunt lung injury. Raghavendran et al. induced blunt lung injury in 54 rats with a falling mass and monitored the rats at intervals starting at

8 minutes after impact, to 4, 12, 24, and 48 hours after impact, and finally 7 days after impact. PC was more pronounced at 24 and 48 hours after impact than at previous times, and at 7 days, findings consistent with BOOP were found in the rats. Hypoxia was seen immediately following impact, and while PaO_2/FiO_2 levels eventually reached the same level as controls at 7 days post-impact, readings consistent with ALI were observed up until 24 hours after impact. Abnormalities in lung pressure-volume mechanics were most evident at 24 hours after impact.(Raghavendran, Davidson, Woytash, et al., 2005) A different study performed by the same group found that varying the impact energy still found the same trends in the oxygenation ratio and contusion progression over time, with even severe, sub-lethal impacts inducing PC without rib fracture.(Raghavendran, Davidson, Helinski, et al., 2005) For rat lungs impacted after a lateral thoracotomy, a PET scan was performed following 1 day, 1 week, and 1 month after impact. The PC response was significant at 24 hours, diminishing but still present at one week and one month. At one month after impact, the PC volume was only present closest to the site of impact indicating the tissue directly under the focal of impact is damaged the greatest, and lasting scar tissue remains a possibility.(Stitzel et al., 2005) Gayzik et al. impacted rats after right lateral thoracotomy(Gayzik et al., 2007) in 4 different groups: Group 1 – severe; Group 2 – high penetration, low velocity; Group 3 – low penetration, high velocity; and Group 4 – mild. Percent of PC with respect to total lung volume peaked at 24 hours after impact in all cases save Group 2 which had a PC peak at 48 hours.(Gayzik et al., 2011) This is an interesting finding that may indicated a trade-off between impact velocity and displacement that affects the timeline of PC development; however, more data would be needed to confirm such connection.

Rats are a more manageable animal surrogate when compared to larger surrogates, and the ease of access to a multitude of specimen numbers is a great commodity. Nonetheless, there exists issues with smaller animal surrogates in comparison to the human body model. Scaling and/or creating transfer functions for a variety of physiological attributes makes the meaning of the experimental data cloudy, as rat versus human physiological parameters have great difference (Table 2.4.1).(Tenney & Remmers, 1963) Thus, there is push in the scientific community for further exploration of blunt lung injury using large animal surrogates. The porcine surrogate has been the surrogate of choice amongst the literature, recognized as a size equivalent for human lungs and producing similar results as a human body model.(Prat, Rongieras, Sarron, et al., 2012; Rater, 2013; Shen et al., 2008b; Tenney & Remmers, 1963; Viano & Warner, 1976) Physiologically, porcine have comparable lung mass and alveoli size to humans, and it is possible to connect human lungs to a porcine's circulatory system to preserve living tissue.(Hozain et al., 2020; Judge et al., 2014) Further, it is advantageous to work with a living model for impact studies so that pathological

and physiological data can be collected.(Prat, Rongieras, Sarron, et al., 2012) Like with all surrogates, the use of the porcine model also has its limitations. Differences in biochemical factors between porcine and humans may alter the precision of physiological readings and collection of symptoms. In blunt impacts to the thorax, it was found by Prat et al. that the chest wall behavior between live porcine and postmortem human specimens (PMHS) may differ significantly. The porcine surrogates had greater measures of chest deflection than the PMHS, leading to possibly greater magnitude of injury than in a comparative human model.(Prat, Rongieras, de Freminville, et al., 2012) However, due to the nature of post-mortem tissue and the fact that porcine used for experimentation may be representative of a younger population when compared to humans, the exact differences between porcine and human models are not conclusive.(Prat, Rongieras, de Freminville, et al., 2012; Prat, Rongieras, Sarron, et al., 2012)

The largest dataset of physiological testing on large surrogates for specific insight into blunt lung injury exists in the blunt thoracic subcategory of BABT research. Much of the clinical research of blunt impact thoracic experimental testing utilizes porcine as a large animal surrogate. Most live-porcine BABT testing is centered around the National Institute of Justice's (NIJ) method for approving body armor. The NIJ requires body armor to not exceed a back-face deformation (BFD) limit of 44 mm.(U.S. Department of Justice, 2008) The motivation exists to determine the effect of BFD measures on living surrogates to assess the outcome on lung injury from BABT. There have been a multitude of studies done to replicate the BABT effect on porcine using a rifle shot from 10 m away unto a porcine protected by various types of body armor (Table 2.4.2).(Arborelius et al., 2004; Drobin et al., 2007; Gryth et al., 2007, 2008; Rocksén et al., 2012, 2020; Sondén et al., 2009) Most of these studies reported BFD depth according to the NIJ standard, which can help to connect impact conditions with physiological occurrences. All aforementioned studies included mean arterial pressure (MAP) and/or mean pulmonary arterial pressure (MPAP) which can be seen re-graphed together in Figure 2.4.1. Other reported physiological parameters included cardiac output,(Arborelius et al., 2004; Drobin et al., 2007; Gryth et al., 2007; Rocksén et al., 2020) respiration,(Arborelius et al., 2004; Rocksén et al., 2020) PaO$_2$,(Arborelius et al., 2004; Rocksén et al., 2020) SaO$_2$,(Arborelius et al., 2004; Drobin et al., 2007; Gryth et al., 2007; Rocksén et al., 2012, 2020; Sondén et al., 2009) VO$_2$,(Arborelius et al., 2004; Drobin et al., 2007; Rocksén et al., 2012) heart rate,(Arborelius et al., 2004; Gryth et al., 2008) lactate,(Drobin et al., 2007; Rocksén et al., 2012) pH,(Arborelius et al., 2004; Rocksén et al., 2012) and many others. It should be noted that for these various studies data collection was limited to two hours. In comparison between controls and exposed (BABT) animals, arterial saturation, respiration, and arterial pressures seemed to all be affected by BABT, while pH and lactate seem to have differing significance throughout studies.(Drobin et al., 2007; Gryth et

al., 2007; Rocksén et al., 2012) In exposed porcine, these factors seemed to have greatest difference compared to controls from time of impact to about 1 hour after impact. At 2 hours after impact, in almost all cases of surviving animals, a trend can be seen towards return to the control value.(Arborelius et al., 2004; Gryth et al., 2007; Sondén et al., 2009) PC was reported to occur in all cases of exposed animals, and a study performed by Prat et al. indicates that PC from BABT on porcine can result in contused volumes up to 52% of the total lung.(Prat et al., 2010) These types of studies on live animal surrogates are essential in looking at possible changes in physiological readings that could correlate with PC. However, not all studies reported the same findings, and more work needs to be included within the literature for any definitive conclusions to be drawn.

2.4.1 Recommendations

There is a distinct lack of experimental testing on live large animal surrogates and blunt PC on focuses other than BABT. In general, more live testing on PC needs to be performed with large animal surrogates so that there is a better understanding on injury progression and comparability to human lungs. Porcine testing would be most beneficial to compare to existing experimental data. There should also be a push to perform testing for longer periods of time, perhaps 24 hours or a week, in order to report on the full severity of induced PC. Shorter observation times are useful; however, the full extent of PC may not appear within a two-hour timeframe. Methods of diagnoses of PC should be clearly outlined, whether with imaging or at necropsy, so that it can be determined if the PC volume can be compared to clinical diagnoses or the full extent of mechanical failure within the tissue.

Table 2.4.1

Table 2.4.1 - Values for mammalian lung reported by Tenney and Remmers.[59] First row of data indicates values for a human man. Following rows indicate the animal, and in parentheses, the percent difference from man for the column property. Animal percent differences are sorted lowest to highest. Equation for percent difference can be seen in the left column with M representing the value for man and S the value for the given animal.

	Body Weight (kg)	Lung Volume (L)	Oxygen Consumption (mL/min)	Alveolar Surface Area (m²)	VO₂ (mL/kg/hr)	Alveolar Diameter (µm)
Value for Man	Man (80)	Man (6.5)	Man (243.5)	Man (65)	Man (216.5)	Man (193)
Animal (Percent Difference from Man) Sorted from lowest to highest percent difference	Bear (1.8%)	Pig (34.3%)	Bear (4.4%)	Dugang (7.6%)	Pig (0.12%)	Porpoise (7.6%)
	Porpoise (68.3%)	Porpoise (38.6%)	Goat (40.1%)	Manatee (8.9%)	Bear (2.9%)	Whale (13.7%)
	Pig (72%)	Bear (41.4%)	Dog (48.8%)	Goat (34%)	Armadillo (13.2%)	Monkey (30.9%)
	Goat (93.4%)	Goat (50.9%)	Pig (57.6%)	Dog (34%)	Whale (18.2%)	Raccoon (31.6%)
	Manatee (97%)	Cow (56.5%)	Dugang (61.1%)	Porpoise (48.8%)	Porpoise (42.3%)	Bear (41%)
	Dugang (117.3%)	Manatee (94.7%)	Manatee (81.9%)	Pig (49.2%)	Raccoon (53.4%)	Cat (49.2%)
	Cow (138.2%)	Dog (118%)	Porpoise (119%)	Bear (58.2%)	Cow (56%)	Goat (58.5%)
Percent Difference $= \frac{|M-S|}{\left[\frac{(M+S)}{2}\right]} \times 100\%$	Dog (138.5%)	Dugang (143.2%)	Cow (142.8%)	Cow (131.9%)	Dog (56.9%)	Pig (65.7%)
	Raccoon (178.1%)	Raccoon (166.2%)	Raccoon (142.8%)	Raccoon (140.3%)	Sloth (66.2%)	Cow (66.3%)
	Whale (>180%)	Whale (178%)	Cat (162%)	Cat (159%)	Monkey (81.3%)	Sloth (67.5%)
M = value for man	Armadillo (>180%)	Cat (>180%)	Monkey (164%)	Rabbit (159.7%)	Rabbit (90.7%)	Dog (69.1%)
S = value for animal	Monkey (>180%)	Monkey (>180%)	Rabbit (168.5%)	Armadillo (169.1%)	Cat (92.9%)	Woodchuck (74.5%)
	Rabbit (>180%)	Mormot (>180%)	Woodchuck (171.5%)	Woodchuck (173.3%)	Goat (100.6%)	Rabbit (85.5%)

Cat (>180%)	Rabbit (>190%)	Armadillo (174%)	Monkey (179.9%)	Woodchuck (104.6%)	Armadillo (88.5%)
Mormot (>190%)	Armadillo (>190%)	Whale (>190%)	Whale (>180%)	Rat (111.5%)	Rat (93.4%)
Guinea Pig (>190%)	Guinea Pig (>190%)	Guinea Pig (>190%)	Guinea Pig (>190%)	Guinea Pig (117.5%)	Guinea Pig (98.8%)
Rat (>190%)	Rat (>190%)	Rat (>190%)	Rat (>190%)	Mouse (153.6%)	Mouse (122.2%)
Mouse (>190%)	Mouse (>190%)	Shrew (>190%)	Shrew (>190%)	Dugang (>180%)	Shrew (143.1%)
Shrew (>190%)	Shrew (>190%)	Mouse (>190%)	Mouse (>190%)	Manatee (>180%)	Bat (146.5%)
Bat (>190%)	Bat (>190%)	Bat (>190%)	Bat (>190%)	Shrew (>180%)	Dugang (160%)
				Bat (>180%)	Manatee (160%)

Figure 2.4.1

Fig 2.4.1 - MAP and MPAP readings for porcine BABT as reported by studies. MAP is indicated in the upper portion of the graph while MPAP is in the bottom portion. Specimens used for control are represented with dashed lines, while experimental specimens are represented by solid lines.

Table 2.4.2

Table 2.4.2 - First column indicates particular studies of live porcine BABT testing. Second column details type of armor/protection used for the study along with the BFD in clay.

Study	Armor
Arborelius et al. 2004(Arborelius et al., 2004)	Hard armor, BFD = 23 mm
Drobin et al. 2007(Drobin et al., 2007)	Mark M/94, BFD = 28 mm
Gryth et al. 2007(Gryth et al., 2007)	Altered Mark M/94, BFD = 40 mm or 34 mm
Gryth et al. 2008(Gryth et al., 2008)	Mark M/94, BFD = 28 mm

MAP and MPAP Readings for Porcine BABT as Reported by Studies

mmHg

Time (min)

MAP

MPAP

Reported MAP

Arborelius et al. 2004
— Exposed
—·—· Control

Drobin et al. 2007
— Exposed
—·—· Control

Gryth et al. 2007
— 34 mm
— 40 mm
—·—· Control

Rocksen et al. 2020
— Exposed
—·—· Control

Sonden et al. 2009
— Exposed
— Exposed & TAB

Reported MPAP

Gryth et al. 2008
— Exposed
—·—· Control

Rocksen et al. 2012
— Exposed
—·—· Control

Rocksen et al. 2020
— Exposed
—·—· Control

Sonden et al. 2009
— Exposed
— Exposed & TAB
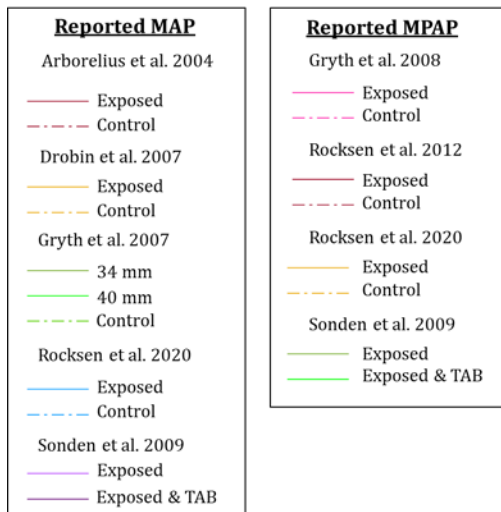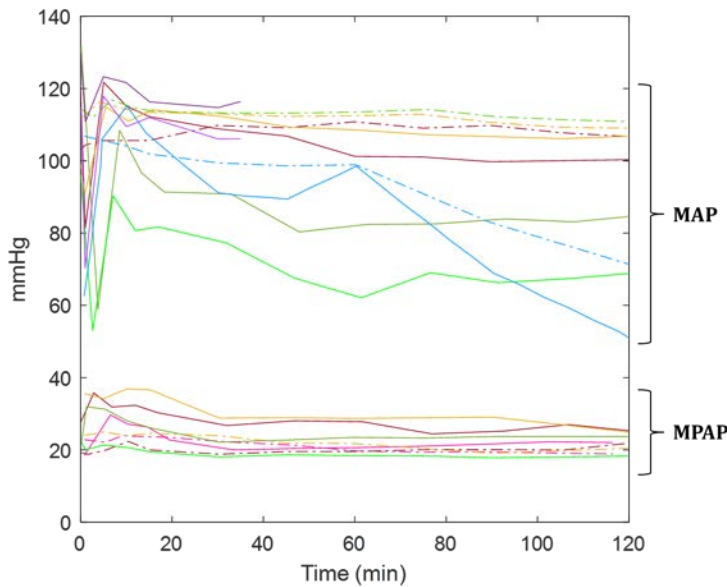
Rocksén et al. 2012(Rocksén et al., 2012)	Altered Mark 98, BFD = 42 mm
Rocksén et al. 2020(Rocksén et al., 2020)	Hard armor, BFD unknown
Sondén et al. 2009(Sondén et al., 2009)	Mark M/94, BFD =28 mm Mark M/94 & TAB, BFD = 19 mm

2.5 DISCUSSION ON PULMONARY INJURY

PC and other forms of blunt lung injury affect nearly a quarter of all occupants in MVC, and can be a leading factor in mortality and morbidity.(Gayzik et al., 2007; O'Connor et al., 2009) Blunt injury in the lung is due to a shearing mechanism resulting in parts of the lung with different densities accelerating at different rates.(Ganie et al., 2013; Yamamoto et al., 2005) The most common cause of PC due to blunt

lung injury is MVC, while in military scenarios BABT is a leading cause of PC and creates a more localized incident area.(Cannon, 2001) Perhaps the most dangerous aspect of PC from blunt impacts is the high probability of missed diagnosis or under diagnosis. Radiographic imaging is known to be unreliable in achieving an accurate measure of PC, and even CT falls short when compared to autopsies and necropsies.(Erickson et al., 1971; Schild et al., 1989) In all patients presenting with injuries received from thoracic blunt trauma, it would be beneficial for medical personnel to gain awareness of the presentation of PC symptoms, and the understanding that PC may peak 24 – 48 hours from initial injury. In this way, patients can be triaged towards the mitigation of future morbidity linked to PC such as ALI and ARDS, ARDS in particular occurring in up to 80% of patients with severe PC.(P. R. Miller et al., 2001)

The most important information that can be gained from insight into injury mechanism and PC instance within the field lies in possible predictors indicating the level of severity of PC or clinical indicators of mortality and likelihood of further disease. Presence of PC is a known independent predictor of pneumonia and ARDS, but has not been proven to be an independent predictor of mortality.(Cohn & DuBose, 2010; C. Miller et al., 2019; O'Connor et al., 2009) Presence of PC has also been connected with BOOP instances in rats, but the connection of BOOP and PC in humans has yet to be determined.(Raghavendran, Davidson, Woytash, et al., 2005) Also in rats, PaO_2/FiO_2 levels were seen as a predictor of PC if taken 4 – 24 hours after injury, returning to the level of controls at 48 hours after injury.(Raghavendran, Davidson, Helinski, et al., 2005) This agrees with most findings from retrospective patient studies,(Alisha, 2015; Kollmorgen et al., 1994) with the only discrepancy coming from a study that observed readings taken at admission.(P. R. Miller et al., 2001) Studies also showed that factors such as age, BMI, and severity of impact can also be predictors of PC levels.(Kollmorgen et al., 1994; O'Connor et al., 2009) Retrospective studies are useful for long term outcome; however, when looking to determine physiological predictors of PC severity in a controlled environment, live animal surrogate testing is the most informative. Not only can the specimens be immediately sacrificed and necropsied to determine PC progression at specific intervals, but there also exists the information that can be gained from control specimens monitored throughout. From this type of testing performed on porcine for insight into BABT, deviations in readings as per the controls give possible predictors of PC. These predictors include PaO_2, SaO_2, respiratory rate, MAP, and MPAP, causing symptoms of apnea, hypoxemia, and pulmonary shunt.(Arborelius et al., 2004; Rocksén et al., 2012) It has also been found that SpO_2 is likewise as good a predictor as SaO_2 with more ease of access.(Magnan et al., 2004) All in all, beneficial insights can be made from the monitoring of specimens during live animal testing, as it offers an understanding that cannot be gained from hospital patient information alone.

Future work in the area of PC within the clinical entity is needed in order to fill the considerate gap within literature. Recommended areas of further research as highlighted from this review include additional retrospective studies and testing on live large animal surrogates. Within databases such as CIREN or in individual hospitals, additional exploration into the correlation between PC and age, PC and occurrence of rib fracture, and/or all three should be explored. Moreover, a greater number of possible predictors of PC as motivated by the porcine BABT studies (SpO_2, MAP, etc.) should be assessed to define measurements that can be taken at a patient's admission to hospital. For the live animal surrogate testing, problems arise in that not all studies report the same physical readings. The available porcine studies also are short-term, and PC is known to have a longer term effect. A 48-hour porcine impact study would shed light on the development of PC and would be more comparable to patient studies. In addition, the only live large animal testing with clinical measures is with porcine, no other animal surrogates, and is only for the loading condition of BABT. While useful, BABT is more localized a blunt impact than other mechanisms of thoracic injury like MVC, falls, or crush injuries. More information could be gleamed from different types of impact scenarios. The addition of future focused work in the area of PC is crucial in determining the exact effects as well as mitigation strategies for blunt lung injury.

2.6 SMALL-COMPONENT MECHANICAL TESTING

Perhaps the most important starting point in the field of biomechanics is the small-component mechanical testing of tissues. Small-component is referring to a smaller sample taken from a whole organ (e.g. bone coupon, swatch of skin, piece of lobe from a solid organ, etc.). This type of testing is crucial in determining the mechanical properties of a material for later mathematical modeling. Surrogates for this type of testing vary, but emphasis is put on surrogates that closely resemble human lung properties such as PMHS or large mammals. It is also important to note that this section is concerned with the strictly mechanical testing of material, and not with pressure/volume based testing that is more relevant for finding the more physiological parameters associated with the function of lung. There is a bridge to that gap, however, in instances where mechanical equations are implemented to characterize the response in pressure changes, for example Hildebrandt's model of cat lung.(Hildebrandt, 1970) Although scientifically sound and good information, this work is focused on blunt lung injury and will therefore not fixate on more pressure-based characterizations that would matter more for the blast injury mechanisms than the blunt.

Astoundingly, there is little information on small component lung testing in shear despite the proposition that shear is the main injury mechanism in blunt injury. The closest experiment to shear lung testing comes in the form of a derivative of the Split Hopkinson Pressure Bar, called the Kolsky bar technique, which is a form of both shear and compression testing. Simply, a sample is placed between two bars, and one of the bars is struck; pulses are captured from either end which can be used to calculate material properties. This testing configuration was originally designed for harder materials such as metals, but has since been configured for softer biological materials. Whether the testing is valid for biological tissues has not been proven, but PMHS lung material has been tested in such a manner.(Saraf et al., 2007) The usefulness of the results are in question, though, as the strain rates for these tests are much higher than any lung tissue will experience within the human body in blunt loading, and even higher than can be experienced in blast loading (strain rates of up to 7700/s were tested).(Bass et al., 2008; Saraf et al., 2007) So in the determination of parameters for blunt thoracic impacts, the material properties as reported at extremely high strain rates are not relevant. There are no other shear studies within the literature that can be applied to blunt lung injury. This is an obvious gap within the field of thoracic blunt trauma, and further studies into small sample shearing of lung need to be performed. For testing in compression, there is a study performed by Weed et al. that proves the isotropic behavior of porcine lung tissue, and, the testing was performed within the boundary of blunt impact conditions. These tests on porcine lung parenchyma in different orientations involved a small sample's compression between two platens, which resulted in stress-strain curves.(Weed et al., 2015)

While data is sparse for testing in shear and compression, that is not the case for testing in tension which forms the backbone of mechanical knowledge on lung. Many of the earlier testing used canine as a surrogate, resulting in various stress-strain curves and moduli.(Hoppin et al., 1975; Vawter et al., 1978; West & Matthews, 1972) From these tests comes on of the most applied set of lung material properties, the study done by Vawter et al. on fresh canine lung in uniaxial and biaxial tension configurations.(Vawter et al., 1978) Vawter et al.'s canine lung testing has been the basis for the most widely used constitutive and finite element models for the human body, despite canine lung being disproved as a 1:1 surrogate for human lung material properties. Zeng et al. performs matched testing to Vawter et al.'s canine experimentation using previously frozen PMHS.(Vawter et al., 1978; Zeng et al., 1987) Zeng et al. concludes that there are three major differences separating canine lung from PMHS lung: for the same stress, canine lung stretches more; for the same stretch ratio, PMHS develops more stress; and the model-fitting constant determining overall stress is three times smaller for canine. This reportedly shows that PMHS lung is noticeably stiffer than canine lung, indicating that canine lung material properties should

not be used as a direct representation of human lung properties.(Zeng et al., 1987) However, this conclusion is dependent upon the assumption that previously frozen lung tissue is comparable to fresh lung tissue, which has not been directly tested within literature. During the freezing and thawing process of lung, ice crystallization could have an effect on the micro-structure and elasticity. Therefore, the possibility of material property changes should be properly noted and considered for studies in which previously frozen tissues are used.

There are only two other instances of small component lung testing using PMHS. The first consists of uniaxial tension testing of fresh PMHS tissue to compare populations with chronic lung diseases (e.g. tuberculosis, emphysema, cancer, etc.). Usable data for mechanical modeling purposes comes from the controls for the study, which consist of specimens without any known factors affecting the lungs.(Sugihara et al., 1971) The final use of PMHS in material testing comes from Gao et al. and is biaxial tension tests resulting in stress/strain curves. The limitations of this study lie in the strain rates being relatively low for use in blunt trauma, and 2 out of the 7 PMHS had a cause of death from pulmonary issues.(Gao et al., 2006) Tensile testing on rat lung, while not directly comparable to human lung, determined definitively that lung cannot be considered incompressible.(Bel-Brunon et al., 2014; Rausch et al., 2011) The remaining tension experimentation in the literature that can be used directly for blunt impacts consists of reported quasi-static and step-hold tensile loading of canine lung, however the origin of this reported data was too vague to be discerned.(Suki & Bates, 2011)

The largest gap in biomechanical lung literature is the low amount of small component testing on any kind of lung parenchyma. Shear testing, which seems to be the most evident injury mechanism in blunt lung trauma, is noticeably absent. Further, the absence of different rates of testing such as quasi-static or any strain rate above 0.1 m/s that is not from a Kolsky setup, is very evident. These types of testing should be used as a basis for mathematical modeling and further exploration into computational modeling, yet this database is not large or diverse enough to conclude anything about the behavior of human lung under blunt loading. Another problem is the various surrogates and their unknown connection to human. PMHS can be considered a 1:1 surrogate for human lung, but the number of results available for PMHS is small. It should also be noted that when using PMHS as a live human surrogate there are many qualities that are present in vivo that cannot be directly replicated in vitro in a laboratory setting. Specifically, without proper attachment to vasculature and the rest of the respiratory system, fluid flow and in vivo pressures within the lung are difficult to replicate. There may also be issues with premortem fluid inhalation, along with the clotting of blood within vasculature and some alveolar structures, limiting the amount of flow at a micro-scale. Nonetheless, any knowledge of material

properties that can be improved using PMHS samples can be used as a starting point for future computational modeling and would be an improvement on preexisting computational models. Small sample PMHS lung tissue can be viewed as an 'equilibrium' pressure within the lung: neither inflated or deflated but rather the resting position of the structure itself. This state in particular is a good starting point for determining lung properties and future studies can use equilibrium as a basis for the introduction of inflation in FE modeling. The biggest issue moving forward in the mechanical modeling of lung tissue is that there is no testing to failure. The mechanical failure threshold, in any metric, is not known for blunt impacts to lung, nor can any be gained without further testing of lung parenchyma.

2.6.1 Recommendations

A greater number of small-scale tissue sample studies on the mechanical properties of lung is needed. These studies can incorporate testing procedures already existent in the literature for use on other soft biological tissues. For instance, classical shear testing would be beneficial to be performed on lung tissue, since shearing within tissue is thought to be the leading cause of failure in blunt trauma events. Tissue appropriation should be prioritized to include fresh, never frozen, tissue samples since the differences in material properties between fresh and previously frozen lung tissue are not well known. Care should also be taken in choosing a human surrogate, whether that means assuming a 1:1 ratio such as with PMHS, or using another species and determining scaling. Aforementioned in the previous paragraph, a mechanical failure threshold for lung needs to be found. Once properly defined, mechanical failure can be addressed within material modeling and used to link to clinical PC.

2.7 SURROGATE MECHANICAL TESTING

This section refers to whole-organ testing or whole-surrogate testing, i.e. no pieces of lung are excised and/or the surrogate in its entirety is involved in experimentation. While mechanical failure thresholds of lung material cannot be gained directly, this type of experimentation is essential in determining metrics for injury or mortality threshold. For this work, mechanical failure is defined as material failure of lung tissue, while injury consists of a physiological response, e.g. respiratory distress or bleeding, which cannot be directly proven to connect with the failure of the structure of lung. These types of testing are more manageable and have lower cost when performed on small animal surrogates as opposed to large animal surrogates. In a test series of rabbits that observed how pressure and weight

changed the properties of lung, it was proposed that the maximum principal strain could be an indicator of lung trauma.(Y. C. Fung et al., 1988) Lau and Viano performed thoracic impacts on rabbits that resulted in PC and concluded that impact velocity and chest compression displacement could be indicators of injury.(Lau & Viano, 1981; Viano & Lau, 1988) The final rabbit thoracic impact testing consisted of whole excised lung subjected to a pellet gun. It was found that velocity of impact, and velocity of impact multiplied by the chest deflection were the greatest determiners of injury.(Yen et al., 1988)

Small animal surrogate mechanical testing consists entirely of rabbits and rats. In rats, impact energy has been considered a good indicator of mortality due to PC. Wang et al. found that an injury threshold for PC in rats lay somewhere between his low impact group (1.7-2.4 J) which had no PC, and his medium impact group (2.9-5.1 J) which had PC in 82% of cases. A mortality threshold was harder to determine, however, since of the 43% that died in the medium impact group, both cardiac failure and PC were present.(N. Wang et al., 2003) The threshold for mortality in rats due to PC becomes clearer when it is discovered that an impact of 2.7 J causes 33% mortality.(Raghavendran, Davidson, Helinski, et al., 2005) A threshold is always appreciated, yet impact energy as a metric is not always clear, as impacts with low velocity and high mass can have the same energy as an impact with high velocity and low mass. This is also seen in the case of an injury metric of paired velocity and chest displacement. Recalling Gayzik et al.'s rat thoracic impacts, there was Group 1 of severe impacts, Group 2 with high penetration and low velocity, Group 3 of high velocity and low penetration, and Group 4 of mild impacts. Interestingly, even though Group 3 had a lower displacement into the thorax than Group 2 it resulted in a higher force, indicating that velocity of impact may have more of an effect on PC than chest displacement.(Gayzik et al., 2011) This could be particularly true for more localized blunt impacts. Gayzik et al. goes on to conclude that strain and strain rate might be better predictors of PC in rat.(Gayzik et al., 2007, 2011)

Although insights can be gained from small animal surrogates, large animal surrogates are closer in scaling to the human body model. One of the first blunt thoracic experiments involving large animal surrogates were tests on goats for the development of the NIJ clay standard for testing body armor. The 44 mm BFD standard was decided upon based on the lack of serious injury or death in goats wearing soft body armor and shot with a .38 caliber bullet.(Hanlon & Gillich, 2012) Further testing of thoracic impacts in goats wearing soft body armor concluded the mortality findings, but found PC in 20 of 25 cases with only 6 instances of rib fracture. It was concluded that impact placement on the body was a major determiner of severity of injury.(Carroll, 1978)

A large portion of thoracic impacts to large animal surrogates with the major outcome being PC and little to no other injuries was done in the field of BABT research on porcine. There are instances of

known or possibly calculated impact conditions (e.g. body armor density, round caliber, firing distance, etc.) that reportedly resulted in PC in porcine, yet the severity of PC is not detailed.(Arborelius et al., 2004; Gryth et al., 2007; Sondén et al., 2009) These studies are useful for later validation of models, but cannot be used to define any injury or mortality thresholds. A study by Liden et al. reports impact conditions and grossly estimated area of PC, and accounts the important fact that blood was seen in both lungs at necropsy. The impacted lung was filled with blood due to PC while the contralateral lung contained blood due to aspiration.(Liden et al., 1988) This could be the reason for some discrepancies in the literature detailing single lung versus bilateral lung PC, since PC and blood aspiration are similar in appearance on imaging. Large animal surrogate testing in which the exact level of PC is known is rare.(Cui et al., 2021a; Magnan et al., 2004; Prat et al., 2010; L. Wang et al., 2013) Prat et al.'s study on porcine BABT and less-lethal kinetic weapons (LLKW) contains very pertinent information in filling the gap between known input conditions and the outcome of PC severity. Both projectile type and protection (i.e. body armor) are noted for all 30 specimens, and included is exact percentages of PC relative to total lung volume gained from methodical slices of the lung at necropsy. PC ranges from 0% to 52% of the total lung, and number of rib fracture is also denoted.(Prat et al., 2010) Another study utilizes CT imaging of impacted porcine to receive a volume of lung contused. This allows for their chosen injury metric, strain energy density, to be able to be correlated to methods of diagnosis in hospital.(Cui et al., 2021a) Similarly, Shen et al. impacts 30 specimens with one of two impact masses with a relatively constant initial velocity. CT imaging was used to determine PC volume, yet it is only reported that an average of 10% PC occurred, despite the two separate testing conditions. It is also reported that pressure in the bronchi had a 70 kPa to 100 kPa threshold for PC when modeled in a finite element model.(Shen et al., 2008b, 2012) While pressure flowing out of the lungs during impact may have relevance elsewhere, it has not been proven as the causation of blunt lung injury. Therefore, pressure in the lungs can only be considered an effect of impacts, similar to increased spinal acceleration due to thoracic impact, electrical activity seen in the brain due to thoracic impact, etc. Further, this pressure measure comes from the recreation of experimental testing, not directly measured from the testing itself, so the actual pressure within the bronchioles of the porcine is unknown. There is also the question of porcine surrogates correctly exhibiting responses characteristic of humans, and while there has not been extensive research specifically with the comparison of lung, Viano and Warner bridge the gap with thoracic impacts. In their study they performed matched testing on live porcine and PMHS for a ranging input velocity, measuring spinal and sternal accelerations, pressure in the lungs, applied thoracic force, and chest deflection. Their findings indicated

that the live porcine response matched the cadaver response, and PC was present in the porcine surrogates.(Viano & Warner, 1976)

PMHS is a difficult surrogate for testing the response of lungs. Even if perfused, postmortem clotting may prevent realistic pooling of liquid or other forms of edema within tissue, leading to false contusion or erroneous lack of contusion. Notwithstanding, experimentation on PMHS can still inform a great deal on the boundary conditions of thoracic impact and on mechanical failure of tissues rather than physiological injury. Work has been done in the field of BABT in attempt to correlate the NIJ clay standard with PMHS data to give insight into the standard's effect on the human body. Bass et al. performed BABT tests on PMHS primarily to investigate the injury risk to the sternum, but also characterized the shape of the armor BFD from such events.(Bass et al., 2006) Eaton et al. used this characterization to create a projectile that mimics the shape of the armor BFD in order to simplify boundary conditions associated with BABT events. The study involved a preliminary correlation between penetration depth in the NIJ clay standard and penetration depth within a PMHS, which could be useful insight for future correlations with soft tissue injury and specific boundary conditions.(Eaton et al., 2020) Results of these types of studies, including BFD depth and boney injury, make transitions to finite element (FE) modeling easier by taking guesswork out of the equation, especially when data such as thoracic organ pressures is matched with the NIJ clay standard.(Iwaskiw et al., 2020) The understanding gained from PHMS and paired clay testing can be further evaluated through FE models and then validated with accounts of BABT survivors,(D. Cronin et al., 2018) leading to better intuition within the mechanics of BABT events.

Another way to tie in valuable PMHS testing to the field of soft tissue injury is a method known as the viscous criterion (VC), developed by Viano and Lau, and is described as the product of velocity of deformation and chest compression.(Viano & Lau, 1988) This method of injury severity prediction has been correlated with AIS (Abbreviated Injury Score) in both cadaveric and animal experimental models.(Sturdivan et al., 2004) Although, the ability to correlate VC to AIS stems from the fact that both methods cover a wide range of area on the body, leading to multiple smaller injuries summed up into one definitive measurement. VC was investigated for its use specifically in lung response and PC through a study performed by Yuen and Cronin using previous PMHS studies and FE simulations. They found that while VC predicted a range of lung injuries, the VC method was too global in that the measures were too dependent on direction of impact and loading conditions.(K. F. Yuen & Cronin, 2010) Albeit its shortcomings, VC as an injury metric for PC remains as one of the only links between cadaveric test data and a method for predicting lung injury.(Prat, Rongieras, Sarron, et al., 2012; K. F. Yuen & Cronin, 2010) In fact, it is only rivaled by associating rib fractures in PMHS with lung contusion severity. This involves

assuming the AIS score due to rib fractures will be the same as the AIS score for the lungs during whole PMHS side-impact pendulum tests. The readings from a pressure gauge in the lungs of the PMHS during the various pendulum tests act as the indicators of contusion severity for FE analysis.(D. S. Cronin et al., 2021a; Shen et al., 2008b; Viano, 1989) There are drawbacks to this method of lung injury prediction; it has been aforementioned that severity of rib fracture does not necessarily correlate to PC. For example, a patient may have a rib/thoracic AIS of 1, but a pulmonary AIS of 3 and severe PC, while another patient may have a rib/thoracic AIS of 4 with no PC at all. This method of determining PC relies on rib injury and PC severity to be the same, which does not have to occur, leading to a possibly invalid assumption. Also, for blunt impacts, it has not yet been proven that bronchial pressures correlate to any concrete level of contusion volume, or that bronchial pressures in a FE model are the same as in a live human subject. Although, pressures have been obtained using an anthropomorphic testing device (ATD) that mimics human lung structure.(Danelson et al., 2011) Despite the assumptions, these methods of large-scale prediction of lung injury or PC remain the best option thus far. There are no strictly mechanical damage criteria for blunt lung injury within the public literature.

2.7.1 Recommendations

Understanding blood flow into injured areas of the lungs and progression of PC starting at impact should be an objective of future surrogate mechanical testing. Gaining a knowledge of PC volume progression through time can lead the way to connecting visual blood volume in the lungs with volume of structural damage. This way, a more accurate method of injury prediction in intact lungs can be achieved. In vitro studies on excised whole lungs may also be crucial to control and determine levels of ventilation at impact. Specifically, air flow during high-velocity impacts can be addressed to define pressure differences within the lungs and wave propagation.

2.8 CONSTITUTIVE MODELING

The most common way to transform experimental data into a usable model is to perform some form of constitutive modeling. There are a variety of ways that this can be achieved, and for lung, there have been different methods that have progressed through the years. One of the first strain energy density (SED) functions developed specifically for lung was done by Fung and involved a micro-scale approach, where lung tissue was not considered a continuum and instead alveolar structures were

individually modeled.(Y.-C. Fung, 1974) Micro-scale constitutive models are beneficial for modeling more physiological occurrences such as injury from gastric inhalation and minute pressure differences.(Clayton & Freed, 2020; Freed et al., 2012; Y. C. Fung, 1975; Y.-C. Fung, 1974) However, when looking at blunt impacts to the lung, a gross mass of tissue is involved, necessitating the use of macro-scale constitutive models for a continuum approximation. It was determined that Fung's original micro-scale constitutive model was not the most effective when working with a continuum approximation.(Lee & Frankus, 1975) Again, Fung was one of the first to develop a SED function to encompass the continuity of lung tissue, and the constitutive model still remains popular. Fung developed a relation for the strain energy per unit mass, W:

$$\rho_o W = \frac{1}{2} C \exp(\alpha I_1^2 + \beta I_2) \qquad\qquad (1)$$

where ρ_o is lung density, I_1 and I_2 are the strain invariants, and C, α, and β are constants.(Y. B. Fung et al., 1978; Vawter et al., 1979)   This model has been used in many cases to accurately depict the response of lung tissue in both strictly mathematical fitting and computational material models.(Gao et al., 2006; Gayzik et al., 2007; Vawter et al., 1978, 1979; Zeng et al., 1987) Within FE modeling, the material 'Lung Tissue' (*MAT_129 in LS-DYNA) consists of the Fung SED with an additional term to have a representative surface energy density,(Deng et al., 1999; Vawter, 1980) thus showing how accepted the Fung-type model is for use in lung biomechanics.

While the Fung-type SED function is prolific within the biomechanics literature, there are other constitutive methods that have produced good results in comparison to experimental data. There have been experimentation and the subsequent modeling for pressure-based studies,(Hildebrandt, 1970; West & Matthews, 1972) and while useful to the scientific community, the relevance of pressure studies to blunt injury mechanisms in the lungs have not proven to be the correct direction for material and damage analysis. However, a hyperelastic model based on the Fung-type SED function relating pressure to density may join pressure-based lung theories with methods used to evaluate blunt lung injury.(Cui et al., 2021a; Shen et al., 2008b) Other types of constitutive models for lungs have been intermittent, but include homogenous viscoelastic and homogenous isotropic linearly elastic frameworks.(Bel-Brunon et al., 2014; Grimal et al., 2004; Plank et al., 1998; Roberts et al., 2005, 2007) While easier to compute, linear models have been shown to not be the best choice for representation of lung material, seeing as lung material behaves non-linearly or quasi-linearly.(Freed et al., 2012; Freed & Einstein, 2011; Y. B. Fung et al., 1978; H.-C. K. Wang & Yang, 1995) Some of the more unique models developed specifically for lung include a hydrodynamic method and utilizing a free energy approach to constitutive modeling.(Clayton & Freed,

2020; Shen et al., 2012) Overall, it seems that the Fung-type model or variations thereof are the most predominant in the literature, but due to the relatively low number of studies of lung as opposed to other biological tissues, it is unclear if the reason lies in representation of the material or solely ease of mathematical implementation. It would be interesting to perform model fitting on experimental lung data using a variety of constitutive models designed for other materials, to see how the models fare in representing lung. This could include models currently used for other biological soft tissues, soft foams, low density rubber, and cellular foams.

2.8.1 Recommendations

A greater number of studies producing material property values for existing constitutive models of lung tissue would be beneficial. As it stands, there is variation of lung material properties within the literature, and not enough data to determine which parameters more accurately depict the kinematics of lung tissue in blunt impact scenarios. It may also be valuable to explore different material models than the ones previously discussed. Using material models that have been developed for other soft tissues may help give insight into what is missing in the mathematical modeling of lung. There is a possibility that different material models may more closely match the response of lung tissue seen experimentally.

2.9 FINITE ELEMENT ANALYSIS

A more modern approach to the characterization of lung tissue involves incorporating chosen constitutive models into a computational model for finite element analysis. FE analysis has been used extensively in the study of the thorax and pulmonary injury in order to supplement and go beyond the capabilities of PMHS and animal experimental models. Over time, these lung FE models have been developed and grown in complexity to better represent the response of the lung in impact scenarios and capture their dynamic properties.

Lung FE models were first introduced as research on lung mechanics was in its early stages. West and Matthews presented an initial study that analyzed the stresses and strain within functional alveolar tissue during inhalation and exhalation to understand how the lung is deformed under its own weight.(West & Matthews, 1972) Due to the unavailability of suitable data for lung tissue properties, values for material properties such as modulus of elasticity and Poisson's ratio were assumed or were derived from excised canine tissue and were meant to be replaced with future studies.(Vawter et al., 1978; West & Matthews, 1972) However, these values would be assumed accepted within the field and used in future work to model the human thorax.(Sundaram & Feng, 1977) Some of the most pivotal studies for lung FE models are based on studies performed by Vawter et al. and continue to build upon other previous work with lung tissue mechanics.(Vawter, 1980; Vawter et al., 1978) Utilizing the Fung-type constitutive model, Vawter et al. formulated a constitutive equation for lung tissue elasticity to develop a lung FE model to consistently apply finite elasticity and take the effects of surface tension into consideration.(Vawter, 1980) These studies presented the groundwork for future work to apply their findings to more detailed and updated human body models (HBM) that would begin to capture the dynamic properties of the lungs. Much of the newer work with thoracic and lung HBM built upon these initial works to apply the HBM to MVC,(Deng et al., 1999; H.-C. K. Wang & Yang, 1995; K. F. Yuen, 2009, p. 200) and blunt trauma due to ballistic impact.(D. S. Cronin, 2012; D. S. Cronin et al., 2021a; Roberts et al., 2005; Shen et al., 2008b) Many of these improvements have centered on updating lung geometries, introducing new material parameters in the material model, and the use of updated lung material properties from experimental material testing efforts. Tables 2.9.1 and 2.9.2 detail the Fung-type parameters used in FE modeling and material constants within literature respectively.

Table 2.9.1

Table 2.9.1 - Upper portion indicates parameter usage in SED function. Lower portion lists reported parameters within the literature, along with the surrogate used to gain parameters.

SED Function(Y. B. Fung et al., 1978; Vawter et al., 1979): $W = \frac{C}{2\Delta}\exp\left(\alpha I_1^2 + \beta I_2\right) + \frac{12C_1}{\Delta(1+C_2)}[A^{(1+C_2)} - 1]$

$$A = \frac{4}{3}(I_1 + I_2) - 1$$

				SED Function Parameters					
Study	**Surrogate**	**C**	**Δ**	**C₁/Δ (kPa)**	**α**	**β**	**C₁/Δ (Pa)**	**C₁**	**C₂**
Vawter 1980	dog			2.45	0.183	-0.291	19.3		2.71
Deng 1999	dog			2.45	0.183	-0.291	19.3		2.71
Stitzel 2005	rat	5.035e-4	0.0702		0.08227	-2.46		6.535e-6	2.876
Gayzik 2007	rat	1.187e-3	0.0702		0.4451	-3.95		1.949e-5	1.918
Gayzik 2008	rat	5.035e-4	0.0702		0.08227	-2.46		6.535e-6	2.876
Shen 2008	dog			0.592	5.85	-3.21	19.3		2.71
Yuen 2008	PMHS, dog			0.592	5.85	-3.21	19.3		2.71
Nsiampa 2013	PMHS, rat	5.035e-4	0.0702		0.08227	-2.46		6.535e-6	2.876

Table 2.9.2

Table 2.9.2 - Material parameters listed within the literature, along with the surrogate used to gain parameters. The term ρ indicates density, E Young's modulus, K bulk modulus, G0 the short term shear modulus, G∞ the long term shear modulus, and v the Poisson's ratio.

Material Parameters							
Study	Surrogate	ρ (kg/m3)	E (MPa)	K (MPa)	G_0 (MPa)	G_∞ (MPa)	v
Matthews and West 1972	dog	230					0.2-0.4
Vawter 1979	dog		0.0017				0.45
Plank 1998	dog	917	0.00172 & 0.00707	2875	7387	2.358	
Ruan 2003	dog	600		0.22	0.02	0.075	
Roberts 2005	dog	600		2880	7.39	2.36	
Kimpara 2005	dog	600	0.01				
Grimal 2004, Grimal 2005	dog	600	0.713				0.3
Stitzel 2005	rat	118		0.1124			
Gayzik 2007	rat	118		0.1384			
Gayzik 2008	rat	118		0.1124			
Shen 2008	dog	200					
Yuen 2008	PMHS, dog	200		24.5			
Nsiampa 2013	PMHS, rat	118		0.118			
Rater 2013 (a)	dog, pig	600		1112.44	0.03	0.00075	
Rater 2013 (b)	dog, pig	1000	0.1				

In the realm of automotive HBM, Wang and Yang introduced internal organs, including lungs, while updates were later made by Ruan et al. and include assumed lung parameters that were 10 times the experimental stress-strain curves produced by Vawter et al. as a result of model tuning.(Ruan et al., 2003; Vawter et al., 1979; H.-C. K. Wang & Yang, 1995) These material parameters were in turn used by Kimpara et al., but with the disclaimer that there is a lack of experimental data of soft tissues in high loading scenarios, and that the material constants chosen are somewhat arbitrary and subjective.(Kimpara et al., 2005) Yuen et al. went back to the original framework of Vawter et al. for determining lung material properties and, to account for differences in canine lung, added PMHS information to achieve different constant parameters (α and β).(Vawter, 1980; K. Yuen et al., 2008) Many studies change the exact value of the parameters through tuning the HBM for MVC,(Danelson & Stitzel, 2015; Gaewsky et al., 2017; Rater, 2013) yet the experimental basis, or lack thereof, remains the same throughout the decades.

HBM have also been used to evaluate BABT and other types of combat trauma. Just as for the automotive HBM, many studies utilize the parameters estimated by Wang and Yang, or the values from canine lung reported by Vawter et al.(Nsiampa, 2011; Raftenberg, 2003; Shen et al., 2008b; Vawter et al.,

1979; H.-C. K. Wang & Yang, 1995) Grimal et al. developed a FE model in order to simplify the interaction in BABT to three layers: a medium representing muscle, one representing bone, and the last representing lung.(Grimal et al., 2004, 2005) While a unique method, it did not gain traction due to the advancement of HBM in the automotive world. There have also been cases where the internal organs in a HBM share material parameters albeit having different geometries.(Roberts et al., 2005, 2007) This is particularly disadvantageous when looking at stiffness, since the parameters usually reflect a midpoint between lung and heart. Cui et al. took a large step in progressing the evaluation of lung response in BABT scenarios.(Cui et al., 2021a) Data obtained from live porcine subjected to projectile testing, done by Shen et al., were turned into subject specific porcine FE models.(Cui et al., 2021a; Shen et al., 2008b) This permitted matched-pair experimental testing and FE analysis, allowing for validation and a surrogate comparison to human. The most detailed HBM boundary conditions for BABT were developed by Cronin et al. and are validated with human BABT survivor cases.(D. S. Cronin et al., 2021a) The lung material model is supplemented with PMHS experimental data, adding accuracy to the HBM response.(D. S. Cronin et al., 2021a; Gao et al., 2006; Zeng et al., 1987) Cronin et al. also uses a dynamic FE projectile, so that the impact onto the HBM precisely represents the changing profile of the BFD of armor through time. This dynamic projectile was also compared to a sphere of similar diameter and it was found that the HBM resultant forces did not have statistical difference. Matched-pair testing was performed between the FE HBM and BABT survivor cases, thus taking a huge step in validating any FE model for BABT conditions.(D. S. Cronin et al., 2021a) While current lung models have their applications, most HBM are only validated as part of an entire thoracic HBM using whole body kinematics from automotive impact tests. The future of FE modeling of lung material properties lies in the advancement of material parameters through use of case-specific experimental data, and there should be a push against the continued use of parameters without an origin in mechanical testing.

In addition to HBM, animal FE models have also been utilized in the literature to study blunt thoracic impact. As discussed previously, experimental animal models are useful due to their ability to be tested in vivo with larger sample sizes that cannot be replicated with post-mortem human tissue. This also allows for more robust FE model generation due to the ability to validate models across a range of loading conditions. Some studies have utilized these methods to study strain-based injury metrics for pulmonary contusion in a rat model. Sitzel et al. developed a detailed rat lung model based on segmented CT scans, with a final mesh consisting of both lungs, heart, mediastinum, trachea, and a sheath to represent the chest wall and diaphragm.(Stitzel et al., 2005) Like previous models, their lung material model utilized the strain energy function presented by Vawter et al., and used optimization techniques to adjust material

parameters.(Stitzel et al., 2005; Vawter, 1980) Their results were validated with results from in vivo rat lung impacts.(Stitzel et al., 2005) Gayzik et al. continued this research by validating the rat model developed by Stitzel et al. through in vivo lung impacts in rats at varying velocities.(Gayzik et al., 2007, 2011; Stitzel et al., 2005) This led to a recommended FE injury metric for PC based on the volume of contusion and first principal strain.(Gayzik et al., 2011) While these models are useful, they do have their limitations. It is unknown how animal-based injury metrics scale from animal models to human models. Additionally, these models are only validated at low-rate loading conditions that are much slower than those experienced in MVC or BABT. However, these animal models can be a useful tool for researchers to better understand the injury mechanisms of PC in other species, which can be used to better understand PC in humans.

Assumed lung parameters are still in use, even though they may be arbitrary, because those parameters are known to make the FE model "run well," meaning that the model runs to completion without an excess of errors. The danger, however, lies in a well-running model that does not represent the actual material, so readily achieved results may not be in any form correct. Here is also where the lack of mechanical failure data from small component testing is pronounced. No experimental damage thresholds for lung in blunt impact scenarios means a FE model cannot accurately predict damage. Many damage thresholds have been suggested based on good correlation with field data and FE results including pressure,(Bush & Challener, 1988; Shen et al., 2008b; K. Yuen et al., 2008) strain,(Gaewsky et al., 2017; Gayzik et al., 2011; Stitzel et al., 2005; K. Yuen et al., 2008; K. F. Yuen & Cronin, 2010) strain rate,(Gayzik et al., 2011; K. Yuen et al., 2008; K. F. Yuen & Cronin, 2010) the product of strain and strain rate,(Gayzik et al., 2007; K. Yuen et al., 2008) principal stress,(Roberts et al., 2007) SED,(Cui et al., 2021a; Shen et al., 2012) and assumed injury level based on AIS of rib fractures.(D. S. Cronin et al., 2021a; H.-C. K. Wang & Yang, 1995; K. F. Yuen & Cronin, 2010) These injury metrics for lung in blunt impact are some of the best possible interpretations and connections that can be made within the current literature. However, the need for future addition of mechanical damage data of a human surrogate is plain. For the advancement of lung injury prediction for the most common lung injuries, structural lung damage must be evaluated.

2.9.1 Recommendations

Likewise to the recommendations in the previous section, it may benefit the field to explore different material models in the representation of lung. This would be a good method of determining which material parameters may be lacking or not fully demonstrating the response of lung tissue. Problems with

material parameters may also arise from the lack of experimental studies to determine values for modeling purposes. Matching the kinematics of these experimental studies to the output of an FE model should be emphasized, rather than relying on historic parameters that have been used to model lung. Implementing a lung failure threshold into FE modeling is crucial, and should be based on mechanical failure from experimental testing of lung parenchyma. The field should aim to move away from previous lung damage thresholding as more information becomes available with the literature.

2.10 DISCUSSION ON MECHANICAL DATA

It is well recorded that PC can lead to complications and be life-threatening.(Cohn & DuBose, 2010; C. Miller et al., 2019; P. R. Miller et al., 2001) The most common cause of PC is blunt impact, motivating a closer look into a common injury mechanism. Only through the mechanical testing and mathematical and computational modeling can the material of lung be fully evaluated from a biomechanics standpoint for blunt impact trauma. Understanding how and when PC occurs within lung tissue can go towards better diagnosis and mitigation of PC and its effects, leading to lowering cases of morbidity and mortality.

For blunt lung injury, there are still many unknowns both medically and mechanically. In vivo, confined compression is not possible for the types of rates seen in most cases of blunt thoracic trauma, instigating the theory that in the cases of blunt impacts soft organs like the lungs failure is in shear from the difference in strain rates of neighboring areas of tissue.(Ganie et al., 2013; Yamamoto et al., 2005) However, actual damaged areas of lung tissue are not easy to discern since PC is defined as areas of blood or bleeding. This pooling of blood within the alveolar spaces can disguise the areas of structural damage, making a clear volume of damage almost impossible with current imaging techniques. The lack of noticeable tissue damage makes it difficult to connect with mechanical testing in that excised tissue does not bleed, so the blood volume in lungs resulting from specific stresses/strains is not well understood. Paired with the fact that there does not exist within the literature a damage threshold for any human lung surrogate in blunt impact, this becomes a real conundrum. Without that structural damage threshold, further investigation such as FE models and any HBM cannot have validated structural lung failure prediction. Further, development of appropriate lung injury criteria can help bridge the gap between clinical injury and biomechanical injury. The future of blunt lung research lies in the correlation of clinical data and mechanical testing to achieve a FE model that accurately represents lung parenchyma and can be used as a tool for diagnosis and mitigation.

That is not to say, however, that there has not been much needed advances in the experimental testing of lung tissue for blunt-type loading. While blast lung studies paved the way for interest into lung injury, the high rates of strain and deformation are not applicable to the more commonly occurring blunt thoracic trauma.(Bass et al., 2008; Bowen et al., 1968) This inspired a number of studies to populate the literature with small-sample mechanical testing.   The great majority of these studies tested lung in tension,(Bel-Brunon et al., 2014; Gao et al., 2006; Rausch et al., 2011; Sugihara et al., 1971; Vawter et al., 1978; Zeng et al., 1987) which is appropriate for determining FE material properties. Of the many tensile studies, data comes in the form of cyclic testing, stress relaxation, a look into hysteresis, and includes uniaxial, biaxial, and triaxial configurations.(Hoppin et al., 1975; Sugihara et al., 1971; Suki & Bates, 2011; Vawter et al., 1978) The only compression study determined that lung tissue, as a continuum, is isotropic.(Weed et al., 2015) Even though tests in tension are the preferred testing setup for later FE analysis, other types of testing are necessary to represent the entire scope of lung tissue responses. Two separate testing mechanisms are needed for material validation, and for that the literature is sparse. The addition of shear testing may be a good choice considering it is the mechanism of injury in blunt impact, but other testing such as macroscopic indentation and unconfined compression could be equally valuable, especially as a separate validation to lung FE models. Also, a wider range of testing rates (strain, velocity, etc.) is severely lacking. Most small-component lung tissue testing occurs at a strain rate too low to be directly compared with impacts such as MVC. Blast-type testing has strain rates too high for blunt impacts, so there exists a large gap of rates in which the response of lung tissue is unknown. There is likewise no quasi-static testing from which a basis of material parameters can be achieved. Another consideration is the type of surrogate used for these experimental tests as well as the subsequent modeling. Most FE lung parameters are from studies done using canine lung tissue,(Vawter, 1980) even though it has been determined that canine cannot be used as a direct surrogate for human.(Zeng et al., 1987) This creates another knowledge gap between clinical testing since the majority of those types of tests are performed with porcine surrogates.(Arborelius et al., 2004; Prat, Rongieras, de Freminville, et al., 2012; Sondén et al., 2009) What is needed is more systematic lung tissue testing using a variety of rates and methods on a fresh human surrogate, preferably one that can be directly compared with human lung function.

While FE HBM as a whole have been progressing with both better organ/part geometries and more advanced materials, the material properties incorporated for the lungs have been noticeably stagnant. This can in part be attributed to the lack in volume of easily convertible small-component material testing. However, the other part is attributed to the 'tuning' of FE lung models resulting in parameters that are arbitrary and not significant in order to have a smoothly running model.(Kimpara et

al., 2005) These parameters have been used time and again due to the stability they sustain, but as a result the FE lung does not behave like an in vivo lung. A push has been made to incorporate more experimental testing from appropriate surrogates and resultant constitutive models.(D. S. Cronin et al., 2021a; Cui et al., 2021a; Shen et al., 2008b; K. Yuen et al., 2008; K. F. Yuen & Cronin, 2010) This trend should continue in conjunction with relevant material testing. Eventually, the possibility of connecting FE analysis of lung injury metrics with a clinical timeline of function deterioration due to lung damage should be explored.

2.11 CONCLUSIONS

Over the years, great strides have been made in characterizing a tissue that is difficult to model. Many breakthroughs and properties of lung tissue have been attained, and a better understanding of lung injury mechanisms have been accomplished. In order to fill in the gaps of knowledge and answer the questions of the unknowns, future work is a necessity. From the review of literature related to blunt lung injury biomechanics, various holes to be filled have been identified within the length of this current work. The most important future work to be done includes a better understanding of the clinical timeline of PC, better evaluation techniques of clinical injury, small-component lung tissue testing in a variety of rates and methods, whole lung testing using a human surrogate that does not requiring scaling or for which scaling is known, FE material models that are derived directly from constitutive modeling of experimental lung data, and finally, a structural damage threshold for blunt impacts to lung. Additionally, with the completion of future mechanical testing on a range of surrogates, scaling mechanisms need to be developed and analyzed for proficiency in using surrogate models to represent human lung. All of this future work can accumulate into a FE tool to be used to span the differences in identification, prediction, and mitigation of blunt induced PC and other lung injury resultants between the clinical entity and a biomechanical standpoint. The path forward includes further exploration into aspects pertaining to blunt lung injury. Specifically, recommendations are listed with reference to the topics of this work:

Section 2.1: Anatomy and Injury Blunt lung injury leading to PC needs to be more clearly defined to relate both clinical diagnosis and mechanical occurrence. Clinically, PC seems to be referring to gross failure within the lung, but that gross failure is caused by smaller tears within the micro-structure of the lung. More research is needed to determine at what point small mechanical failure leads to PC diagnosis via

imaging. Specifically, how to define PC so that it may be relevant for deducing a mechanical failure threshold requires examination.

Section 2.2: Causes of Blunt Thoracic Trauma In automotive PC, wider ranges of consideration should be explored in cumulative studies through databases such as CIREN. Other databases such as the National Automotive Sampling System should be consulted, because specific mechanisms of PC may be absent from certain databases. Exploring a number of databases may give more information surrounding PC occurrence that can be examined for insight into injury mechanism. The relation between blunt injury mechanisms and pressure-based injury should also be investigated to gain better insight into the effect of wave propagation in development of PC.

Section 2.3: Retrospective Studies The significance, if any, between age, number of rib fracture, and PC should be fully explored. If found, significance may lead to one of the factors acting as a predictor for PC and aid clinicians in diagnosis. It may also help in lessening the amount of missed or underdiagnosed PC that is thought to occur in younger populations. Further, research should look into the differences in diagnostic practices between age populations, specifically pediatric and elderly. Care should be taken when evaluating the effect of comorbidities on presence and severity of PC.

Section 2.4: Animal Surrogates and Experimental Testing More testing needs to be performed on live large animal surrogates. For BABT large animal testing, data should be recorded for a longer period than two hours to investigate evolving PC and subsequent vital readings. Other, non-BABT studies on blunt lung injury should be performed on large animal surrogates to examine different blunt mechanisms besides a localized high-energy impact. For all animal surrogate testing, care should be taken to thoroughly outline resulting PC volume and the diagnostic technique.

Section 2.6: Small-Component Mechanical Testing More lung parenchyma testing is needed using methods and techniques already developed and used in the testing of other types of organs. Specifically, classical shear testing may be of great benefit due to the theorized mechanism of PC defined as shearing within the lung. Through further research recommended in Section I above, small-component failure

testing needs to be addressed. Once a physical failure mechanism for blunt PC is defined, this definition should be put to use to develop a failure threshold. This would combine clinical injury with mechanical failure to be used later in computational models to predict PC.

Section 2.7: Surrogate Mechanical Testing The field would benefit from research studies on large animal surrogates investigating blood flow into the lungs throughout impact and the development of PC. Gaining an understanding of the progression of blood volume in the lungs through time is crucial. Studies on excised, whole lungs could also be used to determine the relation between structural response and levels of ventilation at impact.

Section 2.8: Constitutive Modeling More investigation into the material property values used to propagate constitutive models is needed: more specifically, a better consensus on magnitude of various parameters. A wider variety of material models should be considered for use in the representation of lung since only a small number of constitutive models has been explored.

Section 2.9: Finite Element Analysis In regards to the recommendation in Section VIII, better care should be taken in choosing a realistic material model for the representation of lung tissue. There should also be a push to involve more experimental studies on lung parenchyma when determining parameters for FE modeling. Focus should be towards the matching of the kinematics in experimental studies, and FE modeling should move away from the assumed parameters for lung. Failure thresholds in FE models should be based on future experimental testing to failure. Previously used thresholds based on rib fracture or similar should be phased out as soon as more information on PC is available.

CHAPTER 3: Small Sample Testing of Porcine Lung Parenchyma

The development of a validated material model for lung begins with lung tissue testing in order to inform the parameters of the model with experimental data. This is the first crucial step towards being able to model lung response in a BABT event.

3.1 MOTIVATION

As per Chapter 2, one of the biggest gaps in the literature with reference to the biomechanics of lung is the distinct lack of experimental small-scale testing data. Blunt injuries to the lung are characterized by high energy impact events without penetration, usually in the form of high velocity impacts that result in quick acceleration or deceleration to the thorax. (Ganie et al., 2013; Yamamoto et al., 2005) In these events, lung tissue failure is due to the tearing of the alveolar structures in shear. When the thorax is compressed, due to the quick accelerations within the lung, alveolar structures are ripped from places of higher density. (D. L. Miller & Mansour, 2007; Wagner et al., 1988; Yamamoto et al., 2005) The shearing of lung tissue due to the compression of the thoracic wall is the leading cause for injurious PC.(D. L. Miller & Mansour, 2007) It follows that a material model for lung that accurately represents the deformation in blunt trauma should have an experimental basis in simple shear (quasi-static shearing), at-rate shear (comparable to biaxial tension), and a validation procedure in a compressive form (macroscopic cylindrical indentation which causes localized shearing in the compressed portions of tissue).

To have an accurate lung material model based in appropriate mechanical properties, experimental testing on a relevant surrogate must be performed as a basis for material modeling. The porcine surrogate was chosen for this study based upon its structural similarity to human lung, (Judge et al., 2014; Rater, 2013; Tenney & Remmers, 1963; Weed et al., 2015) along with the ability to be later paired with physiological results from live-pig testing. (Drobin et al., 2007; Gryth et al., 2007; Rocksén et al., 2012) Further, the porcine lung surrogate is directly comparable to human in terms of overall organ size and mass (see Appx. A.1), making it a better basis for the modeling of human lung than all small mammal surrogates. (Eaton et al., 2022)

Included within this section is a preliminary comparison between the material response of human and porcine lung parenchyma which precludes the assumption that porcine lung can be investigated as a surrogate for human lung without the need for scaling. This is imperative to cost-effective testing methods and availability of testing material. The rest of this work will assume a 1:1 scaling of human to pig lung in the investigation of pulmonary contusion in behind armor blunt trauma.

3.2 METHODS

3.2.1 Material preparation

Fresh porcine lung was acquired ~1 hour after sacrifice from a meat processor (T&E Meats, Harrisonburg, VA). Within this chapter, *samples* will refer to pieces taken from the whole lung organ, and *specimens* will refer to the animal as a whole, e.g. many samples can come from one specimen's lung. Once procured, the lungs were separated, weighed, and prepared for testing (Figure 3.2.1.1a). All

Figure 3.2.1.1

Fig. 3.2.1.1 – a.) is an image of the whole lung for specimen P008 with left and right lungs indicated by L and R respectively. b.) is the extraction location of the right shear samples. c.) is an image of the shear and indentation samples taken from P008.

specimens were tested within 24 hours after sacrifice, and if a specimen was not tested immediately (1-2 hour time window after procurement), the specimen was stored in a cooler to inhibit cellular degradation. For this small sample testing of porcine lung tissue, samples were taken from within the lobes of the whole specimen, avoiding the outer membrane of the organ as well as any large vasculature or bronchiole (Figure 3.2.1.1b). Care was taken to evenly distribute sample location between left and right lungs. Small sample testing of lung tissue was carried out in both shear and indentation testing, so both types of samples were taken from the specimens. The shear samples were rectangular in nature while the indentation samples were cylindrical. Average dimensions of the shear samples were approximately 7x7x7mm (± 0.733mm), and the indentation samples exceeded minimum values of 7mm for thickness and 31mm for diameter so that with a 6.36mm indenter the infinite half-plane assumptions were maintained. Individual sample dimensions can be found in Appx. A.1. After excising the samples and before experimental testing, the samples were kept in an environment mimicking in vivo moisture levels via a misted saline solution. All samples were tested within two hours of being excised from the whole lung (Figure 3.2.1.1c).

3.2.2 Shear and indentation test setup

Three different testing mechanisms were employed: quasi-static shear, step-hold shear, and step-hold indentation. All sample testing was done using a displacement driven bench-top test machine (ElectroForce® 3100, Bose Corporation – ElectroForce, Eden Prairie, MN) along with a 1000 g load cell.

Figure 3.2.2.1
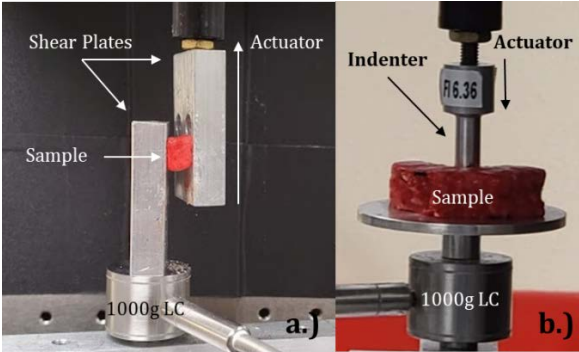
Fig. 3.2.2.1 – a.) depicts the shear setup with the sample in between two shearing plates, one connected to the actuator and the other the load cell (LC). b.) depicts the indentation setup with the sample on a plate connect to the LC and the indenter attached to the actuator.

The shear setup consisted of two aluminum shearing plates aligned vertically, one connected to the load cell and the other to the test machine's actuator. For the shear testing, samples were fixed rigidly to the shearing plates using a thin layer of glue (Loctite®, Henkel Corporation) so that the thickness is the span between the shearing plates (Figure 3.2.2.1a). The indentation samples were placed on an aluminum plate connected to the load cell and uniaxially compressed with a cylindrical indenter (6.36mm) (Figure 3.2.2.1b).

3.2.3 Testing speculations

Quasi-static shear testing was performed at 0.05 mm/s for 220s, and step-hold shear testing was performed by shearing at 1 m/s to 45° then holding the strain level for 30s. These testing procedures resulted in force and displacement time histories that were later used to determine Lagrangian stress and strain. Indentation step-hold testing was performed at the same rate as the shear, 1 m/s to a specific strain level and then held at the strain for 30s. The strain levels in indentation testing varied from 0.1 to 0.45, and all indentation testing was performed to be used for later model validation.

3.2.4 Statistical analysis

A linear mixed model was used to determine specimen (N) and sample (n) numbers required such that the mechanical properties gained are representative of the population. This model is described by $y = X\beta + Zu + o$, where y is the measured response, X and Z are design matrices, u is the fixed-effect vector, and o is an intercept offset. For the simplified case at hand, only random effects are considered such that β is the zero vector, o is the mean of the data, and Z is a sparse matrix that groups sample (n)

Table 3.2.4.1

	P-004	P-005	P-006	P-007	P-008	P-009	P-010	P-011	P-012	P-013	P-014	P-015	P-016	P-017	P-018	P-023	P-024
QS	X	X	X	X	X	X	X	X	X	X							
SH-S											X	X	X	X	X	X	X
SH-I											X	X	X	X	X		

Table 3.2.4.1 – Shows the specimens (first row) and the corresponding testing configurations. QS refers to quasi-static shear, SH-S to step-hold shear, and SH-I to step-hold indentation. An 'X' marks the specimens as contributing samples to the specific testing setup. All specimens were fresh porcine

by their given specimen (N).   For results comparable to the field, the 95% confidence interval must be less than 25% of the mean for that method of testing. To achieve this precision, ten fresh porcine lung specimens (*N*=10) were used for quasi-static testing (*n*=30), seven (*N*=7) were used for shear step-hold testing (*n*=21), and five (N=5) for indentation step-hold testing (n=15).   The specific specimens corresponding to the different testing configurations can be seen in Table 3.2.4.1.

3.3 RESULTS

All experimental testing was completed without reaching failure of the material, determined through the use of high speed cameras and the evaluation of data traces. After mass compensation of the load cell and test fixtures, raw data were processed with a low-pass filter of 150 Hz (frequency determined using fast Fourier transformation) to remove any noise within the data (Appx. A.1). Figure 3.3.1 shows force (N) versus time (s) plots for each of the quasi-static specimens, and Figures 3.3.2 and 3.3.3 show the force (N) versus log time (s) plots of each specimen for the step-hold testing. To achieve the specimen curves, all samples from a particular specimen were averaged together. It should be noted that for these experimental force plots, differences in sample thickness are unaccounted for, causing a false perspective on the spread of the data. Force and displacement time histories were then used to calculate Lagrangian stress and strain for future model fitting (Figures 3.3.4 and 3.3.5).

Table 3.3.1

	Material	Value	Standard Deviation
Density (g/cm³)	Fresh Porcine	0.535	± 0.07
Bulk Modulus (kPa)	Fresh Porcine	900.1	± 346.5

Table 3.3.1 – Values found experimentally, density and bulk modulus, can be found along with the subsequent standard deviations

Values gained experimentally, density (ρ) and bulk modulus (K), can be seen in Table 3.3.1. To ensure that the values achieved for ρ and K were within reasonable limits, the values were checked with the known speed of sound in lung and were found within range (experimental value of 41m/s for literature range of 25-70m/s). (Rice, 1983) Further experimental results can be found in Appx. A.1.
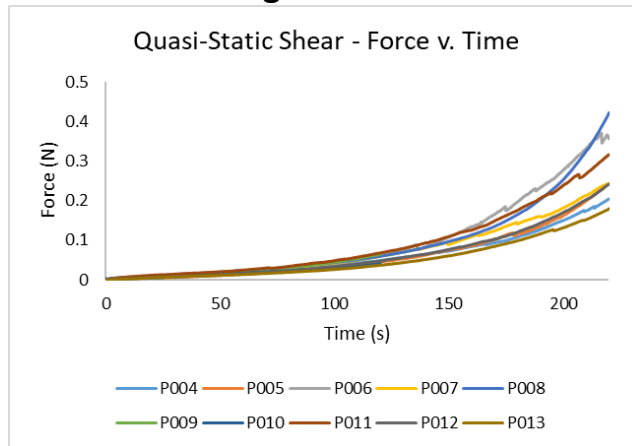
Figure 3.3.1

Fig. 3.3.1 – Depicts experimental force (N) vs. time (s) for the averaged specimen curves for the quasi-static shear testing

Figure 3.3.2
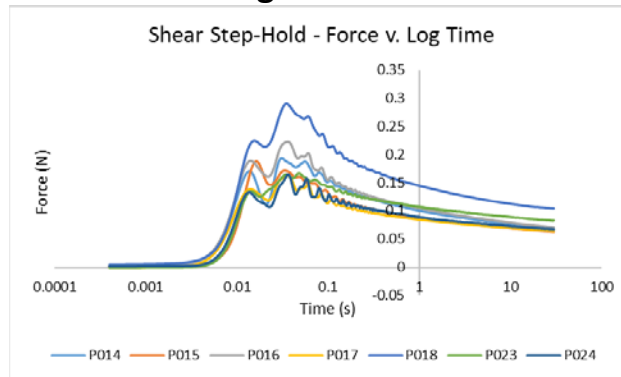
Fig. 3.3.2 – Depicts experimental force (N) vs. log time (s) for the averaged specimen curves for the shear step-hold testing

Figure 3.3.3
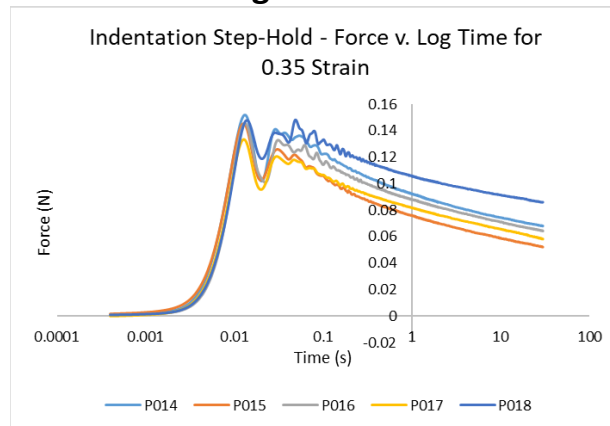
Fig. 3.3.3 – Depicts experimental force (N) vs. log time (s) for the averaged specimen curves for the indentation step-hold testing performed to 0.35 strain

Figure 3.3.4
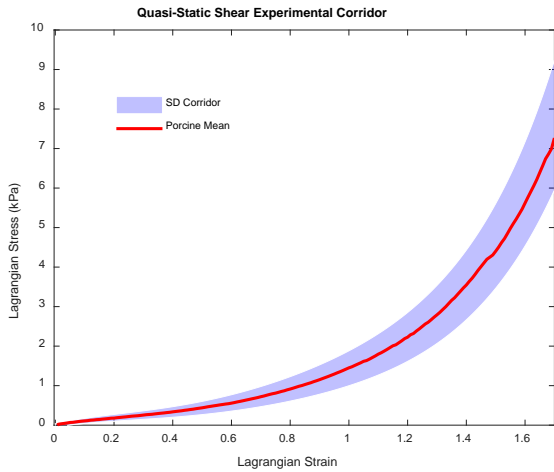
Fig. 3.3.4 – Lagrangian stress versus strain for the quasi-static shear testing. The mean of all specimens is indicated by the red line, while the standard deviation corridor is indicated by the blue shaded region

Figure 3.3.5
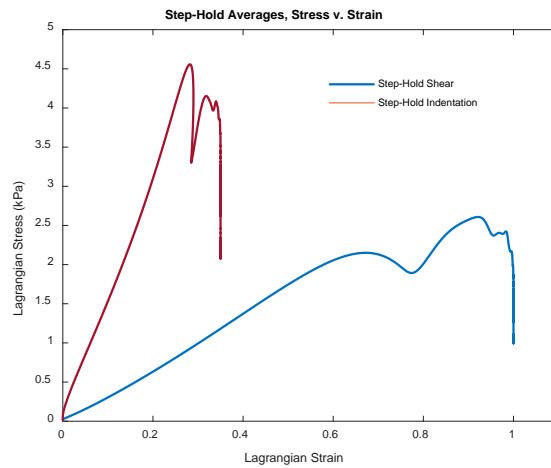
Fig. 3.3.5 – Lagrangian stress versus strain for the step-hold testing means. Shear testing is in blue, and terminates at strain = 1, indentation testing is in red, and terminates at strain = 0.35

3.4 PRELIMINARY COMPARISON TO HUMAN

Due in part to the ease of access of porcine lung specimens, there is great ambition to move from frozen PMHS to a more ideological fresh human surrogate. There is evidence in the literature that porcine lung tissue can be a direct surrogate to human.(Hozain et al., 2020) Pig is the most comparable animal to man, after bear, when observing as a whole: lung volume vs. body weight, alveolar area vs. oxygen consumption, and alveolar diameter vs. metabolic rate, (Tenney & Remmers, 1963) and porcine lung size and functional capacities are very similar. (Lum & Mitzner, 1987; Tenney & Remmers, 1963)

To give some credence to this assumption for the current research, three PMHS were tested with the same setup and methods seen in 3.2. All three, one fresh and two previously frozen, were tested in shear and indentation step-hold, and only one, a previously frozen specimen, was tested in quasi-static shear. It should be noted that the fresh PMHS had a history of smoking, which was also evident in the coloration and odor of the lungs (see Appx. A.1 for all lung images). To give comparison on the previously frozen tissue, two porcine subjects were frozen and tested as well (Table 3.4.1). For the porcine tissue, fresh lungs were acquired and then put into a freezer were they remained for two weeks. For all previously frozen tissue, the lungs were allowed to thaw in a cooler overnight, and then tested the next day when no frozen portions remained.

The outcome of this testing can be seen in Figure 3.4.1, where all of the tested specimen responses, porcine and PMHS, can be seen in log time for step-hold shear testing. Porcine curves are colored red, PMHS colored blue, fresh tissue are represented with solid lines, and frozen with dashed lines. Likewise, the result of the quasi-static shear testing on porcine can be seen with the PMHS subject curve overlaid in black (Figure 3.4.2). This plot is the same as Figure 3.3.4 with the addition of the single PMHS outcome.

Table 3.4.1

	H707	**H984**	**H1002**	**P025**	**P026**
Material	PMHS	PMHS	PMHS	Porcine	Porcine
Fresh/Frozen	Frozen	Fresh	Frozen	Frozen	Frozen
Test Method	SH-S, SH-I	SH-S, SH-I	QS, SH-S, SH-I	SH-S, SH-I	SH-S, SH-I

Table 3.4.1 – Specimens tested in addition to those in Table 3.2.4.1. In the last row, test method, QS stands for quasi-static shear, SH-S for step-hold shear, and SH-I for step-hold indentation.

Figure 3.4.1
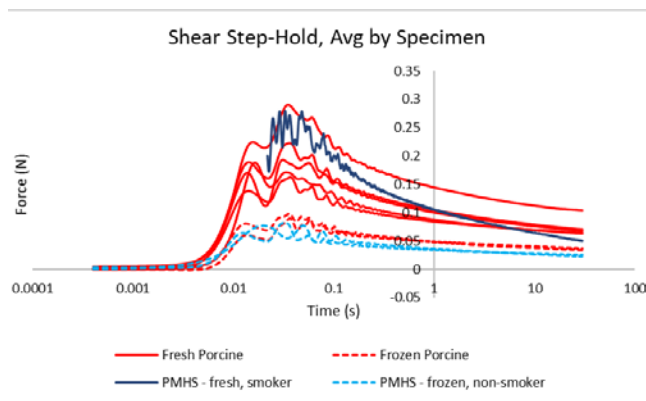
Fig. 3.4.1 – Depicts the specimen averages for step-hold shear in force (N) versus log time (s). Red indicates a porcine specimen, blue PMHS, a solid line fresh tissue, and a dashed line previously frozen tissue. The fresh PMHS does not have the ramp portion graphed due to a noise issue that was fixed in later testing.

Figure 3.4.2
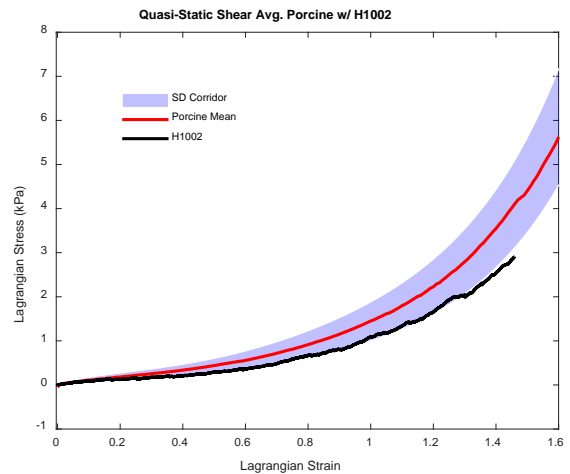
Fig. 3.4.2 – Depicts the porcine mean for quasi-static shear testing in red. The blue shaded region is the experimental standard deviation corridor. The black curve is the one PMHS specimen tested in quasi-static shear.

3.5 DISCUSSION

There only exists a small quantity of experimental lung data in literature, with most material models stemming from a single study.(Vawter et al., 1978) From the successful collection of data and the ability to replicate experimental curve responses, it can be concluded that lung can be treated mechanically as a solid organ and tested accordingly. The experimental SD corridors for the different modes of testing can be used as bases for other types of investigations into the biomechanics of lung. This is the first test series using large mammal lung, and is a crucial step in the overall characterization of lung material for representing human response. Having a material model for lung based in porcine data is a large improvement in the modelling of lung tissue.

Porcine lung is similar to human lung in most categories including alveolar size and whole lung size and mass, and is therefore the best accessible animal surrogate for lung.(Hozain et al., 2020; Judge et al., 2014) This research aids the literature in regards to using porcine as a 1:1 surrogate to human by having a preliminary comparison. As seen in Figure 3.4.1, the peak force of the fresh PMHS lies within the spread of the peak forces from the porcine specimens. The relaxation portion of the fresh PMHS does not seem in line with the porcine specimens; however, that may be caused by the history of smoking present within the tissue of the fresh PMHS. The relaxation portion of the frozen PMHS curves follows the trend of the porcine specimens, further indicating that non-smoker PMHS lung correlates to the relaxation trend seen in porcine lung. Albeit being one specimen, fresh PMHS lies within the bounds of fresh porcine for the step-hold shearing of lung tissue. The previously frozen PMHS specimens have noticeably lower peak forces than any of the fresh specimens, but are similar to the peak forces of the previously frozen porcine specimens. Again, there are only two PMHS specimens, yet these two correlate with two frozen porcine specimens. This indicates that the lower peak force may be a result of the freezing and thawing process, not a result of a different tissue type. The previously frozen nature of the PMHS tissue may also be the reason that the quasi-static results of the PMHS tested falls at the lower bound of the standard deviation corridor as seen in Figure 3.4.2. However, the PMHS quasi-static results still lie within the spread of the porcine data, making that particular specimen indistinguishable from a porcine specimen tested in the same manner.

While this does not statistically validate the consistency in mechanical properties between the two species, the results demonstrate that treating porcine lung tissue as human lung tissue is a valid assumption not yet disproven by preliminary mechanical testing. Within this dissertation, the assumption will be made that porcine lung tissue is the same as human lung tissue.

CHAPTER 4: Development of a Shear-Based Constitutive Model

To develop a validated material model for lung for use in BABT simulations, a constitutive model must be used to fit experimental data. Within this chapter, a shear-based model is derived from a chosen strain energy density function and the procedure for fitting experimental data is described.

4.1 MOTIVATION

In order to fully utilize the experimental data from Chapter 3, a constitutive model needs to be identified and applied to create a mathematical framework. It has been proposed that in all blunt trauma to the lungs (sub-blast) the main injurious mechanism is compression-caused shearing of alveolar structures. (Ganie et al., 2013; Wagner et al., 1988; Yamamoto et al., 2005) Consequently, damage in the lungs caused by BABT is the result of shearing within the lung, and thus the chosen constitutive model is based in shear.

The chosen model was the Hill Foam (Hill, 1978; Storåkers, 1986) due to its highly compressible nature and ability to represent low density foams. The Hill Foam strain energy density function will be derived for the simple shear case, in order to fit the quasi-static shear data achieved in Chapter 3. This way, the parameters for the Hill Foam model can be applied to the step-hold shear data with only the addition of quasi-linear viscoelastic (QLV) fitting. The QLV approach to fitting biological tissues allows for creep and relaxation to be included with a chosen constitutive model. With both quasi-static and step-hold shear represented by the constitutive model, the Hill Foam model for lungs can then be implemented into a finite element model and validated using the experimental step-hold indentation dataset.

4.2 DERIVATION

The Hill Foam strain energy density function (SED), W, takes the form:

$$W = \sum_{j=1}^{m} \frac{C_j}{b_j} \left[\lambda_1^{b_j} + \lambda_2^{b_j} + \lambda_3^{b_j} - 3 + \frac{1}{n} \left(J^{-nb_j} - 1 \right) \right] \tag{1}$$

where C, b, and n are material constants, λ's are the stretches, and J is the Jacobian. The case is for simple shear, so the deformation gradient, F, takes the form:

$$F = \begin{bmatrix} 1 & \dfrac{\partial x_1}{\partial X_2} & 0 \\ 0 & 1 & 0 \\ 0 & 0 & 1 \end{bmatrix}$$

2

which makes the Jacobian, J = det(F) = 1. The deformed and undeformed displacements, x_1 and X_2 are expressed in Figure 4.2.1 for the simple-shear sample. The simple shear case allows the SED to reduce to:

$$W = \sum_{j=1}^{m} \frac{C_j}{b_j} \left[\lambda_1^{b_j} + \lambda_2^{b_j} + \lambda_3^{b_j} - 3 \right]$$

3

The goal of the derivation is to find an expression for the Lagrangain stress, σ, in terms of the SED:

$$\sigma = \frac{\partial W}{\partial \varepsilon}$$

4

where the Lagrangian strain, ε, is represented by:

$$\varepsilon = \frac{\Delta x_1}{X_2}$$

5

again with reference to Figure 4.2.1. In order to relate the strain to the principal stretches, the stretch tensor, U, must be expressed to find the eigenvalues (Horgan & Murphy, 2010). The tensor, U, can be found by relation to the right Cauchy-Green deformation tensor, C:

$$U^2 = F^T F = C = \begin{bmatrix} 1 & \dfrac{\partial x_1}{\partial X_2} & 0 \\ \dfrac{\partial x_1}{\partial X_2} & \dfrac{\partial x_1}{\partial X_2}^2 + 1 & 0 \\ 0 & 0 & 1 \end{bmatrix}$$

6

In finding the eigenvalues of C in terms of the principal stretches, λ, we arrive at the equation:

$$\Rightarrow \ \lambda^4 - \lambda^2 \left(2 + \frac{\partial x_1}{\partial X_2}^2 \right) + 1 = 0$$

7

Solving for the eigenvalues produces the three possible stretches, λ_1, λ_2, and λ_3. One of the stretches, for simplicity we'll denote the third, $\lambda_3 = 1$, and since J = 1 = $\lambda_1 \lambda_2 \lambda_3$, then $\lambda_2 = 1 / \lambda_1$. In solving Eq. 7:

$$\lambda = \frac{1}{2} \left(\sqrt{\varepsilon^2 + 4} + \varepsilon \right)$$

8

where the remaining principal stretch is expressed in terms of the engineering strain, ε, through the geometry in Figure 4.2.1.

Figure 4.2.1
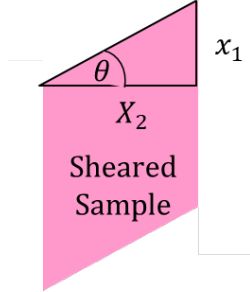
Fig. 4.2.1 – Example geometry of a sheared sample. Indicates the resulting variables for the deformed and undeformed displacements.

Since the three stretches can be expressed as a single term, λ, the SED becomes:

$$W = \sum_{j=1}^{m} \frac{C_j}{b_j}\left[\lambda^{b_j} + \lambda^{-b_j} - 2\right] \qquad 9$$

The overall goal of this derivation was to find σ, so substituting Eq. 9 into Eq. 4:

$$\sigma = \frac{\partial W}{\partial \varepsilon} = \frac{C}{b}\left[b\lambda^{b-1}\frac{\partial \lambda}{\partial \varepsilon} - b\lambda^{-b-1}\frac{\partial \lambda}{\partial \varepsilon}\right] \qquad 10$$

So therefore,

$$\sigma_i(\varepsilon) = \sum_{j=1}^{m} C_j \frac{\partial \lambda}{\partial \varepsilon}\frac{(\lambda^{2b_j} - 1)}{\lambda^{b_j+1}} \qquad 11$$

with σ in terms of ε by substituting in Eq. 8, and

$$\frac{\partial \lambda_1}{\partial \varepsilon} = \frac{1}{2}\left(1 + \frac{\varepsilon}{\sqrt{\varepsilon^2 + 4}}\right) \qquad 12$$

QED.

4.3 PARAMETER FITTING METHODOLOGY

In order to properly fit a model to the experimental lung data, the number of parameter sets (m) must be determined, a fit for the experimental mean established, and then a look into the parameter variance amongst individual specimen means. Experimental quasi-static shear data was fit to Eq. 11 and constants C and b determined by minimizing the sum squared error (SSE) between the experimental shear curves and the predicted model fitting (Excel Solver®, Microsoft®). The Lagrangian stress/strain calculations found in Chapter 3 were used for the stress and strain values in Eq. 11. To begin, the experimental quasi-static traces were used to determine fit without interference of relaxation parameters, starting by determining the overall number of C and b parameters (m) needed to fit the response. All samples were first averaged all together to attain a single mean quasi-static shear curve.

The quasi-static mean was used to determine the number of parameter sets (C,b) that were needed to represent the data. Starting with a single set (C,b), the number of parameter sets were iteratively increased until additional parameters were null valued by the optimization solver. In this manner, it was found that two sets of parameters (i.e. C_1, b_1, and C_2, b_2) were required to properly fit the lung tissue data (Figure 4.3.1), and any additional sets were null valued through optimization. For all subsequent fittings, m=2 (Eq. 11), so the model fit consists of the parameters C_1, b_1, and C_2, b_2.

Once the required number of parameter sets had been established, the quasi-static mean curve was fit to achieve the parameters necessary to fit the average experimental response by optimizing the parameter values to gain the lowest SSE between the model fit and experimental data. These parameters, seen in Table 4.3.1, are considered the best fit for quasi-static lung tissue. In order to achieve an error range on the parameters developed with the experimental mean, the traces of the individual specimens were utilized. All samples were averaged per specimen, so that each specimen had its own single experimental response. Subsequently, each averaged specimen curve was fit to attain specimen-specific C_1, b_1, and C_2, b_2 through the optimization process. The C-parameter ranges were - C_1: 7.12e-4 – 0.125 kPa; C_2: 0.157 – 0.627 kPa; and the b-parameter ranges - b_1: 6 – 12 b_2: 3 – 5, as seen in Table 4.3.1. It should be noted that parameter sets cannot be mixed and matched from different optimized sets, but must be used as a cohesive package. This is due to the nonlinearity of the b parameters.

Figure 4.3.1

a.)

b.)
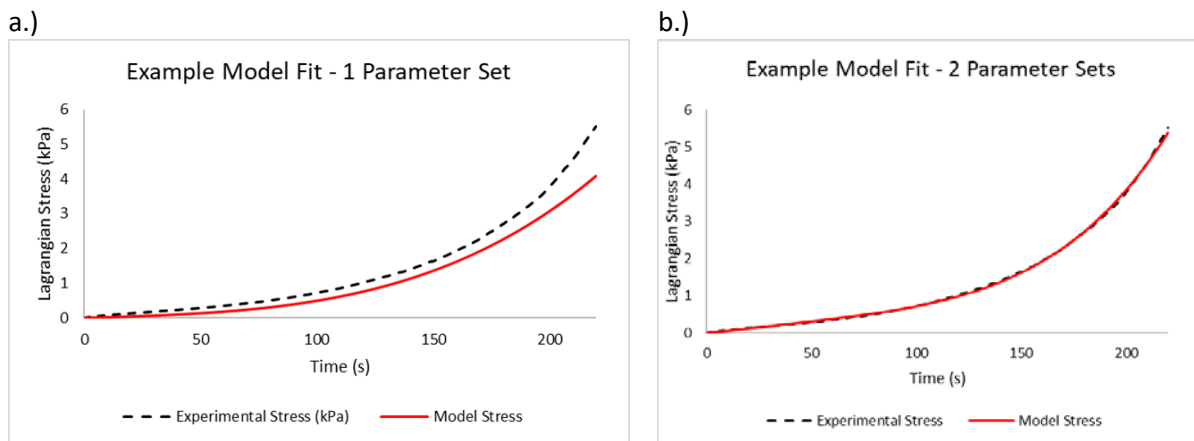
Fig. 4.3.1 – Two example plots comparing the model fit with different numbers of parameter sets. Plot a.) is an example fit of the average quasi-static data with only one set of parameters, and plot b.) is the same experimental data fit with two parameter sets. Experimental data is seen in dashed black, model fits are seen in red.

Table 4.3.1

Specimen	Plotted Results	Parameters				
Mean	Quasi-Static Shear Model Fit - Mean	C_1	b_1	C_2	b_2	SSE
		4.95e-3	10	0.357	4	1.81
P004	Quasi-Static Shear Model Fit - P004	C_1	b_1	C_2	b_2	SSE
		3.41e-3	9	0.205	3	6.38
P005	Quasi-Static Shear Model Fit - P005	C_1	b_1	C_2	b_2	SSE
		6.81e-4	12	0.157	5	11.4
P006	Quasi-Static Shear Model Fit - P006	C_1	b_1	C_2	b_2	SSE
		5.00e-3	10	0.169	5	8.17
P007	Quasi-Static Shear Model Fit - P007	C_1	b_1	C_2	b_2	SSE
		0.125	6	0.519	3	8.60
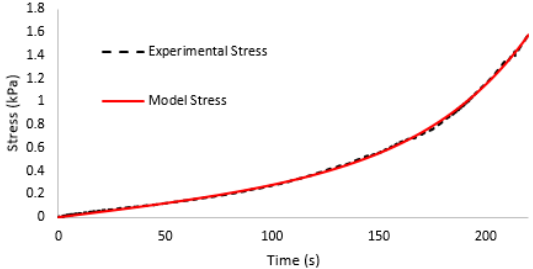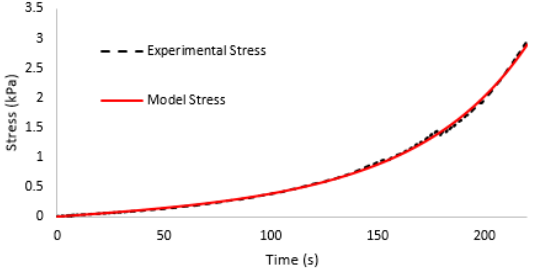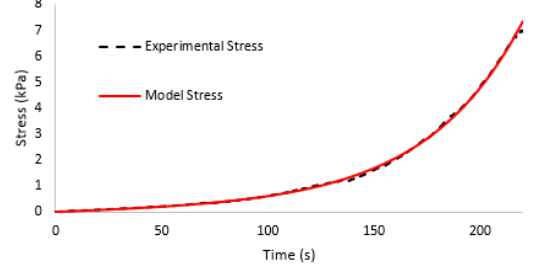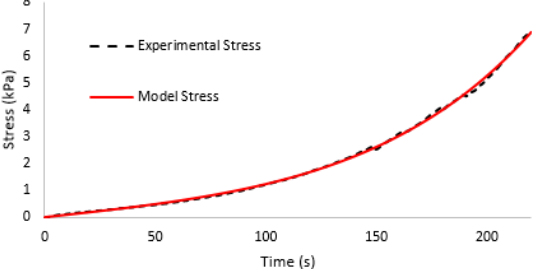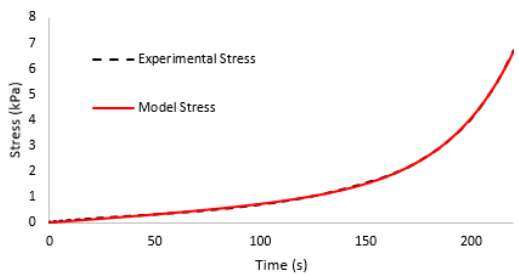
P008		C_1	b_1	C_2	b_2	SSE
		1.18e-3	12	0.522	3	2.09
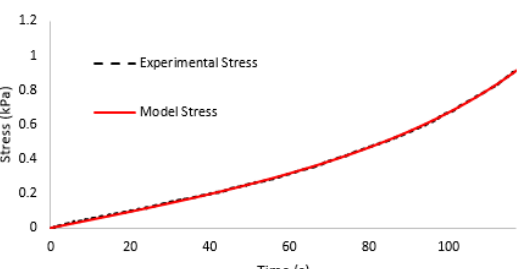
P009		C_1	b_1	C_2	b_2	SSE
		2.77e-3	12	0.309	4	1.32
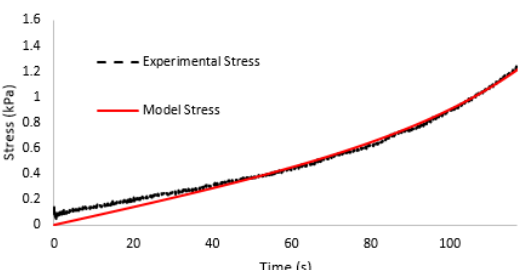
P010		C_1	b_1	C_2	b_2	SSE
		3.44e-3	12	0.587	3	72.7
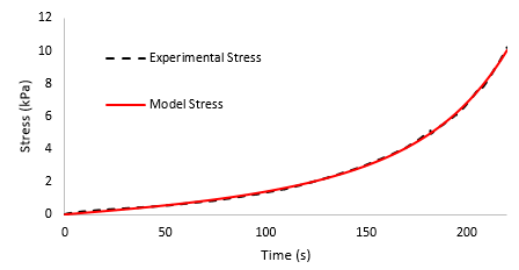
P011		C_1	b_1	C_2	b_2	SSE
		7.12e-4	12	0.627	4	5.97
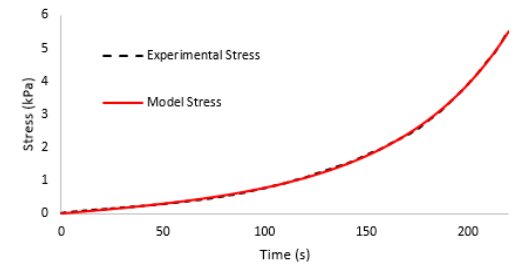
P012		C_1	b_1	C_2	b_2	SSE
		1.15e-3	12	0.318	5	2.15

Table 4.3.1 – The first column indicates individual specimens, with the first row as the mean of all specimens. The second column contains the plotted model fit (red) compared to the experimental trace (black). The third column contains the specific parameters (C's, b's) for the model fit shown with C's in kPa, and the SSE of the model fit.

59

4.4 QUASI-LINEAR VISCOELASTIC FITTING

Once the ranges for the quasi-static constants had been determined, the step-hold shear data were fitted using the quasi-linear viscoelastic (QLV) fitting method to account for the relaxation of the viscoelastic material. QLV was chosen to represent the inelasticity in the data by looking at the effect of different strains in step-hold experimentation (Figure 4.4.1). This method was modified to isolate the quasi-static response in the QLV formulation. This allows the use of the simple shear based SED function. The basic form of QLV is expressed:

$$\sigma(\varepsilon, t) = \int_0^t g(t - t') \frac{\partial \sigma_i(\varepsilon)}{\partial \varepsilon} \frac{\partial \varepsilon}{\partial t'} dt' \qquad 13$$

where t is time, t' the integration variable, σ_i the instantaneous elastic response, and g(t) the reduced relaxation function of the form

$$g(t) = g_\infty + \sum_{j=1}^z g_j e^{-t/\tau_j} \qquad 14$$

in which τ refers to the time constants. Knowing the relationship between σ_0 and σ_∞ (the quasi-static stress, Eq. 11) is

$$\sigma_\infty = g_\infty \sigma_0 \qquad 15$$

then Eq. 13 can be rewritten as

$$\sigma(\varepsilon, t) = \int_0^t g(t - \tau) \frac{1}{g_\infty} \frac{d\sigma_\infty}{d\varepsilon} \frac{d\varepsilon}{d\tau} d\tau = \int_0^t \frac{g(t - \tau)}{g_\infty} \frac{d\sigma_\infty}{d\varepsilon} \frac{d\varepsilon}{d\tau} d\tau \qquad 16$$

A modified relaxation function can be defined:

$$G(t) = \frac{g(t - \tau)}{g_\infty} = \sum_{i=1}^n \frac{g_i}{g_\infty} e^{\beta_i t} + 1 = \sum_{i=1}^n G_i e^{\beta_i t} + 1 \qquad 17$$

where the new linear coefficients of the modified relaxation function are

$$G_i = \frac{g_i}{g_\infty} \qquad 18$$

Here the modified relaxation function goes from some arbitrary value at t = 0 to 1 at t = ∞, whereas the original reduced relaxation function goes from 1 at t = 0 to some arbitrary value at t = ∞. It should also be noted that the original reduced relaxation function is normalized. The final form of the QLV function, using the quasi-static stress function and the modified relaxation function is

$$\sigma(\varepsilon, t) = \int_0^t G(t - \tau) \frac{d\sigma_\infty}{d\varepsilon} \frac{d\varepsilon}{d\tau} d\tau \qquad\qquad 19$$

which is mathematically equivalent to Eq. 13. The original reduced relaxation parameters can be solved from the modified relaxation parameters:

$$g_\infty = \frac{1}{1 + \sum_{i=1}^{n} G_i} \qquad\qquad 20$$

$$g_i = \frac{G_i}{1 + \sum_{i=1}^{n} G_i} \qquad\qquad 21$$

so that the original reduced relaxation parameters can be implemented in other models without the need for any further modification.

The QLV parameters were fitted using the step-hold data in the same manner as the initial SED fitting on the quasi-static data, by minimizing the SSE between the experimental curves and the predicted model fit. However, only one set of QLV parameters can be produced with the available experimental data – those which are based on the mean experimental curves. The modified form of QLV requires matched quasi-static parameters before fitting the relaxation parameters, but in this case, the dynamic step-hold experimental testing was performed on a different set of specimens than the quasi-static testing. The quasi-static response acts in the place of the instantaneous elastic response, so to fit individual specimens with QLV parameters, the individual quasi-static curves for those same specimens are required. The lack of matched-pair specimen testing implies that individual specimen means cannot be accurately fit with QLV parameters, but the overall mean material response can still be determined using the above methodology.

Since the data in the mean experimental curves (i.e. shear quasi-static mean and shear step-hold mean) came from different individual specimens, the linear parameters (C_1, C_2) were first re-optimized to account for the entire population while the nonlinear parameters (b_1, b_2) were left unchanged. This was achieved by setting the starting C values as the C's obtained from the quasi-static mean (Table 4.3.1) and allowing the solver to optimize only the C values while minimizing the SSE of both mean experimental curves without QLV - i.e. G(t)=0. Once the new C values were optimized, they were no longer allowed to vary, and the fitting of the QLV parameters began. Likewise to the material parameters in the SED, the number (z) of relaxation and time constant sets (G, τ) were iteratively increased to find the total set number needed to represent the data. It was found that four sets of the QLV parameters were required to express the relaxation of lung tissue (Figure 4.4.2). Within Figure 4.4.2 the model fitting can be seen when there is no QLV included for the fit of the shear step-hold data (Figure 4.4.2a), when there is just one relaxation parameter (τ=0.1) (Figure 4.4.2b), and when all four parameters are present (Figure 4.4.2c).

The parameters resulting from the re-optimization of the C's and the QLV fitting can be seen in Table 4.4.1. Included in Table 4.4.1 are both sets of reduced relaxation parameters, modified and original, where the 'original' (g's) parameters are normalized and useful for implementation into other models.

Figure 4.4.1
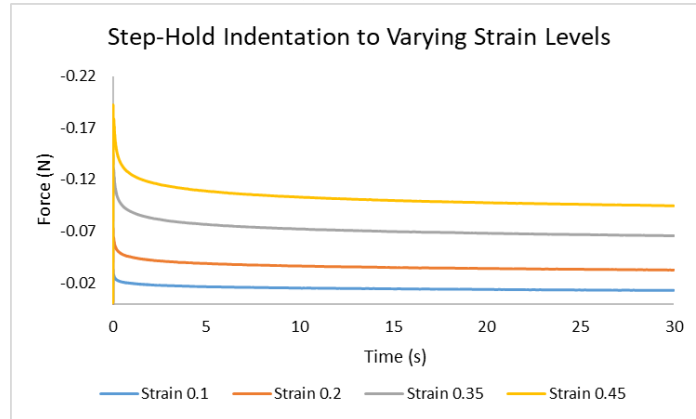
Fig. 4.4.1 – Step-hold indentation experimental testing to strain levels 0.1, 0.2, 0.35, and 0.45. The relaxation of the material is such that the normalization of these curves of varying strain result in the same relaxation trace.

Figure 4.4.2

a.)   b.)

c.)
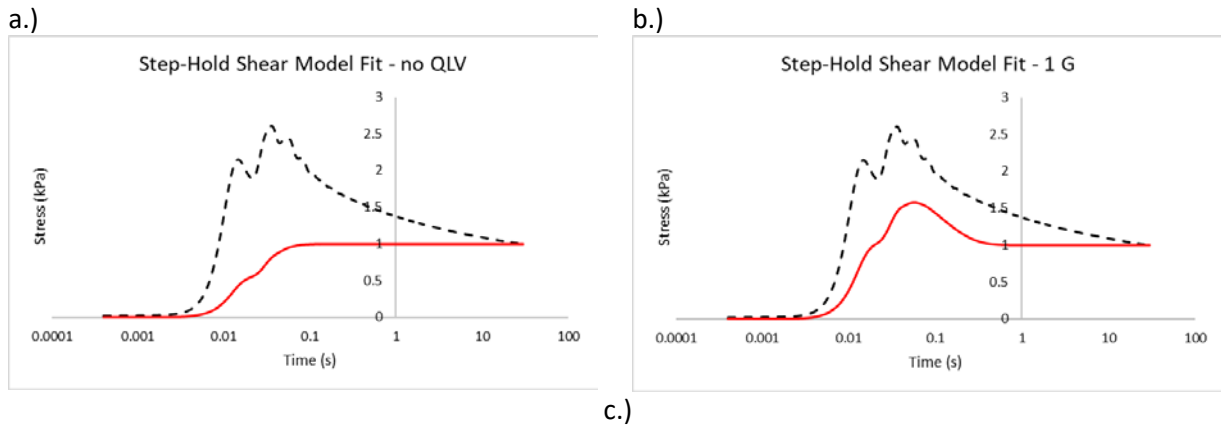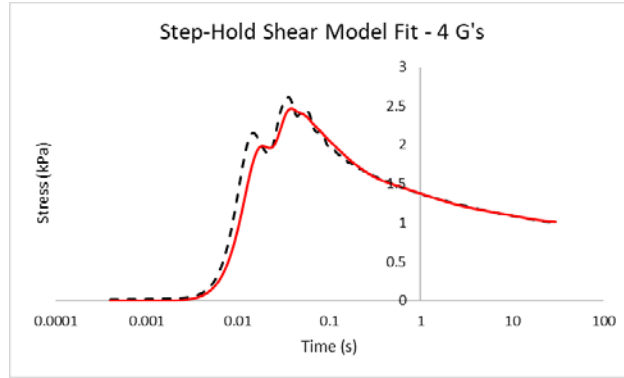
Fig. 4.4.1 – Three example plots comparing number of modified relaxation constants (G) with the QLV model fit of the experimental step-hold shear data. Plot a.) is the shear step-hold data without any QLV fitting applied. Plot b.) is fitted with only one relaxation constant (τ=0.1), while plot c.) is fitted with four. Experimental average is depicted in dashed black, and the model fit is depicted in red.

Table 4.4.1

Linear Parameters		C_1	6.94e-3	C_2	0.205
Modified Relax. Const.	G_1	G_2	G_3	G_4	
	2.5588	0.9388	0.3842	0.2595	
Original Relax. Const.	g_1	g_2	g_3	g_4	
	0.4977	0.1826	0.0747	0.0505	
Time Const. (s)	τ_1	τ_2	τ_3	τ_4	
	0.01	0.1	1	10	

Table 5.3.1 - The table gives the parameters gained through QLV fitting. The first row indicates the re-optimized C parameters in kPa. The G's are the constants from the modified reduced relaxation function, the g's the constants from the original reduced relaxation function, and the τ's are the corresponding time constants in seconds. This fit gave an R^2 of 0.998, this method of error is relevant due to the quasi-linear decline in the relaxation of the material.

4.5 DISCUSSION OF RESULTS

The goal of this Chapter was to develop a shear-based constitutive model for lung tissue, and that was achieved using the Hill Foam model derived specifically for simple shear in Section 4.2. Further, in order to fit the dynamic data of the shear step-hold experimentation, a modified form of QLV was produced to be used in conjunction with the simple shear SED function. Both of these formulations had parameters optimized to experimental shear data through the minimization of the SSE between the experimental data and model fit.

The end result of this chapter consists of values for C_1, C_2, b_1 and b_2, fitting the entire population of experimentally tested specimens, and the known G's, g's, and τ's from the QLV fitting. This fitting, as compared with the experimental data, can be seen in Figure 4.5.1. The quasi-static model fit relies on the parameters from the SED function, C_1, C_2, b_1, and b_2, (Figure 4.5.1a) and the step-hold model fit relies on

the SED function parameters as well as the QLV parameters to account for the relaxation in the material (Figure 4.5.1b). The mean fit resulted in a SSE of 550.7. Because of the discrepancy in specimens, the final mean model fit is the only set of parameters that is valid for modeling dynamic cases. This is due to the modified QLV formulation that requires quasi-static parameters from matched testing data. Therefore, there is only one set of QLV parameters and one set of optimized C and b parameters that are a result of the fitted mean experimental data.

These parameters from the model fit achieved in Chapter 4 are used in Chapter 5 through the finite element (FE) modeling of all three forms of experimental testing: quasi-static shear (simple shear), step-hold shear, and step-hold indentation. The experimental step-hold indentation data is used in conjunction with the FE reproduction as a validation, since as a separate test setup, the indentation data was not used in the production of this material model.

Figure 4.5.1

a.) | b.)
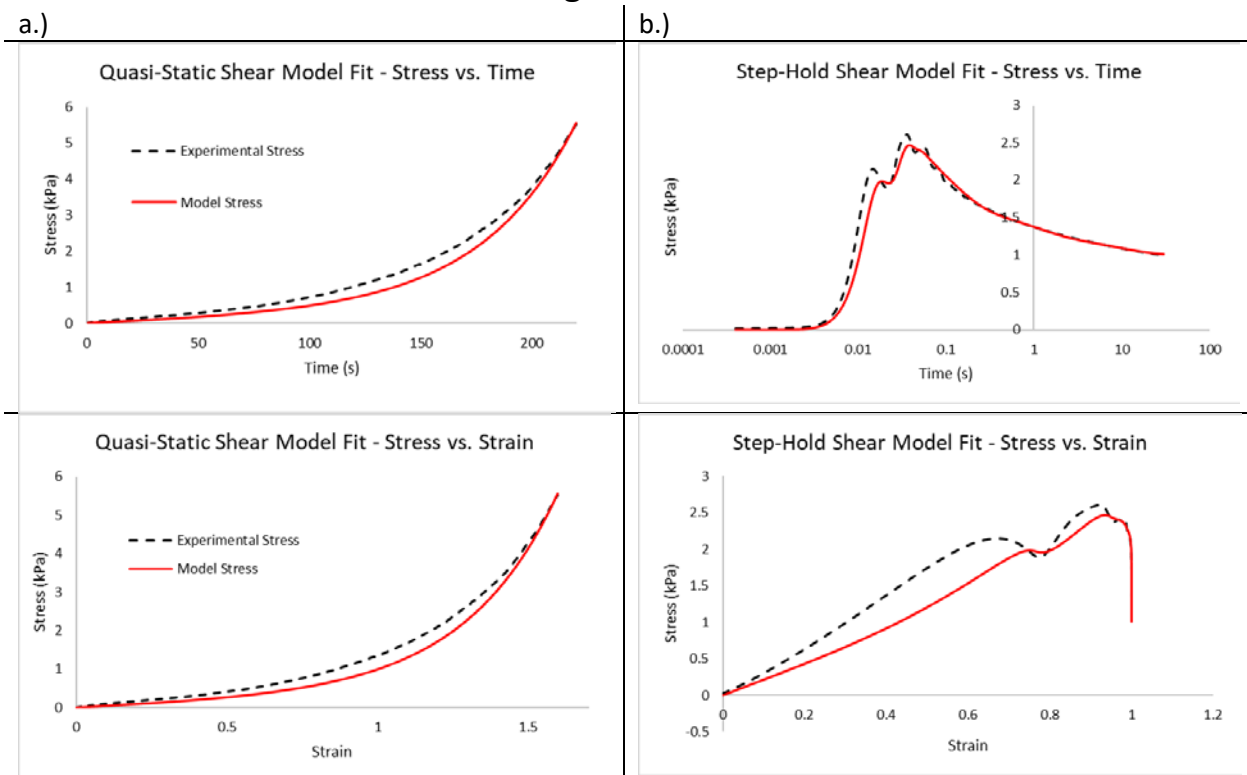
Fig. 4.5.1 – a.) plots are the quasi-static experimental mean compared to the mean model fit, while b.) plots are the step-hold experimental mean compared to the mean model fit. The first row of plots are in stress (kPa) versus time (s), and the second row are in stress (kPa) versus strain. The experimental means are indicated by black dashes, while the model fits are solid red lines.

CHAPTER 5: Development of a Finite Element Lung Material Model

The experimental data from Chapter 3 and the constitutive fitting from Chapter 4 culminate into a finite element model. The current chapter includes validation of this model, so that a validated material model for lung is achieved for later use in BABT loading scenarios.

5.1 MOTIVATION

It follows that the constitutive model developed in Chapter 4 must be implemented in a relevant computational model to fully understand and represent the material characterization of lung tissue. Consequently, this material model is implemented into a finite element (FE) model and validated with experimental data. This way, the finite element model for lung relates directly back to an experimental basis.

As discussed in Section 2.9 of Chapter 2, the experimental basis of mechanical testing for use in a FE model for lung tissue has been conceivably sporadic and varied within literature, and it should be noted that a very limited variety of testing mechanisms are represented (Table 5.1.1). There have been multiple experimental tests on blunt impacts to murine lungs and the subsequent models. (Gayzik et al., 2007, 2011; Raghavendran et al., 2005; N. Wang et al., 2003) However, there has not yet been any type of scaling configuration from, specifically, blunt-type lung data in murine to human, or for any other small mammal. Thus, we turn to large mammal animal models and other surrogate human models. Perhaps one of the most useful studies in the mechanical properties of lungs comes from Zeng et al. and their biaxial tension testing of postmortem human specimens (PMHS). (Zeng et al., 1987) The study is matched testing of the canine tension tests done by Vawter et al.,(Vawter et al., 1978) and a comparison is given between the properties of human and canine lung tissue. Zeng et al. concludes that in model fitting the constant determining overall stress level is three times smaller in canines, showing that PMHS is significantly stiffer than canine lung. (Zeng et al., 1987) Despite these findings, most constitutive models used in FE material modeling of lung have parameters based in the Vawter et al. canine lung experimentation. (Vawter, 1980; Vawter et al., 1978) Table 5.1.2 is a summary of the evolution of the lung material model for BABT with special reference to the animal model used as the experimental basis for fitting parameters. The current research uses porcine as a surrogate, since porcine lung tissue is a close large mammal match to human lung tissue. (Hozain et al., 2020; Tenney & Remmers, 1963)

This work is the first of its kind to create a material model for lung parenchyma based on a large mammal surrogate, and include different testing mechanisms. This allows for the model to fully

Table 5.1.1

Author(s)	Year	Test Type	Material
(Sugihara et al., 1971)	1971	Uniaxial Tension	Fresh Diseased PMHS
(Hoppin et al., 1975)	1975	Triaxial Tension	Frozen Dog
.(Vawter et al., 1978)	1978	Uni- & Biaxial Tension	Fresh Dog
(Zeng et al., 1987)	1987	Uni- & Biaxial Tension	Frozen PMHS
(Gao et al., 2006)	2006	Biaxial Tension	Frozen PMHS
(Saraf et al., 2007)	2007	Kolsky Bar	Frozen PMHS
(Rausch et al., 2011)	2011	Uniaxial Tension	Fresh Rat
(Suki & Bates, 2011)	2011	Uniaxial Tension	Fresh Dog
(Bel-Brunon et al., 2014)	2014	Uniaxial Tension	Fresh Rat
(Weed et al., 2015)	2015	Uniaxial Comp.	Fresh Pig

Table 5.1.1: Small-Sample Testing of Lung Parenchyma

A summary of all mechanical lung component testing and the animal/human surrogate used. 'Frozen' indicates previously frozen then thawed for testing.

Table 5.1.2

Author(s)	Year	Material Model	Experimental Basis
(Y. C. Fung, 1975)	1975	"micro-Fung"	Dog
(Sundaram & Feng, 1977)	1977	Linearly Elastic	Dog
(Y. B. Fung et al., 1978)	1978	"Fung"	Dog
(Vawter, 1980)	1980	Fung	Dog
(Zeng et al., 1987)	1987	Fung	PMHS
(H.-C. K. Wang & Yang, 1995)	1995	Low Density Foam	Dog
(Plank et al., 1994)	1998	Plank	Dog
(Roberts et al., 2005)	2005	Plank	Dog
(Stitzel et al., 2005)	2005	Fung	Rat, Rat*
(Gayzik et al., 2007)	2007	Fung	Rat, Rat*
(Roberts et al., 2007)	2007	Plank	Kolsky Bar PMHS
(Shen et al., 2008)	2008	Hyperelastic	Dog, PMHS*
(K. Yuen et al., 2008)	2008	Fung	Dog, PMHS*
(K. F. Yuen & Cronin, 2010)	2010	Fung-type	Rat, Rat*
(Gayzik et al., 2011)	2011	Fung	Rat, Rat*
(Rausch et al., 2011)	2011	Linearly Elastic	Rat
(Cronin, 2012)	2012	Fung-type	Dog, PMHS*
(Shen et al., 2012)	2012	Hydrodynamic	Dog, Pig*, PMHS*
(Rater, 2013)	2013	Low Density Foam	Dog, Pig*
(Danelson & Stitzel, 2015)	2015	Low Density Foam	Dog, CIREN*
(Gaewsky et al., 2017)	2017	Low Density Foam	Dog, CIREN*
(Clayton & Freed, 2020)	2020	Free Energy	Dog
(Cronin et al., 2021)	2021	Mat_Lung_Tissue	Dog, PMHS, PMHS*
(Cui et al., 2021)	2021	Hydrodynamic	Dog, Pig*

Table 5.1.2: Overview of Lung Material Modeling

A brief overview of lung material models and the experimental basis for the lung material properties. Not all models are represented. The '*' refers to the experimental basis for lung failure criteria, CIREN refers to the database, and PMHS* usually refers to chest compliance thresholds

encompass the response of the lung material in all blunt trauma situations while having a validated material response. This material model for lung will prove instrumental in the development of injury risk and subsequent injury mitigation for behind armor blunt trauma and other forms of thoracic trauma.

5.2 METHODS

The overarching goal within the development of a lung material model was to be able to fit the FE model to the mean experimental curves of all three forms of testing seen in Chapter 3. This was achieved by first fitting the quasi-static data in order to develop the material parameters, C_i, b_i (Chapter 4), without interference from the relaxation parameters present in the QLV framework. The FE modeling will start with the modeling of the quasi-static experimentation as well, with only the Hill Foam SED

function as the complete material model. Once the quasi-static FE model has proven to replicate the analytical solution seen in Chapter 4, the QLV portion will be added and the shear step-hold testing will be modeled using FE analysis. When the results of the shear step-hold FE model have been verified to replicate the analytical solution, the step-hold indentation testing is used as a validation of the material model. The experimental indentation step-hold testing was not used in the creation of the material model in Chapter 4, and thus serves to evaluate the use of the material model in different modes of testing.

LS-DYNA (Livermore Software Technology) was the FE solver used for all simulations. The FE model for the quasi-static shear testing consisted of a single element sample cube (7x7x7mm) with two shearing plates rigidly attached. The shearing plates were modeled as rigid bodies to closely mimic experimental setup (Figure 5.2.1a). The Hill Foam material card (*177_Mat_Hill_Foam) was used to incorporate the material parameters found in constitutive modeling (Chapter 4). The C's and b's present in the final result of Chapter 4 (4.5) were implemented unaltered into the FE model.

In a likewise manner, the shear step-hold testing was represented as a sample cube in a FE model. This sample cube was also rigidly attached to shearing plates with measurements 7x7x7mm and 30x30x30 elements (Figure 5.2.1b). Multiple elements allowed the model to behave dynamically so that the effect of the QLV fitting could be better evaluated. The values gained through QLV fitting were incorporated using the *Mat_Add_Inelasticity card in LS-DYNA. It is extremely important to note that when using this card with the modified QLV formulations presented in Chapter 4, the user must manually account for the infinite reduced relaxation parameter. This was done by dividing the linear constants of the SED function by the infinite reduced relaxation parameter (C_i/g_∞) to remain in line with the analytical fitting done in Chapter 4. This alteration, needed to utilize the *Mat_Add_Inelasticity card, is present in the *Mat_Hill_Foam material card for the dynamic testing. The hourglassing parameters were set to the same values seen in the Global Human Body Model Consortium (GHBMC) for the left and right lung for later ease of implementation of the new lung material model (Appx. A.2). The step-hold FE simulation was displacement-driven using the displacement-time experimental history of the actuator, while a force-time history was taken from the stationary shearing plate. The force-time history of the FE model is compared to that of the experimental tests to ensure it is representative of the analytical fit.

In order to validate that the shear response is representative of the whole material, the material model was also evaluated with indentation testing. A FE step-hold indentation model was created to mimic experimentation. The FE indentation sample was cylindrical with diameter 31mm and thickness 7mm. These dimensions were chosen to represent the minimum requirements of the experimental samples; i.e. the experimental samples exceeded the dimensions required so that the infinite half-plane

assumptions were maintained when paired with a 6.36mm indenter. The indentation sample was meshed so that the compression of the center did not cause geometric element abnormalities (see Figure 5.2.1c). The indenter itself was also a cylinder and was modeled as a rigid body. The sample sat on a rigid body plate with surface contact between the sample and the plate, and this rigid plate acted as the load cell for a force readout. By ensuring that the results of the FE force-time history were representative of the mean experimental indentation data, this has validated the material response of lung tissue in different modes of testing.

Figure 5.2.1
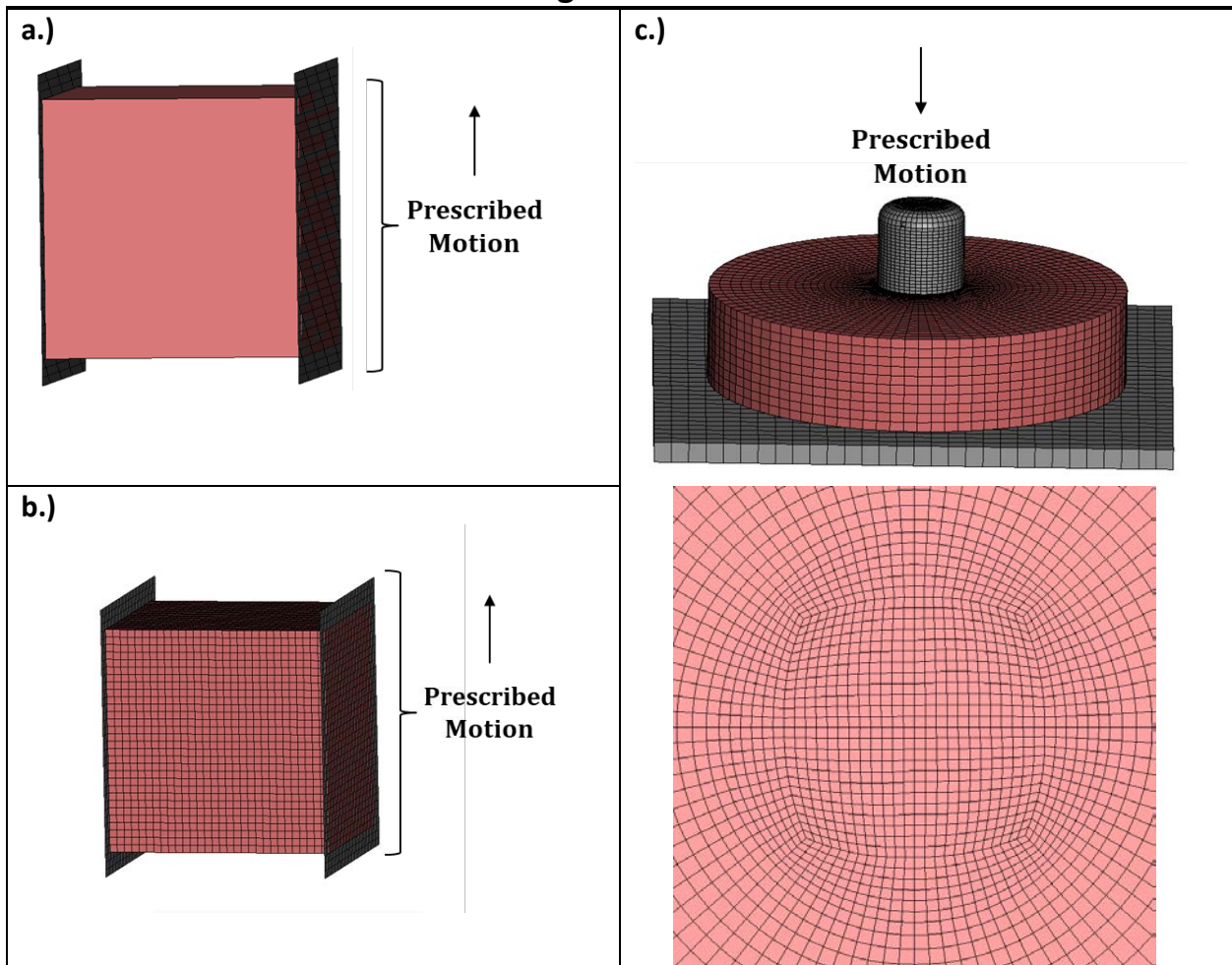
Fig 5.2.1 - Quasi-static FE model is depicted in a.) as a single element shear. Shear step-hold FE model is depicted in b.) and the indentation step-hold in c.) with a picture of the mesh on the center of the sample (top down). Pink colored parts indicate the lung sample, while gray indicates the test fixtures.

5.3 RESULTS

All FE simulations ran without errors, and visual kinematics were observed to match overall displacement and surface deformation seen in high speed video footage. The FE material model was able to run all three experimental setups and be compared to the experimental SD from the matched testing. Seen in Figure 5.3.1, the red lines represent FE model response, while the blue shaded regions are the experimental SD corridors. Also for reference, the average responses of each specimen are included in the graphs as thin black dashed lines. The quasi-static curves are plotted using engineering stress in kPa versus displacement in mm, the step-hold shear curves in engineering stress (kPa) versus time (s), and the step-hold indentation curves in force (N) versus time (s). The quasi-static FE model had parameters seen in Table 5.3.1a, while the other dynamic cases had parameters seen in Table 5.3.1b to include the QLV results.

In order to achieve the FE fits, two additional parameters needed to be determined. These additional parameters are the damping coefficient (mu) and the Poisson's ratio (n) and are part of the material model. Seen in the *FE* section of Table 5.3.2, the damping coefficient (mu) was set to 0.1 after simulations indicated that the value mu changed the whole response of the material only when mu was increased or decreased by two orders of magnitude. Therefore, a range of mu within a magnitude of 0.1 would be sufficient to model the response, and the value of 0.1 is comparable to other materials. The Poisson's ratio (n) for lung varies between values of 0.35 and 0.5. (Al-Mayah et al., 2009) A sensitivity study was done with the material by increasing n in increments of 0.5 from 0.3-0.55. It was found that the value of 0.45 allowed for the best fit within shear experimental SD (Table 5.3.2). Validation occurred in the form of implementing the material model developed using the shear data into the FE indentation model, then using the experimental SD corridor for assessment. The results can be seen in Figure 5.3.1c.

A sensitivity study was performed for the mesh size of the FE shear step-hold model. This exploration is important considering the difference in mesh between the quasi-static and shear step-hold models, and the mesh size of the lungs within the GHBMC. The material model for lung will be implemented into the GHBMC, and the average size of the elements constituting the lungs of the human body model match the size of the shear samples. To understand how the mesh size of the small-sample shear FE models contributes to overall response, the same dynamic step-hold test was performed with varying mesh sizes. The shear step-hold modeling in this chapter was performed with a mesh of 30x30x30 elements, so to test the extremes, the testing was also performed with a mesh of one element, and a mesh of 60x60x60 elements. For this sensitivity study, the dynamic parameter set as seen in Tables 5.3.1 and 5.3.2 was used for all cases. The results can be seen by the plot in Figure 5.3.2, where the dotted

lines are the experimental averaged specimen curves and the model fits are represented as solid lines. From these results, it is apparent that the mesh size of 30x30x30 elements is close to convergence, as using a fine mesh does not drastically change the output. It can also be seen that the single element case, while significantly different than the other mesh sizes, still lies well within the spread of the experimental data. Since the extreme cases of element size lie within the SD corridor, the remeshing of the lungs of the GHBMC is not suggested considering that the material model will still represent overall tissue response even in varying mesh sizes.

Table 5.3.1a

Quasi-Static	C_1	C_2	
Linear Coeff.	6.94e-3	0.205	

Table 5.3.1b

Step-Hold	C_1/g_∞	C_2/g_∞	$g_\infty = 1 - \sum g_i$	
Linear Coeff.	3.568e-2	1.054	$g_\infty = 0.1945$	
Relaxation Const.	g_1	g_2	g_3	g_4
	0.4977	0.1826	0.0747	0.0505
Time Const. (s)	τ_1	τ_2	τ_3	τ_4
	0.01	0.1	1	10

Table 5.3.1 - The table gives the parameters gained through constitutive fitting. a.) gives the linear coefficients used in the quasi-static FE model, in kPa, as well as the g_∞ formulation. b.) gives the linear coefficients and the QLV parameters used in the step-hold FE cases. The g's are the constants from the reduced relaxation function, and the τ's are the corresponding time constants in seconds.

Figure 5.3.1

a.)   b.)

c.)

Step-Hold Indentation to 0.35 Strain Model and Experimental SD
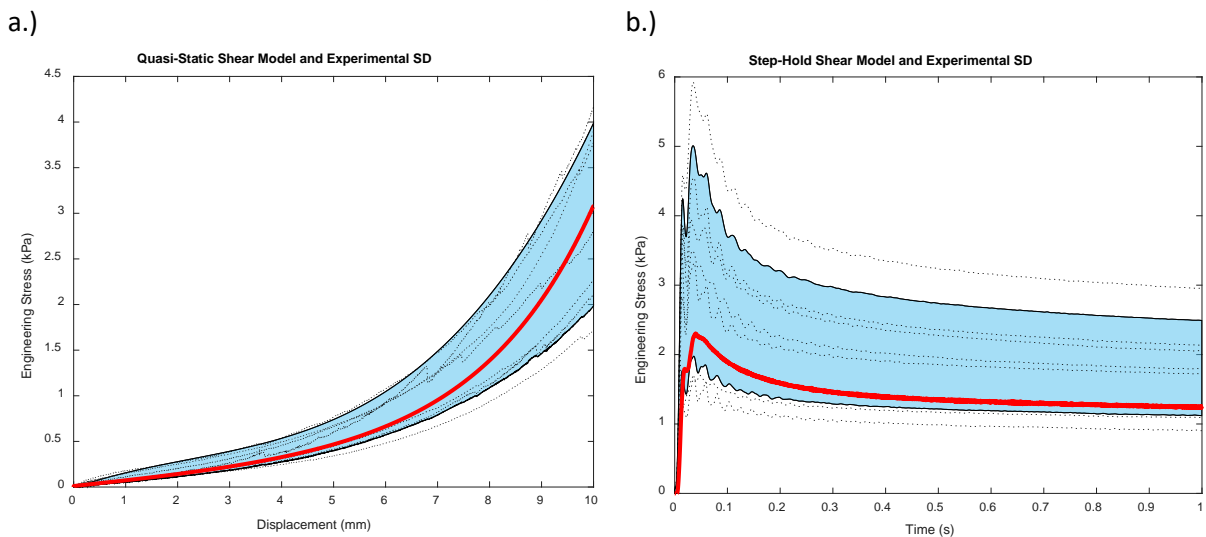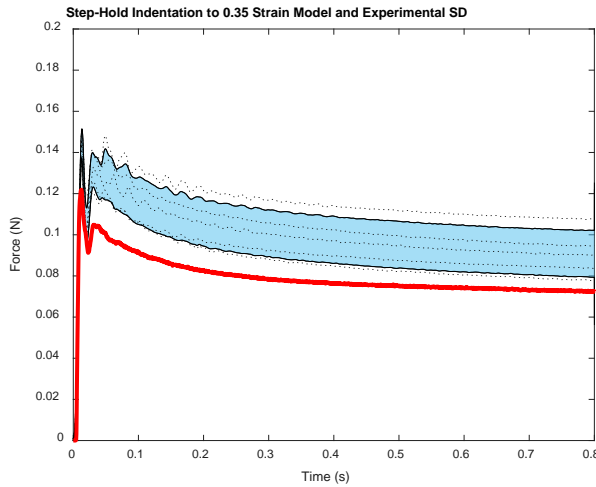
Fig. 5.3.1 - a.) depicts the quasi-static curves in engineering stress (kPa) versus displacement (mm). b.) depicts the step-hold shear curves in engineering stress (kPa) versus time (s) c.) depicts step-hold indentation curves in force (N) versus time (s). In all graphs, the red line is the FE model results, the blue shaded region is the experimental SD corridor, and the thin dashed black lines are average specimen curves (experimental).

Table 5.3.2

	Experimental		Constitutive				FE	
Parameter	ρ (g/cm^3)	K (kPa)	C_1 (kPa)	b_1	C_2 (kPa)	b_2	n	mu
Value	0.53498	900.1	6.94e-3	10	0.205	4	0.45	0.1

Table 5.3.2 - The table is separated into parameters found experimentally, through constitutive fitting, and through evaluation of the FE model. These parameters fill the material card *Mat_Hill_Foam.

Figure 5.3.2
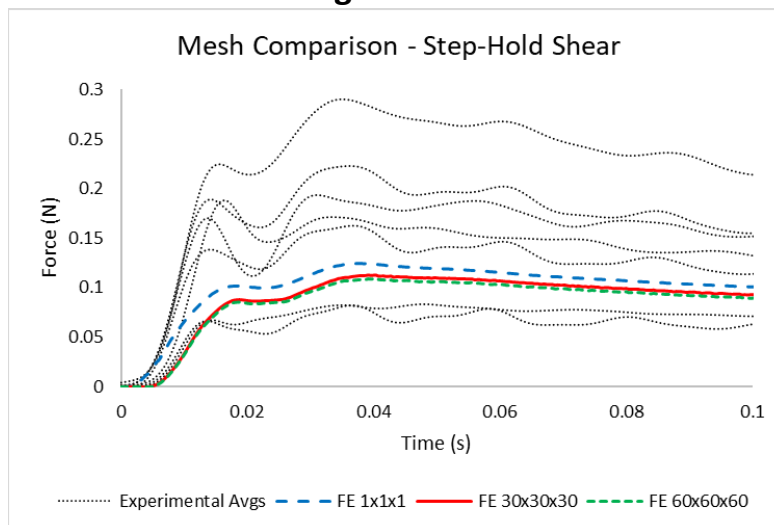
Fig. 5.3.2 – Results of the mesh sensitivity study on the shear step-hold model in force (N) versus time (s). Dotted black lines represent the experimental curves averaged by porcine specimens, the single element mesh is represented in blue dash, the 30x30x30 mesh in red solid line, and the 60x60x60 mesh in green dash.

5.4 DISCUSSION

This current research is set apart from others of its kind within the field mainly due to all other material models for lung having a basis in small mammals, specifically with murine and canine lung data. (Gayzik et al., 2011; Raghavendran et al., 2005; Stitzel et al., 2005; Vawter et al., 1978) Murine and canine data have been known to have significant issues when relating to human lung (Zeng et al., 1987), and no transfer function between responses has been developed. This arises from differences in lobe placement, alveolar size, lung volume versus animal mass, and respiratory function contributing to the mechanical properties of lung parenchyma. (Raghavendran et al., 2005; Tenney & Remmers, 1963) Porcine lung is similar to human lung in most categories including alveolar size and whole lung size and mass, and is therefore the best accessible animal surrogate for lung. (Hozain et al., 2020; Judge et al., 2014) Having a material model for lung based in porcine data is a large improvement in the modelling of lung tissue.

For this work, this is the only material model for lung to be proven usable in three different loading modes: simple shear, dynamic shear (biaxial tension), and indentation (compression). This creates a material model with the ability to be used in a wide variety of scenarios involving deformation of lung. The quasi-static FE curve as seen in Figure 5.3.1a is an exact match to the analytical fit seen in Chapter 4 (Figure 5.4.1a). However, the shear step-hold FE curve has a slight discrepancy in magnitude as compared to the analytical fit from Chapter 4, and this can be attributed to the simple shear SED function being applied to a dynamic, multi-element case. As seen in Figure 5.4.1b, the single element step-hold fit matches the analytical case, while the multi-element case does not exactly match. Regardless, the shear step-hold FE model still lies within experimental SD bounds, thus confirming the reliability of the model. The indentation step-hold experimental data was used as a validation when compared to the indentation FE model. As seen in Figure 5.3.1c, the FE model results can be compared to the experimental range. Contributing factors to the FE model not being within the experimental SD corridor include mesh size and shape as well as lack of experimental data. The indentation SD corridor results from only 5 specimens, and it is possible that with a larger population the SD corridor would be bigger. With an indentation SD corridor from a greater experimental population, it is expected that the FE model will lie within bounds. These results and contributing factors show that there are still minute discrepancies between experimental data and a fully encompassing material model. This is an indication that there is room for improvement using the Hill Foam strain energy density function to represent lung. Improvement can be made in the forms of reevaluating parameters, adding experimental datasets and possibly expanding the number of parameters to achieve a better fit.

One of the advantages in using the Hill Foam model is that this material model is based on a popular strain energy density function that is easily applicable through ready-made FE cards. The low number of parameters involved in the Hill Foam model adds a simplicity factor and does not overcomplicate model fitting or computational runtime. Further, this chosen material modelling method makes it easy to add in QLV parameters to fully represent the viscoelastic relaxation of lung parenchyma.

Having an updated material model for lung is necessary in the evaluation of injury inducing insults to the thorax such as motor vehicle crashes, physical altercations, blunt impacts to the torso, falls, and other thoracic trauma. The material model produced in this study can be used to address these concerns through evaluation using FE models and other mathematical models. This is the only material model for lung to be based entirely on large mammal experimental testing, and is also the only lung material model to be validated using a separate test setup. Creating an accurate material model based on experimental lung testing is a crucial part in the characterization of lung, and will be used as a tool to help mitigate injury. Ultimately, this material model is paired with experimental damage criteria so that the model can encompass the full response of the material.

Figure 5.4.1

a.)   b.)
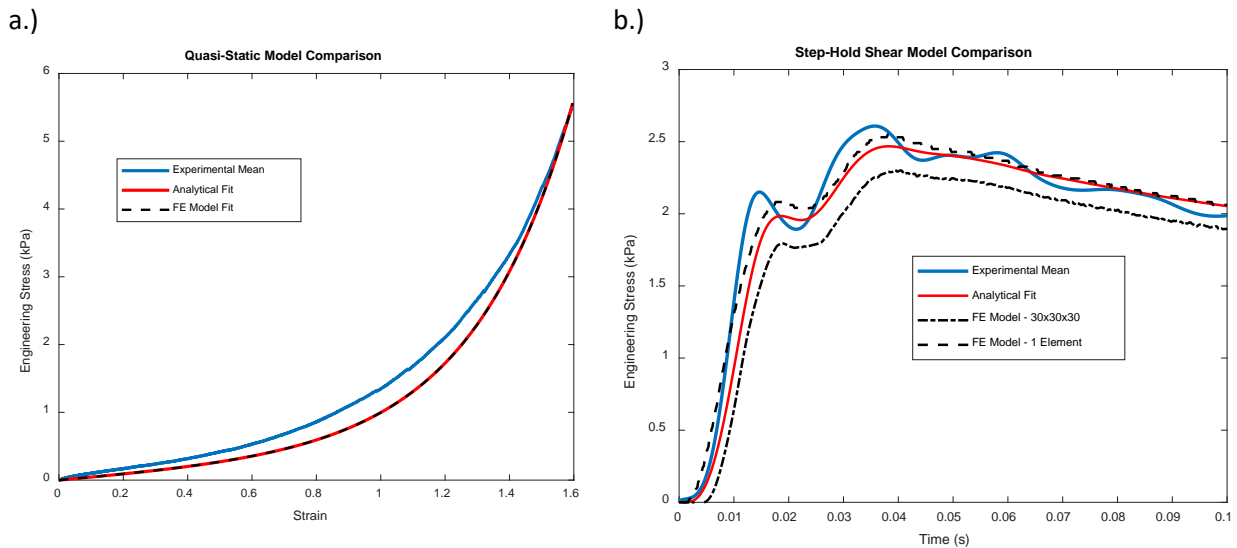
Fig. 5.4.1 – Depicted is the FE model fit (dashed black) as compared to the analytical fit (solid red) and the experimental mean (solid blue). a.) contains the fits for the quasi-static shear test, and b.) for the step-hold shear test. The step-hod plot contains both the FE model fit with 30x30x30 elements (dot-dash) and the FE model fit using a single element (dash).

From this point forward within this dissertation, the material model constants used in the FE material cards *Mat_Hill_Foam and *Mat_Add_Inelasticity contain different values than those described in Chapters 4 and 5.

These material constants produce the FE model fits seen in Figure N.1. The quasi-static result (Figure N.1a) is depicted in engineering stress (kPa) versus displacement (mm), the shear step-hold result (Figure N.1b) in engineering stress (kPa) versus time (s), and the indentation step-hold validation (Figure N.1c) in force (N) versus time (s). The red, dashed lines are the model results presented in Chapter 4, while the solid red lines are the models with the different material constants used from this point forward. The quasi-static FE model lies at the extreme upper edge of the experimental SD corridor, and the indentation FE model lies at the extreme bottom edge of the experimental SD corridor. These fits are a result of the parameters seen in Tables N.1 and N.2, with N.1 depicting the parameters used in the *Mat_Hill_Foam card, and N.2 depicting the QLV parameters used in the *Mat_Add_Inelasticity card. The C's were unchanged for the quasi-static and step-hold FE models. A driving factor for these fits was that all FE model results are close to the experimental SD corridors for all three forms of testing. However, these material model constants do not provide the most accurate analytical fit. Future studies should focus on the material parameters presented in Chapters 4 and 5.

Figure N.1

a.)   b.)
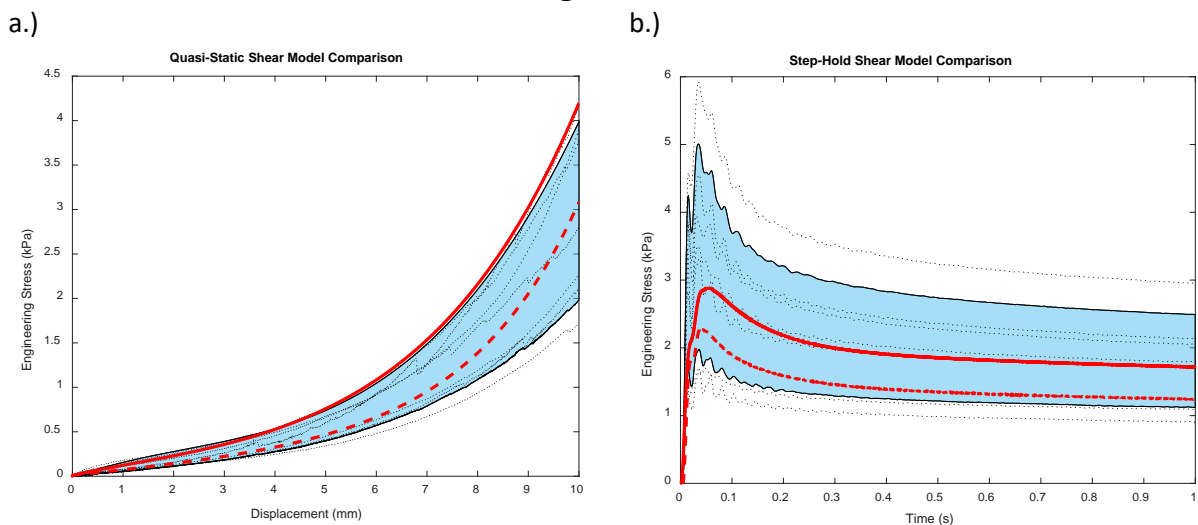
c.)
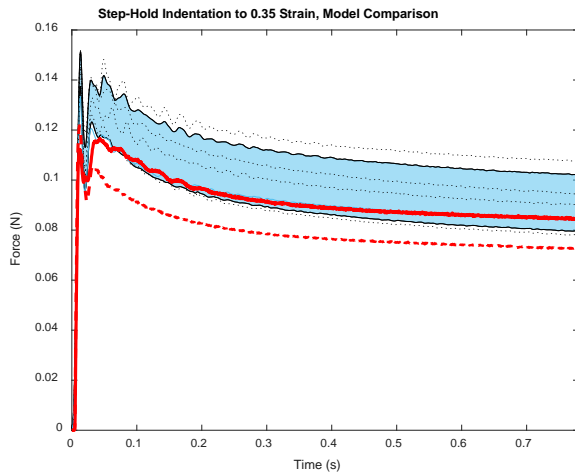
Fig. N.1 - a.) depicts the quasi-static curves in engineering stress (kPa) versus displacement (mm) to account for differences in sample thickness. b.) and c.) are step-hold shear and indentation curves respectively, and are depicted in engineering stress (kPa) versus time (s), and force (N) versus time(s). Since the step-hold curves have a specific strain input, there is no need to account for differing sample thickness. In all graphs, the red line is the FE model results: **the dashed line is the model presented in Chapter 4, and the solid line is the model from this point forward**. The blue shaded region is the experimental SD corridor, and the thin dashed black lines are average specimen curves (experimental).

Table N.1

Parameter	Experimental		Constitutive				FE	
	ρ (g/cm^3)	K (kPa)	C_1 (kPa)	b_1	C_2 (kPa)	b_2	n	mu
Value	0.53498	900.1	0.668	4	0.132	7	0.45	0.1

Table N.1 - The table is separated into parameters found experimentally, through constitutive fitting, and through evaluation of the FE model. These parameters fill the material card *Mat_Hill_Foam.

Table N.2

Relaxation Const.	g_1	g_2	g_3	g_4
	0.0883633	0.365548	0.119346	0.0963434
Time Const. (s)	τ_1	τ_2	τ_3	τ_4
	0.01	0.1	1	10

Table N.2 - The table gives the parameters gained through QLV fitting. The g's are the constants from the reduced relaxation function, and the τ's are the corresponding time constants in seconds. This fit gave an R^2 of 0.998, this method of error is relevant due to the quasi-linear decline in the relaxation of the material.

CHAPTER 6: Validation of Whole Body GHBMC Response to BABT

***See NOTICE after Chapter 5

To determine how to model lung damage in BABT, the GHBMC must be evaluated for its use in BABT events. Using the updated material model for lung developed in the previous chapters within the GHBMC, BABT testing is simulated and the response compared to experimental impacts on a PMHS. Through this comparison, the GHBMC is validated for use in recreating BABT scenarios and can be later used to address lung damage in BABT.

6.1 MOTIVATION

While BABT has been characterized as an emerging issue in both militant scenarios and within law enforcement, (Cannon, 2001) the question of the proper method in which to model the BABT interaction on the human body still remains. Available human body models are useful for modeling a variety of interactions and producing kinematics for comparison to reported cases of injury or insult. However, most widely used human body models are only validated for automotive crashes and other like incidents. Automotive crashes are usually characterized by higher mass and lower velocity impacts that are distributed over a large region of the body. (Danelson & Stitzel, 2015; Prat, Rongieras, Sarron, et al., 2012; Viano, 1989) This creates a discrepancy in the modeling of BABT which is characterized by lower mass and higher velocity impacts that are usually extremely localized on the human body. (Cannon, 2001; Carr et al., 2016; Prat, Rongieras, Sarron, et al., 2012) Due to these factors, there is uncertainty in the ability of these human body models to accurately replicate the body's kinematics during a BABT event.

However, that is not to say that there have not been cases of BABT reproduced with human body models. The most notable in the literature comes from Cronin et al. (D. S. Cronin et al., 2021a). In this study, the previously developed Waterloo Thorax model (WALT) was the human body model utilized. The goal of the study was to assess injury using the WALT by replicating field cases of BABT. The deformation of the body armor in these events was modeled using an impactor with the same profile as the back-face deformation. Ten field cases of BABT were reproduced in this manner, and the human body model was considered a sufficient model for the cases. (D. S. Cronin et al., 2021a)

An important aspect of this study is the example it produces in the usage of human body models in the field of biomechanics. The WALT was developed specifically for automotive uses, (D. S. Cronin et al., 2021a; Deng et al., 1999) and in the study previously described, the WALT was considered operational for BABT type incidents. This shows that within the literature, there exists a precedent for using human

body models validated for automotive loading in BABT events. Notwithstanding, the question of validation of BABT kinematics should be addressed.

As mentioned in Chapter 5, the GHBMC is the FE human body model used to implement the new lung material model, and the GHBMC will also be used to explore the effects of BABT. Likewise to most FE human body models, the GHBMC has its origins in automotive crash safety, and is validated using pendulum impacts on the side of a PMHS to represent an occupant in a near- or far-side crash. (Viano, 1989) Since, to date, automotive loading is the only manner in which whole body kinematics of the GHBMC are validated with experimental testing, there exists the need to ensure the quality of results when performing BABT type simulations. Therefore, an exemplary experimental test on a PMHS will give comparison on the GHBMC response in BABT events. Particularly since this demonstration will be done with only a single subject, the goal is not to match experimental data exactly, but to ensure that collected data follow similar trends to the same FE traces. Peaks of traces gained from FE modeling will be checked to ensure they are within the same magnitude of the counterpart traces gained experimentally.

6.2 EXPERIMENTAL METHODS

In traditional ballistics testing, various interactions and reactions between variables are taking place at the same time, so understanding the outcome due to a single factor becomes indistinct and distorted by the uncontrollable variables. When looking solely at the effect of the back face deformation of armor on a body, it becomes imperative to limit the experimental scope to a single precise interaction. The testing setup designed and constructed for this BABT experimentation was meant to simulate conditions seen in a BABT event while restricting the number of variables and reducing the risks associated with traditional ballistics testing. An impactor was made to mimic the exact shape and dimensions of the body armor's deformation resulting from an impact of a high-caliber round or piece of shrapnel. (Bass et al., 2006) This 3D-printed carbon fiber impactor was cylindrical with a quasi-hemispherical front, measuring 10.16cm in diameter and hollow to accommodate a wireless accelerometer sensor/data acquisition system (Figure 6.2.1a). Instrumented mass of the impactor was 227g. The test rig, the Differential Rate Air Gun (DRAGun) was comprised of a 6m long aluminum launch tube with an inner diameter of 10.16cm and a pressurized locking mechanism at the loading end of the launch tube. The DRAGun was connected to a system of three volumetric tanks capable of 175psi and an impactor launching speed of 100m/s. At the launch-end of the DRAGun were 25.4 cm slits to allow for a controlled free flight. The launch-end also contained an optical velocity gate to measure free flight velocity at impact.

Figure 6.2.1

a.) b.) c.)
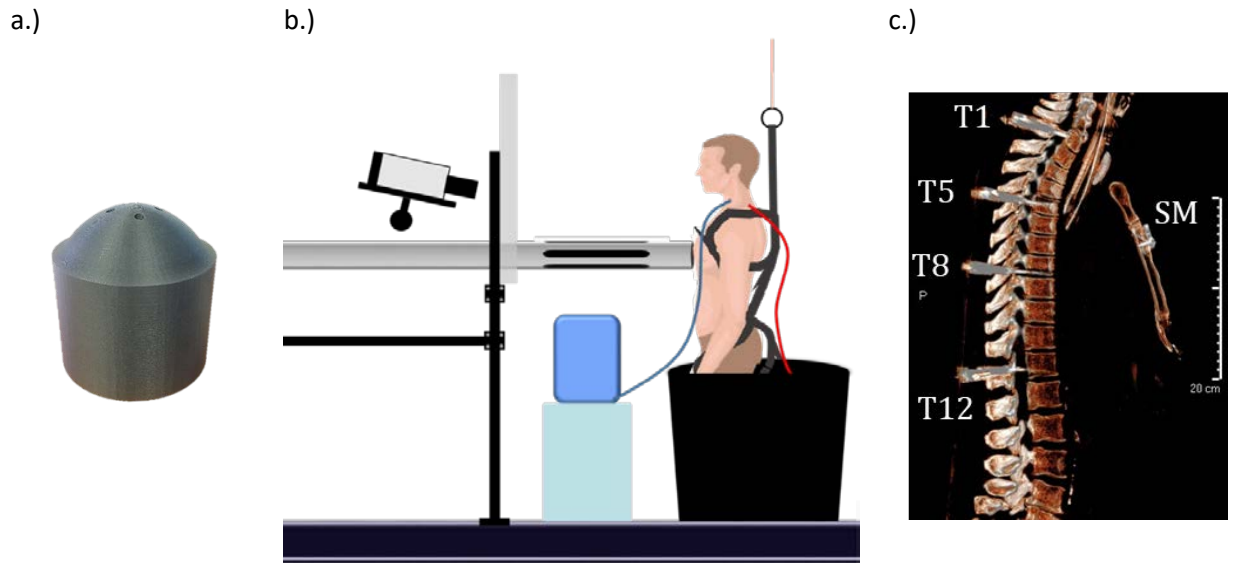
Fig 6.2.1 – a.) carbon fiber impactor used for BABT testing b.) schematic of PMHS positioning at launch-end of the DRAGun c.) X-ray image showing placement of spinal accelerometers (T1, T5, T8, T12) and sternal mounted accelerometer (SM)

Whole body testing was performed on a PMHS thorax. The test protocol was reviewed and approved by an internal oversight committee from the University of Virginia (UVA), the UVA IRB (CAB 2018-13), and the US HRPO. The specimen was aged 56 years and was a 50th percentile male (anthropometric data in Appx. B.2). The PMHS was suspended in a standing position at the launch-end of the DRAGun using a five-point harness that left the torso bare (Figure 6.2.1b). The specimen's vasculature was perfused for every test, and before each test the lungs were exercised and then left open to air. In addition to perfusion, other instrumentation included 20 strain gauges (Micro-Measurements, Raleigh, NC) on the ribs and sternum, 4 spinal mounted accelerometers (6DX PRO, DTS, Inc. Seal Beach, CA) with six degrees of freedom (Figure 6.2.1c), 3 pressure transducers in the lungs and right atrium (SPR-524, Millar, Houston, TX), and a sternal mounted accelerometer (A243111, DTS, Inc.). All sensors had an acquisition rate of 100 kHz. High speed cameras were utilized to validate impact velocity. Velocities of the back face deformation of body armor during BABT events is known to vary between $10 - 80$ m/s, (Prat, Rongieras, Sarron, et al., 2012; Wen et al., 2015) so two velocities were chosen for the testing of the PMHS: low and high. Three tests were performed: two low speed tests over the lungs in quadrants I and III (upper right and lower left), and one high speed test over the heart in quadrant II (upper left). Specific testing velocities and placements on the thorax of the PMHS are shown in Figure 6.2.2.

6.3 FINITE ELEMENT MODELING

The GHBMC was used to simulate the experimental impacts described in the previous section. All parts and materials remained unaltered from the GHBMC M50-O v.6 except for the lung material card, which was changed as described in Chapter 5. The 3D-printed impactor described in the previous section was meshed from the CAD as a rigid shell element (Figure 6.3.1). The instrumented weight and the dimensions of the FE impactor were the same as in experimental testing. The impactor's motion was

Figure 6.3.1
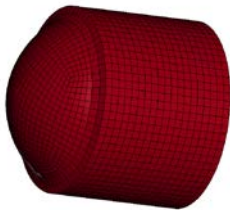
Fig 6.3.1 – Meshed BABT impactor (rigid shell)

limited to the x-direction to simulate the controlled free flight within the launch tube. Other than the restricted degrees of freedom, the impactor was given a prescribed initial velocity in the x-direction, but was otherwise allowed to react to the impact with the GHBMC with differing x-accelerations and velocities. The GHBMC was subjected to gravity and element erosion for boney parts was turned on to allow for fracture. Otherwise, the GHBMC was not constricted in any form.

All three experimental tests were simulated using the GHBMC. The prescribed initial velocity of the impactor was matched with the experimental velocity at impact, and location of the impact was recreated according to experimental test placement (Figure 6.3.2). Nodes in the placement of the sensors used in the experimental test were marked and set to output kinematics to compare with the accelerometers. The impactor was positioned near the impact point with the torso without contact to allow for shorter computation time. The FE simulation was set to run for 20 ms, which included initial impact and reaction as seen by the experimental results.

Figure 6.2.2
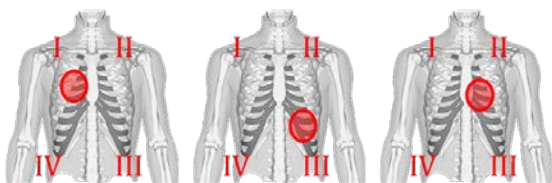
Test	Velocity (m/s)	Quadrant
1	28	I
2	29	III
3	59	II

Fig 6.2.2 – The test matrix for PMHS testing: diagram indicates thoracic quadrants and impact locations, table contains hit velocities

Figure 6.3.2
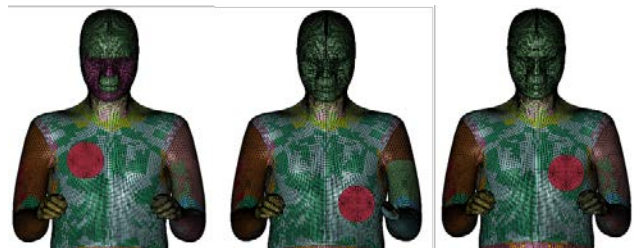
Fig 6.3.2 – Images detailing impact locations for the FE simulations on the GHBMC

6.4 RESULTS

The two low impacts to the PMHS resulted in no known damage to the torso, while the third high velocity impact resulted in rib fractures and cartilage damage seen in Figure 6.4.1a. Due to the postmortem nature of the subject, contusion cannot be fully accounted for, but some pleura damage over the third impact sight can be seen in Figure 6.4.1b. It should be noted that the damage and fracture patterns were discovered via autopsy. Likewise, the two low impacts to the GHBMC in the FE simulations did not result in any cases of fracture, and the third hit resulted in four cases of rib element erosion.

All accelerometer, strain gauge, and pressure data were processed using a CFC 1000 filter to remain comparable to other whole body PMHS testing. (Bailey et al., 2015) All PMHS sensor data can be seen in Appx. B.2. After review of the data, it was apparent that the most meaningful sensors for a frontal thoracic impact were the impactor and sternal accelerometers. The spinal accelerometers produced data only indicative of full body motion, which is not relevant for the specific case of BABT where localized trauma needs evaluation. Since this exercise is to validate the GHBMC for specifically BABT type scenarios, comparison of deformation into the body and local torso velocity are most significant. This stems from the NIJ standard for approving body armor, which deals solely in back-face deformation displacements, (U.S. Department of Justice, 2008) and measures of internal velocities from localized impacts. (Viano & Lau, 1988) Displacement measures into the body of the PMHS were achieved through integration of the impactor acceleration curve paired with high-speed video footage. Displacement into the GHBMC was measured from impactor contact with the torso to peak displacement of the impactor in the negative x-direction (Table 6.4.1). Sternal velocities were gained from the PMHS via the integrated sternal accelerometer trace. The sternal velocities from the GHMBC come from the kinematic response of a

Figure 6.4.1

a.)

b.)
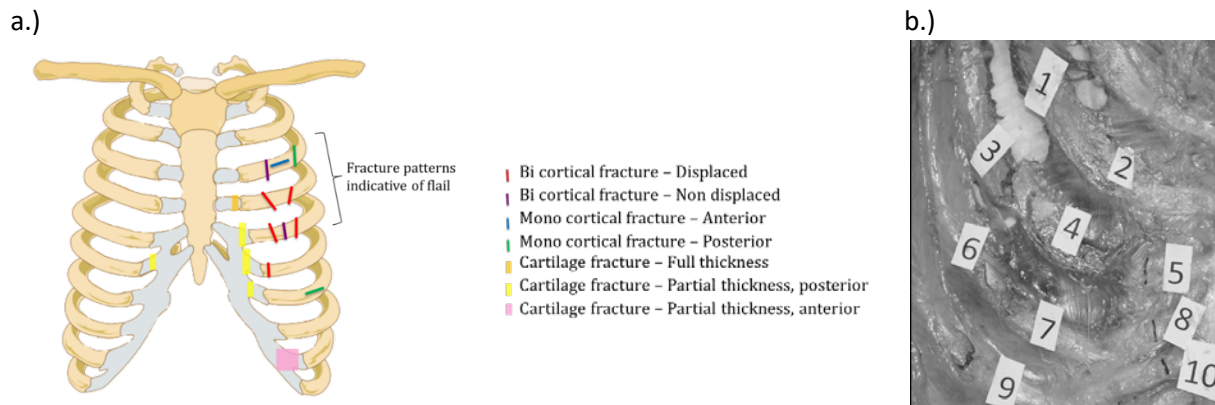
Fig 6.4.1 – a.) Diagram of ribcage fracture patterns as a result of the third PMHS test b.) Image of the posterior view of the ribcage; the darker coloring is pleura damage over the impact site

designated node in the same placement as the sternal accelerometer on the PMHS. The compared velocity traces can be seen in Figure 6.4.2 while the peaks are listed in Table 6.4.1.

Table 6.4.1

	PMHS			GHBMC		
	Test 1	Test 2	Test 3	Test 1	Test 2	Test 3
Max. Disp. (mm)	40 ± 4	46 ± 4	67 ± 7	56	49	87
Peak Vel. (m/s)	-1.26	-0.52	-3.1	-1.86	-0.5	-2.2

Table 6.4.1 – First row of data depicts the maximum displacement at the impactor in mm, second row depicts the peak sternal velocity in m/s. The three tests to the left correspond to the values for the PMHS, while the three to the left correspond to the GHBMC.

Figure 6.4.2
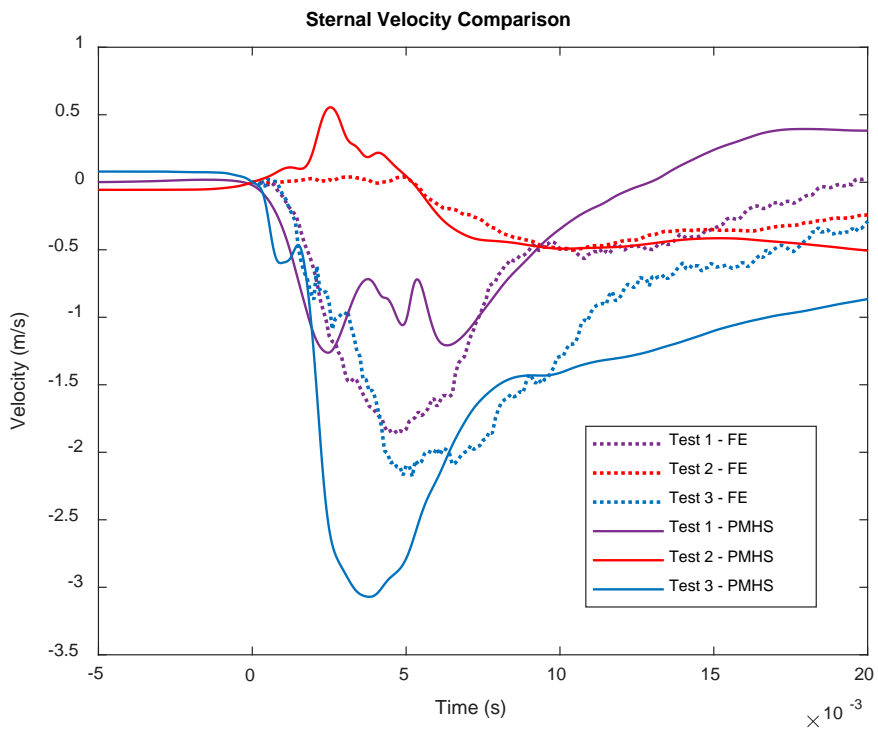
Fig 6.4.2 – Comparison of sternal velocities between the PMHS and GHBMC. PMHS tests are solid lines while GHBMC model results are dotted lines. Model lines have the same color as the experimental counterparts.

81

6.5 DISCUSSION

The objective of this chapter was to determine the GHMBC's capability in reacting to a BABT event. This was done by simulating experimental tests of a PMHS undergoing a BABT impact, and comparing the results of both the experimental sensor readings and the FE simulations. Observationally, the FE model visually matched the high-speed video footage of the PMHS in that only the torso was greatly affected by movement. Other areas of the body had only secondary visual motion in reaction to the thoracic impact (e.g. swinging from the gantry or shifting in reaction to the torso being pushed). Similar boney injuries were seen with the PMHS as with the GHBMC; the two low speed hits produced no fractures. While autopsy revealed a number of boney fractures from the high speed hit on the PMHS (Figure 6.4.1a), a radiologist reported only three fractures when reading a post-test CT scan of the subject (Appx. B.2). This compares very well to the rib element erosion seen with the GHBMC, possibly indicating that boney fracture on the GHBMC is relatable to radiological imaging rather than autopsy results.

Differences in displacement measures and peak velocities (Table 6.4.1) were well within intra-specimen variations seen within the field. (Bailey et al., 2015) For instance, when the PMHS displacements are counted on the upper edge of the error (i.e. 40 ± 4 = 44), the average discrepancy between PMHS and GHBMC displacements is 8mm. This is not a large discrepancy when considering the fact that the PMHS's chest depth measures approximately 30mm less than the measure for the 50th percentile male (see anthropometry in Appx. B.2). Differences can also arise from bone quality, temperature, and other minute differences seen in fresh biological material. With this in mind, the FE simulation can be considered comparable to the response in a BABT event.

Through these interpretations of the results, the GHBMC can be considered valid for use in thoracic BABT simulations. As with any model, this validation comes with limitations. Only specific measures were investigated to compare, and those measures involved the integration of experimentally collected acceleration traces. This comparison was also only performed with one PMHS. More specimens need to be experimentally tested to ensure the validity of the results, and to create an experimental standard deviation range. Nonetheless, this exercise was sufficient in demonstrating that the GHBMC can be used for BABT simulations.

CHAPTER 7: Threshold for Failure in Lung Tissue

To reach the goal of modeling lung damage in BABT, a metric for lung damage must first be ascertained. The determination of a threshold for lung tissue failure is achieved by experimental testing to failure in small-scale shear samples. This testing results in a failure threshold to be implemented into the GHBMC during BABT events so that a lung damage volume can be gained.

7.1 MOTIVATION

As aforementioned (Chapters 2 & 3), there is a gap in the literature regarding small-scale testing of lung tissue for material properties. However, there does exist in the literature some studies on the mechanical characterization of lung parenchyma – that is not the case for a failure threshold of lung tissue based on the actual material, lung tissue, for humans or comparable human surrogates. Damage metrics have been proposed for lung, but mostly in blast loading which has strain rates too high for thoracic impacts. (Bowen et al., 1968) Lung damage criteria not based in blast have included murine data and pressure thresholds. (Gayzik et al., 2011; Viano & Warner, 1976) The murine data are not comparable to human directly, and no form of transfer function has been made, while the pressure thresholds focus on pressure readings in the upper bronchi from impacted PMHS, and include no proven correlation with definite lung damage. In all of these proposed methods, it is also assumed that the damage metrics are corresponding directly to PC and not mechanical lung failure. From a biomechanics standpoint, this is problematic due to the fact that PC refers to a blood volume that changes over time and not a static measure of the physical failure point of a material.

As a specific example and critique of a lung damage metric, the most significant contribution to modeling PC risk in BABT comes from Cronin et al. (D. S. Cronin et al., 2021b). The study includes well-detailed interactions found in BABT, and the experimental basis for fitting lung material parameters is not solely based in canine data – including PMHS lung material data as well. However, the injury metric is not proven to be accurate. Cronin et al. has the assumption that a thoracic AIS 3 corresponds to a high risk of developing ARDS. The connection is then made through Miller et al. that the highest risk of ARDS cases comes from severe PC (≥20% lung contused). (P. R. Miller et al., 2001) So using a thoracic pressure gained from the FE modeling of pendulum tests on a human body model that resulted in AIS 3 rib fractures, Cronin et al. uses this as an individual FE injury threshold in the lungs. (D. S. Cronin et al., 2021b) This popular injury metric is essentially ignoring all cases of PC without severe rib fracture, and then only links PC with the correlation of higher number of ARDS cases. As discussed in Chapter 2, there is no evidence

correlating rib fracture and severity of PC, as patients can have severe PC without severe rib fracture and vice versa. (O'Connor et al., 2009)

The goal of the current research is to define a damage metric that allows for detection of structurally induced failure that can be linked with PC in BABT events. This is achieved through small-scale testing of porcine lung tissue to failure in shear. This research will be the first of its kind to include damage based on mechanical tissue testing and to have both the material and damage model fitted from the same material type.

7.2 METHODS

Characterizing the material of lung through experimental testing and constitutive modeling only depicts the behavior of the material sub failure. Therefore, the objective exists to find a threshold for mechanical lung damage using the same surrogate as the characterization. For this BABT research, the damage metric will be defined as a small sample (7 - 5mm cube) reaching ultimate failure (visible ripping) (Figure 7.2.1). In this way, the damage metric for small samples of lung can be directly related to the damage threshold for a single element of lung in a FE model.

Since common experimental data acquisition tools such as accelerometers or strain gauges are unusable for in vivo tissue like thoracic organs, measures of organ velocity in instances similar to BABT need to be determined via a less direct route. In studies done using rabbits, pigs, and PMHS in thoracic impact scenarios, it has been estimated that the lung

Figure 7.2.1

Fig 7.2.1 - This figure shows a time lapse of a sample failing in shear. The top picture shows the sample before the start of the test. The bottom picture shows the sample at the end of the test. The white arrows indicate the area where failure occurs.

velocity relative to the body is less than 3 m/s. (Magnan et al., 2004; Prat, Rongieras, de Freminville, et al., 2012; Rater, 2013; Viano, 1991) To check this measure for BABT scenarios, the information gained in the experimental testing in Chapter 6 will be utilized. (Eaton et al., 2020) Using impactor displacement, sternal displacement, sternal velocity (Figure 7.2.2), and body velocity, all gained from accelerometers, it was concluded that the assumed velocity of the lungs relative to the body was indeed ≤ 3 m/s. From this, it was decided that at-

Figure 7.2.2

Fig 7.2.2 – Sternal velocities (x direction) for upper and lower bound BABT impacts on PMHS; the left depicts a mild case of BABT while the right depicts a more severe case

rate failure testing would be performed for small lung samples at 1 m/s. In this way, the failure testing is comparable to the testing done for material characterization.

The experimental methodology for shear failure testing will be the same as in the small sample testing section (Chapter 3), but for the exception that all displacements will be to failure. Once the material has been prepared and the samples excised, the shear samples were placed between the shearing plates, rigidly fixed, and sheared at 1 m/s until failure occurred. The use of high-speed video cameras were employed to ensure that actual material failure was reached, and not an error caused by the test fixture or failure of adhesive (Figure 7.2.1 shows still frames of high-speed footage). Force and displacement time plots were also utilized to ensure that the curve was characteristic of a material reaching the yield point.

7.3 RESULTS AND STATISTICAL ANALYSIS

Once failure was thought to have occurred for a sample, the observed failure time point from high-speed video footage was corroborated with the failure time point seen from Lagrangian stress-strain calculations. For example, a sample plot indicative of failure can be seen in Figure 7.3.1a, with the yield point of the material indicated by the peak followed by a steep decline. There did occurred instances where the material failed, but due to excessive noise or partial adhesive failure, a time point for failure could not be matched. An example of this case can be seen in Figure 7.3.1b, and in cases such as these the sample was not counted as having failed and the data not included in the determination of a failure threshold.

85

Figure 7.3.1

a.)   b.)
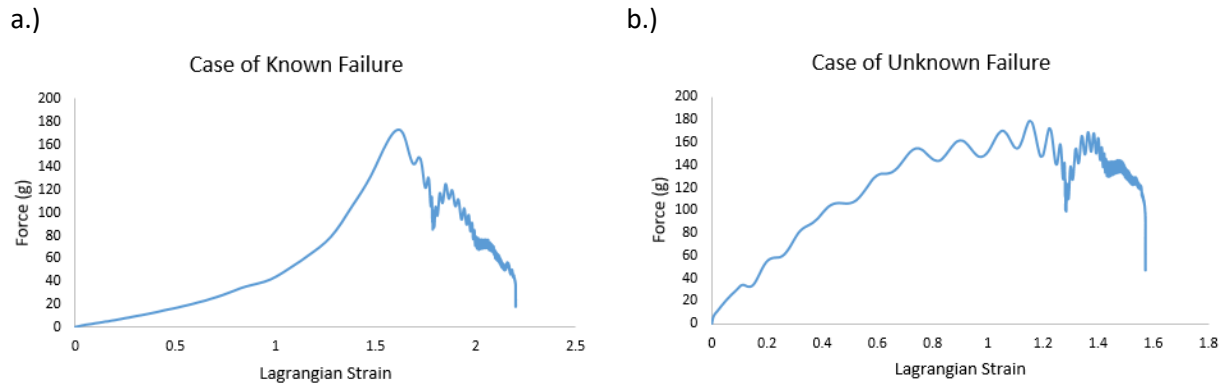
Fig 7.3.1 – The left plot depicts a sample in which failure was easily discerned (P019 L1), the right plot depicts a sample in which failure was obscured by noise. In the case of the right plot, the data was not used for threshold determination. Both plots are Force (g) versus Lagrangian Strain.

To find a suitable variable indicative of failure, stress and maximum strain were investigated as per other lung injury threshold investigations on murine data. (Gayzik et al., 2007, 2011) Also investigated within the literature was strain rate, along with the product of strain and strain rate (Gayzik et al., 2007); however, for the current research, strain rate did not vary independently of strain since the testing velocity remained constant among all tested samples. Therefore, investigating strain rate or the product of strain rate and strain would not have yielded more information than examining strain alone. The goal in finding a predictor of mechanical failure was to have the 95% confidence interval for the data less than 20% of the mean, as was the case in Chapter 5 to remain comparable with other works within the field. Strain was found to be the best predictor, with a 95% confidence interval less than 10% of the mean, and the threshold value, in true strain, along with the standard deviation can be seen in Table 7.3.1.

A linear mixed model was utilized to not only achieve the number of samples (n) needed to gain statistically valid results, but also the number of specimens (N) from which the samples came. This negates any bias from any one specific sample and ensures that there are enough samples to represent the population so that the data is not skewed. Through this statistical analysis (Chapter 3), it was found that 7 samples were needed (n=7) from 5 specimens (N=5) to determine the threshold of failure in lung tissue (Table 7.3.1). For more data regarding individual samples and corresponding plots, see Appx. A.1 and B.1.

Table 7.3.1

Specimen	P016	P017	P017	P018	P018	P019	P022
Sample	L2	L3	R3	R2	R3	L1	L2
Strain	0.928	0.806	0.904	0.916	0.971	0.963	0.908
		Average:	0.914	SD:	0.054		

Table 7.3.1 – List of failed samples with corresponding specimen and true strain measure. L refers to a sample from the left lung, R from the right lung. Average failure strain and standard deviation are shown for the failed samples.

7.4 DISCUSSION

Knowing the failure point of biological materials is one of the most important steps in modeling and predicting injury within the human body. Without a mechanical failure threshold of the tissue, any modeled injury predictions are just estimates based on secondary or tertiary effects or symptoms. Biological systems are all different, so it does not suffice to depend on symptoms or predictors that have been known to vary widely with specimen geometry, medical history, unproven correlations between different organs and even species, etc. Thus, the need for a mechanically based failure measurement of the tissue is necessary to accurately provide information on possibly injury metrics. This research is the first of its kind to include damage based on mechanical tissue testing and to have both the material and damage model fitted from the same material type.

With the preliminary human correlation findings in Chapter 3, it can also be assumed that porcine lung failure can be used in a 1:1 ratio when investigating the failure of human lung tissue. This paired with the fact that the failure threshold of lung parenchyma proved to be a simple strain measure for at-rate loading, allows for a breakthrough in the field of lung biomechanics and injury prediction and prevention. Never before within the literature has the failure point of lung tissue been found, or a failure prediction method based in physical damage been considered.

This strain threshold for damage within lung tissue is easily applicable in instances such as FE modeling, where elements within the lung that reach the strain threshold can be counted as having failed. The dimensions of the failed experimental samples were determined for ease of applicability and implementation into the GHBMC parts for lungs. The mean size of the failure samples matches the mean size of the elements that make up the left and right GHBMC lungs. Therefore, physical damage seen experimentally relates directly to an individual element failure in the FE lung model. The directly relatable measure of damage revolutionizes the possibilities for injury prediction using human body models, in that it provides increased accuracy for the determination of damaged regions through a proven connection to

tissue failure. Past formations for blunt injury prediction in lung fall short by using unproven correlations such as injury in other organs or pressure measurements that may not be affected by parenchyma damage. The current research outlined in this chapter is crucial to the advancement in understanding of lung injury and paving a path forward in future mitigation strategies. Without a damage metric for lung tissue, alleviating injuries in blunt thoracic trauma through the discovery of prevention strategies would not be possible.

CHAPTER 8: Determination of Clay Displacement and BABT Relationship

In determining how to model lung damage in BABT, a problem arises in the ability to recreate live-porcine BABT testing present in the literature with a FE model. A way to match the input conditions of both the BABT of the live-porcine specimens and the GHBMC becomes a necessity. The problem is solved by relating the back-face armor deformation into clay, as reported by the live-porcine studies, with the velocity of the BABT impactor used in the GHBMC simulations.

8.1 MOTIVATION

The pass/fail of body armor is almost solely dependent on its back-face deformation (BFD), or how the armor deforms when struck with a projectile. The official measuring of BFD comes from the National Institute of Justice (NIJ), and uses an oil-based clay (Roma Plastilina No.1) as a backing material and measuring standard. The passing limit of the armor is set at 44 mm: the BFD into the clay cannot exceed 44 mm in more than 20% of the hits with a confidence of 95%, and the armor fails if BFD reaches 50 mm or higher (7.8.8 (U.S. Department of Justice, 2008)). However, this method for testing armor, specifically using a single measure of BFD, has never been correlated with injury risk or severity. The clay used in NIJ standard testing was picked for its close material response to that of 20% ballistics gel. 20% ballistics gel was the first medium used to measure the effects of BABT, but was replaced with clay to lower cost, omit the need of high speed cameras, and to be able to utilize a reusable material. The 44 mm BFD limit was picked based on data from a .38 caliber round in 20% ballistics gel, for soft body armor, and has no proven relevance to higher velocity rounds. (Hanlon & Gillich, 2012) Furthermore, the NIJ clay standard has been used for many decades without development of novel or reformed procedures for more modern projectile types and newly developed composition materials in body armor. This becomes extremely relevant in the current push for more effective lighter body armor, where the effects due to BABT are unknown and are possibly unattainable through traditional clay-centered testing.

Despite the decades Roma Plastilina No.1 has been in use for testing armors, a thorough characterization of the clay's properties has not been achieved. This is due to the variance in the clay properties due to temperature as well as the extreme plasticity of the material. A FE model that encompasses the clay's characteristics for all levels of strain rate is nearly impossible because of these variant properties. This can be seen in the study by Roberts et al. (Roberts et al., 2007) where the authors created a FE model of the clay to be used in a BABT simulation then compared results to a human surrogate computational model undergoing the same conditions. However, the experimental clay data

used to propagate the FE model was achieved through a one half to two-meter ball drop test onto bare clay, and the BABT simulations consisted of a 9mm bullet fired at body armor-covered clay. In some instances, this results in a kinetic energy difference by a factor of 10^6, which renders their assumptions and findings inadequate for further study. Due to the plastic nature of the clay, any experimentation toward BABT needs to be at BABT rates to gain an accurate BFD measure for comparison. Similar drop-test or indentation-style testing has been done on Roma Plastilina No.1, but only at low- to mid-rate velocities and strain rates or without an indentation pattern comparable to BABT. (Buchely et al., 2016; Hernandez et al., 2015)

Since the clay is difficult to model mathematically, other models have been proposed for determining the corridor for BABT. For biological models, both porcine and cadaveric (PMHS) materials have been widely used, with PMHS being the preferred choice since it is best to evaluate human tissue for human injury. (Bass et al., 2006; Gryth et al., 2007; Prat, Rongieras, de Freminville, et al., 2012) Various gels have also been proposed in place of the clay, including the 20% ballistics gelatin for which the clay model was chosen. (Mauzac et al., 2012; Merkle et al., 2008) Despite the numerous alternative methods in evaluating body armors, the NIJ has given no indication of switching or altering its methods for testing armor. From this, the scientific community should focus on assessing the clay standard and connecting the BFD limit with human injury data.

The goal of this chapter is to connect clay displacement with an input energy, and determine how to mimic body armor BFDs of differing clay displacements. The reason for this objective stems from the only data within the literature on full-scale BABT testing: armored live-porcine. In live-porcine BABT testing, various hard armors are hit by a NATO 7.62 bullet, which causes the armor to deform and impact the porcine specimen. The only known variable concerning this impact is the depth into clay when clay replaces the specimen as a backing for the armor. (Arborelius et al., 2004; Drobin et al., 2007; Gryth et al., 2007; Rocksén et al., 2012; Sondén et al., 2009) The BABT impactor developed and used in Chapter 6 is sufficient in mimicking the impact between the armor and the specimen, but input conditions to recreate the exact impact energy are unknown. The solution is to discern the relationship between the clay displacements and the BABT impactor velocity; i.e. know which impactor velocity will result in a certain clay displacement so that impact energies can be matched between live experiments and FE simulations. This is investigated by first determining the environmental factors to condition the clay according to the NIJ standard, and then by using the BABT impactor at differing velocities to impact the clay so that a relationship can be formed.

8.2 EXPERIMENTAL METHODS

All clay preparation was undergone as outlined in the NIJ standard section 4.2.5, *Armor Backing Material*. (U.S. Department of Justice, 2008) Only one type of clay can be used for the NIJ standard in testing body armor, Roma Plastilina No.1 made exclusively by Sculpture House (USA). This gray-green clay is oil-based and therefore will not dry out if left open to the atmosphere. The clay fixture was made of rigid wood (4.2.5.2 (U.S. Department of Justice, 2008)) with dimensions compatible with the minimum shot-to-edge distance (7.6.1 (U.S. Department of Justice, 2008)). Clay calibration is in the form of a drop test from 2m with a steel sphere (P/N 3606, Salem Specialty Ball Co., West Simsbury, CT) with mass 1043g and diameter 63.5mm. For the clay backing material to be validated for testing, it must be heated, allowed to cool to a specific temperature, and then undergo the ball drop test. The drop test must consist of at least five drops with a depth measurement mean of 19mm, and no indentation shall be more than 22mm or less than 16mm (4.2.5.6 (U.S. Department of Justice, 2008)). It is important to note that the depth measurement must be done from the outside edge of the clay which represents the initial surface; it cannot be done from the edge of the crater, as this is a common and imprecise mistake.

The exact temperatures for the clay in accordance with the standard are not listed in government documents available to the public or in the literature, so the results of the calibration tests will be documented here for further use. There are two unknown temperatures: the preconditioning temperature and the testing temperature. Preconditioning temperatures of 30-55°C were tested, and it was found that the preconditioning temperature only mattered for the uniform smoothness of the clay: the clay becomes liquid around 55°C. Otherwise, the most important aspect of the clay validation is having a uniform testing temperature. Through execution of the drop test calibration depths, the testing temperature was found to be at ≈27.22°C.

Figure 8.2.1

Fig 8.2.1 – Image depicting clay BFD from high speed testing

This indicates that any testing with the clay at room temperature (≈22°C) is invalid for the NIJ standard for testing body armor.

The impacts into the clay were performed using the DRAGun test setup and BABT impactor described in Chapter 6. The clay was positioned at the launch-end of the DRAGun so that the smoothed impact surface was perpendicular to the open end of the tube. The clay was preconditioned before each test to the testing temperature, and was tested within 10 minutes to eliminate any temperature variances. The clay was tested at the same two speeds as the PMHS (Chapter 6): a low speed of around 28m/s and

a high speed of around 64m/s (Figure 8.2.1). Five tests were performed at the low speed, four of those at 27.22°C, and three at the high speed, two at 27.22°C. To look at the effects of prolonged exposure to room temperature on the ballistics clay, one run from each velocity level was brought to testing temperature and then allowed to rest for an hour before testing. This resulted in a clay temperature of 25.56°C. Once impacted, the clay BFD was measured in accordance with the NIJ standard (4.2.5.4-6 (U.S. Department of Justice, 2008)) by using the non-impacted edges of the fixture as a reference surface for the indentation, not the risen edges of the indentation. After each test, the clay was reconditioned and smoothed for subsequent tests. See Appx. B.2 for images corresponding to the clay testing process.

8.3 IMPACTOR FOR SIMULATING BABT

The DAS within the impactor along with outside sensors described in the methods of Chapter 6 result in measures of acceleration, velocity, and displacement for the interaction between impactor and clay. Paired with the known mass of the impactor, energy at the time of impact (t=0) can be achieved. This energy measure can thusly be associated with specific clay displacements and used as a form of comparison in the field of BABT research. More importantly for the current research, the velocity of the impactor at time of impact is known and sufficiently correlated with displacement into ballistics clay. This makes the impactor the best choice to be used in future BABT simulations.

The BABT impactor, through the testing described in Chapters 6 and 8, has the most amount of correlation to body armor and the clay standard than any other method currently in use for modeling BABT. By taking the armor itself from consideration, this allows focus on the interaction between BFD and the backing, whether ballistics clay or a wearer of body armor. The FE impactor part (Chapter 6) allows for directly comparable boundary conditions seen in both the experimental testing of a PMHS and the experimental tests determining displacements into the clay. This also follows the precedent set that when modeling BABT, the BFD interaction is achieved through the use of a projectile acting on a human body model. In the study done by Cronin et al., the authors even indicate that a hemisphere produces the same results as a dynamic BABT BFD shape, (D. S. Cronin et al., 2021a) thus proving that the BABT impactor profile can be applied for different hard armors. Therefore, the impactor used here is hereby used for all BABT simulations.

8.4 DISCUSSION OF RESULTS

Table 8.4.1 contains a summary of BFD measures for all testing. The low speed clay tests at 27°C had average velocity 27.72m/s and clay depth 16.63mm, with standard deviations ± 0.5 m/s and ± 0.75 mm (95% CI ≤ 2% of the mean for both cases). Since the variance in displacement for a specific velocity is much smaller than the difference in displacement for differing velocities, it is sufficient to use single data points to represent each of the different velocities. Likewise, a data point for the same velocity with differing temperature is sufficient to represent the trend, since inter-temperature variance of tests with the same velocity is much lower than values for differing temperatures. Knowing that the clay may be sitting outside the conditioning chamber and open to environmental temperatures for an extended length of time during body armor testing, this temperature-dependent response needs to be addressed. The ballistics clay was chosen for its repeatability, so it can be assumed that most error in clay displacement measures of body armor come from temperature differences while testing. This is evident in a study performed by Sonden et al.; a uniform rectangular piece of hard body armor was placed in front of clay, shot, and the BFD measured. The BFD measure was 28mm, yet despite having uniform armor and identical testing conditions, the authors report a range of BFD of 24 – 31 mm. (Sondén et al., 2009) Since all of the equipment was the same, it must be assumed that the error in BFD in clay comes from temperature differences.

With the results outlined in Table 8.4.1, a relationship between clay displacement and impactor velocity can be determined (Figure 8.4.1) using an exponential fit ($y=17e^{0.03x}$). (Buchely et al., 2016; Hernandez et al., 2015) Due to the quasi-linear nature of the data for the BABT-range of strain rates, goodness of fit is measured by r^2, which calculates at 0.9987. The error corridor was made using the low temperature data (25.5°C); the corridor is the estimated error on variance in temperature utilizing the fitted data. Because the impactor velocity and clay displacement relationship is quasi-linear for BABT strain rates, differing displacements at other temperatures can be assumed quasi-linear as well.

This correlation found relating clay displacement and BABT impactor velocity through energy at impact is important to the future modeling of BABT events. The results outlined in this chapter are further verified by Wen et al. The study observed BFD into gelatin using high speed video, and profile shape, displacement, and velocity measures from the study are in line with the current research. (Wen et al., 2015) By limiting impacts to a single interaction, and connecting impacts to a widely used standard, outcomes from BABT are more easily identified and recorded. This chapter has established an accurate method for quantifying the effect of BABT clay information, and proven the utility of a standard impactor to compare BABT data from different sources. As far as modeling BABT interactions, the relationship

gained between impactor velocity and clay displacement allows for matched testing of the live-porcine studies and FE human body simulations. This is possible by matching the energy input of the actual impact into the specimen, whether live-porcine or GHBMC. Through this current chapter's research, and the research described in Chapters 6 and 7, BABT interactions that include lung damage can be modeled, and that model can be used to compare and recreate BABT experiments found in literature.

Table 8.4.1

Test	Velocity (m/s)	Displacement (mm)	Temperature (°C)
Clay 1	27.9	9	25.5
Clay2	26.7	16	27.2
Clay 3	27.8	16	27.2
Clay 4	27.8	17	27.2
Clay 5	27.7	17.5	27.2
Clay 6	58.3	37	25.5
Clay 7	72.0	49.5	27.2
Clay 8	64.2	46	27.2

Table 8.4.1 – Table depicting the specific velocity, BFD measure (displacement), and clay temperature at time of test for each test performed

Figure 8.4.1
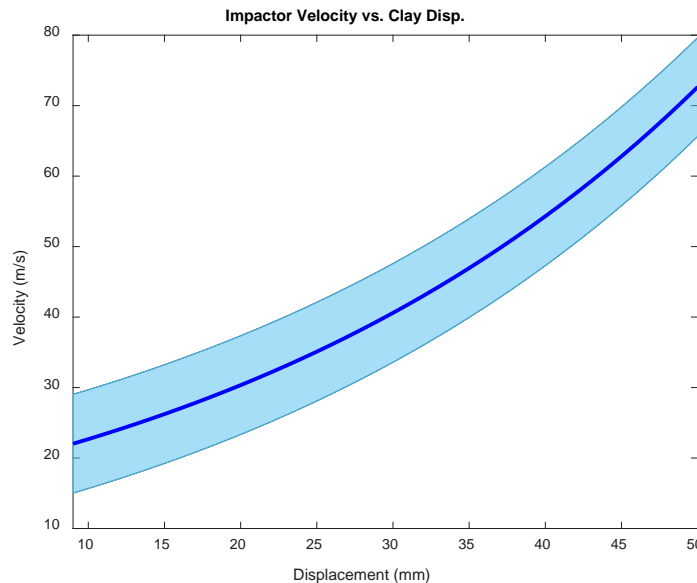
Fig 8.4.1 – Relationship between impactor velocity at impact and displacements into clay. Dark middle line represents the fitted data, while the shaded corridor is the error based on temperature difference found during testing

94

CHAPTER 9: Prediction of Pulmonary Contusion from Lung Damage

***See NOTICE after Chapter 5

Once a method for modeling lung damage in BABT is established, attention can be turned towards methods for determining volume of PC from BABT-type impacts. First, this is explored through connecting the volume of lung damage output from the model with reports of PC volumes from live-porcine experimental testing present in the literature. For BABT impact testing, the methods of modeling impacts as determined by Chapters 6, 7, and 8 allow for matched input conditions between the GHBMC and the live-porcine testing to achieve a damage volume in the lung.

9.1 MOTIVATION

Pulmonary contusion (PC) has been reported to peak within 24-48 hours after initial injury, respiratory distress peaking as much as 72 hours later. (Cohn, 1997; Cohn & DuBose, 2010) This provides an immediate problem for ease of diagnosis considering most patients are imaged only upon admission to hospital. Not only is the timeframe of imaging essential, but also the method of imaging. Computed tomography (CT) has long been known to be the best method for diagnosing PC, although many cases rely on X-rays at initial visit. (Cohn & DuBose, 2010; Gayzik et al., 2007; Schild et al., 1989) In the study performed by Schild et al. on live dogs, all specimens with PC could be diagnosed with CT immediately after injury yet only 37% were immediately diagnosable through X-ray. After six hours post-injury, 21% of PC occurrence was missed with X-ray, and at necropsy, it was found that even CT scans underestimated the volume of contusion. (Schild et al., 1989) Due to this discrepancy in findings, cases of PC are only split into two categories: severe PC where ≥ 20% of the whole lung is contused, or moderate PC which is any percentage of contusion under severe. (Jin et al., 2014; C. Miller et al., 2019; P. R. Miller et al., 2001) A method of indicating the volume of PC in patients by means other than imaging would be beneficial since severity of PC may be underdiagnosed or missed altogether.

The need for PC prediction in BABT events is necessary since factors such as immediate respiratory response or early X-ray may not indicate the presence of severe contusion. In military scenarios where combat readiness and mobility are of import, it is a necessary ability to assess risk of PC without imaging techniques to properly mitigate any lung injuries to reduce morbidity. Individuals may not feel symptoms of PC until up to 24 hours later, (Kishorkumar et al., 2015; Meese & Sebastianelli, 1997) and in theater could result in a warfighter risking another BABT event which may worsen existing PC to a severe case. Patients with severe PCs have a higher risk (82%) of developing acute respiratory distress syndrome (ARDS) and pneumonia (50%), along with being admitted to the ICU and requiring intubation – capabilities

that are not common in field. (C. Miller et al., 2019; P. R. Miller et al., 2001) This chapter results in prediction of PC based on lung damage volume, and for BABT uses the identified BFD displacement from the armor's approval with the clay standard – a known variable. In this way, mechanical properties of lung will be linked with damage and PC, so that in-field cases of BABT can be properly triaged and severe cases are not missed.

Since the GHBMC has been assessed for its use in cases of BABT (Chapter 6), it can be used as a tool to relate structural lung damage with PC. The evaluation of PC through mechanical data is possible through the use of live-porcine BABT studies recorded in literature. The determination of the relationship between mechanical damage and physiological PC will be done through two parts: (1) verifying the relationship between PC and damage volume, and (2) using a separate experimental setup to validate the volume of contusion. As mentioned previously in Chapter 3, the assumption remains that porcine data is directly transferable to human body models.

9.2 METHODS

9.2.1 FE model failure volume

The first step in correlating mechanical lung damage with PC is to establish a relationship using an FE model with lung failure criteria and a known volume of PC from a thoracic insult reported in live-animal experimental testing. This consists of FE model runs recreating the live-porcine experimental testing performed by Shen et al. The testing series impacts porcine specimens over the right lower lobe (RLL) of the lung using a cylinder (Ø = 7.52 cm, m = 76 g). These impacts have initial velocities 40.5 – 51.4 m/s and reportedly result in an average of 10% PC volume of the right lung. (Shen et al., 2008b) The GHBMC with updated lung material undergoes the same testing using the boundary conditions described by the study, and an output of lung damage volume is realized through use of the lung failure threshold found in Chapter 7. This strain failure threshold indicates when an element in the lung fails, and all element failure is then volumetrically added to receive total lung volume failure.

As in Chapter 6, the GHBMC M50-O v.6 is used unchanged save for the updated lung material cards. All lung failure thresholding is done in post-process from the LS-DYNA binary output (Appx. B.3). A rigid cylindrical shell was meshed with the dimensions and mass of the cylindrical impactor described in the study, (Shen et al., 2008b) and the placement can be seen in Figure 9.2.1.1. The placement of the impactor was also matched to the study, contacting the torso in the area of the RLL. The cylinder was

Figure 9.2.1.1　　　　　　　　　　**Figure 9.2.2.1**
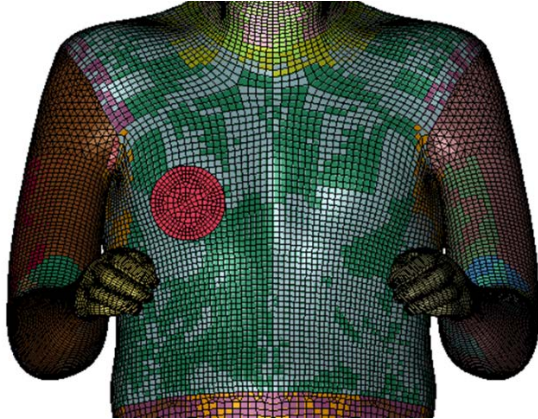
Fig 9.2.1.1 – Image depicting the placement of the cylindrical impactor on the GHBMC thorax
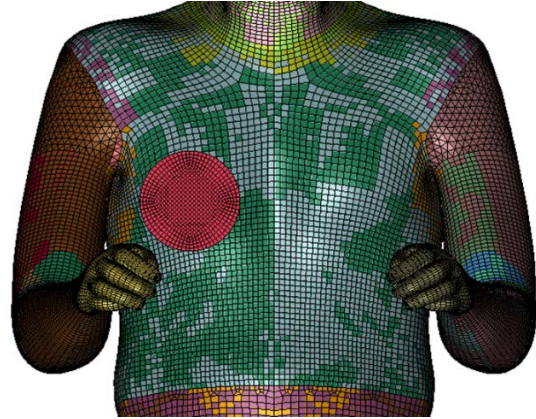
Fig 9.2.2.1 – Image depicting the placement of the BABT impactor on the GHBMC thorax

bounded to movement in the x-direction so that a direct impact could occur. All parts were subjected to gravity, and no other boundary conditions were employed onto the GHBMC so that it may react organically.

9.2.2 BABT validation

Once a relationship is determined between elemental failure and PC using the Shen et al. cylinder, validation from a separate study should occur to ensure the accuracy of results. Since this research is focused upon predicting pulmonary damage in BABT, a live-porcine BABT study will be used to confirm the correlation. In the study performed by Sonden et al., porcine subjects were subjected to BABT while wearing either hard plate armor (ceramid and aramid body armor) or hard plate armor in conjunction with a trauma attenuating backing (TAB). These had reported depths into clay (via the NIJ clay standard) of 28 mm and 19 mm respectively, which can be transferred into input conditions usable for FE modeling. (Sondén et al., 2009) From Chapter 8, the BABT interaction in the porcine specimens can be recreated through a FE model since the relationship is known between BFD of clay, reported by studies, and the BABT impactor from Chapter 6, used with the GHBMC.

Just as in the above section, the GHBMC is used for all simulations with the same boundary conditions. The difference in model setup is the exchange of impactors and initial impact energy. The BABT impactor is positioned with the same centroid as the cylinder; both cited studies indicate an impact position on the RLL of the lung (Figure 9.2.2.1). (Shen et al., 2008b; Sondén et al., 2009) The BABT impactor is given initial velocity 38 m/s to match the impact energy from a 28 mm insult into clay and 29.5 m/s to

match the 19 mm insult. In this way, the impact energies seen in the study from use of hard body armor and the addition of TAB are recreated. The impactor is restricted to movement in the x-direction, and save for a prescribed initial velocity is otherwise unbounded.

The study by Sonden et al. reported an average PC measure for each category of experimental testing. The mean PC reported was an area measure from X-ray imaging, which was 56 ± 22 cm^2 for the standalone hard armor, and 19 ± 6 cm^2 for the armor paired with TAB. To achieve a PC volume to be comparable to other studies, a method was employed to convert PC seen by X-ray to a volumetric PC measure such as those calculated from CT. The methodology, described thoroughly in Appx. B.3, produced volumetric PC of 25.5% ± 10% (armor) and 8.7% ± 4% (armor + TAB) for the right lung. These volumes are used for comparison to the simulation output for failure volume.

Figure 9.2.3.1
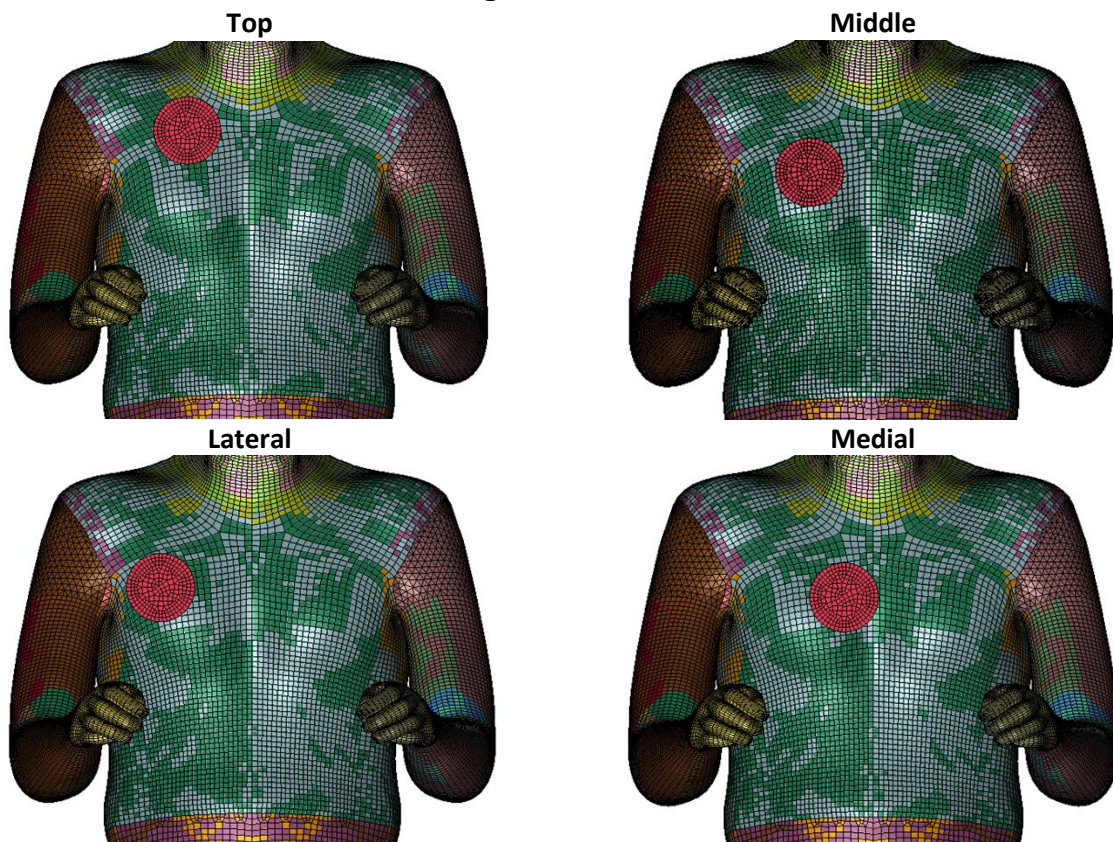
Fig 9.2.3.1 – The impact locations of the location sensitivity study with the cylindrical impactor. "Top" refers to a position on the upper lobe of the right lung, "middle" is a central location, "lateral" and "medial" are determined from the middle location.

9.2.3 Location sensitivity study

While Shen et al. gives an exact impact location for the right lung, this is not necessarily the case for other live-porcine BABT studies. (Shen et al., 2008b) Additionally, intra-specimen variability can cause different effects in the spread of PC after injury. To make certain of the effectiveness in PC injury prediction, a location sensitivity study was performed by varying the impact location on the right lung. With consideration for the size of impactors, four additional locations were chosen to explore impacts on all areas of the right lung: top, middle, medial, and lateral. Top refers to the upper lobe of the right lung, middle to a central location, and medial and lateral are in respect to the center of the right lung (Figure 9.2.3.1).

Both studies simulated in this chapter had varied location runs to determine the sensitivity per impactor type. The Shen et al. location runs, seen in Figure 9.2.3.1, were performed at the median velocity impact of 45.53 m/s. (Shen et al., 2008b) To further develop an understanding of the impact's damage result in regards to location about the ribs, an additional sensitivity study was performed in which rib element erosion was turned off. All locations for the cylindrical impactor were tested both with allowing rib failure and subsequent element erosion, and without any allowed boney failure. The Sonden et al. location runs were simulated with the BABT impactor using the same centroid coordinates as the cylindrical impactor. For the location study, the impact velocity corresponding to the 28 mm clay depth was chosen in order to represent an unaltered hard body armor.

Table 9.3.1.1

Run	Initial Vel. (m/s)	Energy (J)	Damage Vol.
1	51.4	100.4	6.3%
2	41.8	66.4	4%
3	42.29	68	4.3%
4	40.5	62.3	3.6%
5	46.96	83.8	5.2%
6	45.53	78.8	4.9%
7	45.66	79.2	5%
8	46.24	81.2	5.1%
9	45.14	77.4	4.8%
10	45.53	78.8	4.9%

Table 9.3.1.1 – Results of the Shen et al. simulations. Initial velocity is referring to that of the cylindrical impactor, and energy is the energy at impact. The damage volume is the output of the model, to be compared to ~10% reported (Shen et al., 2008b)

9.3 RESULTS

9.3.1 Failure to PC

Impacting the thoracic region of the GHBMC and applying the lung failure threshold (Appx. B.3) resulted in a volume of lung damage with respect to whole lung volume. The Shen et al. simulations consisted of replicating ten specimen runs with impactor velocities seen in Table 9.3.1.1. These experimental tests resulted in "about 10%" of PC located in the RLL. (Shen et al., 2008b) The damage volume for the right lung from each of the FE simulations can be seen in Table

9.3.1.1, and had a mean value of 5% ± 1%. Since the failure volume was well within a magnitude of the PC volume and that is the precision limit of prediction for the GHBMC, there is therefore no need of a scale factor or transfer function. The damage volume resulting from the model reflects the PC volume present an hour after injury.

To validate the relationship between FE lung damage volume and experimentally present PC, simulations with a different impactor and initial boundary conditions were performed. The results from the Sonden et al. runs can be seen in Table 9.3.1.2, along with the calculated volume measures. These two FE simulations represent mean values for the experimental body armor tests (N=10) and the armor with TAB tests (N=5). (Sondén et al., 2009) Since the average value of PC among specimens is reported, the calculated measure of PC from the model can be recognized as the average PC volume response from that level of BABT. Figure 9.3.1.1 shows the frontal and lateral views of the GHBMC right lung from the 28mm and 19mm insult. In the figure, failed elements are colored red to show the pattern of PC.

Table 9.3.1.2

Disp. in Clay (mm)	Velocity (m/s)	Energy (J)	PC Vol. (paper)	Damage Vol. (model)
28	38	166	25.5% ± 10%	21.6% ± 8%
19	29.5	98.6	8.7% ± 4.1%	13.3% ± 4%

Table 9.3.1.2 – Results of the Sonden et al. simulations. Velocity refers to the initial velocity of the BABT impactor, energy is impact energy, PC volume is from (Sondén et al., 2009), and damage volume is the output of the model.

Figure 9.3.1.1

28 mm Insult		19 mm Insult	
Frontal	Lateral	Frontal	Lateral
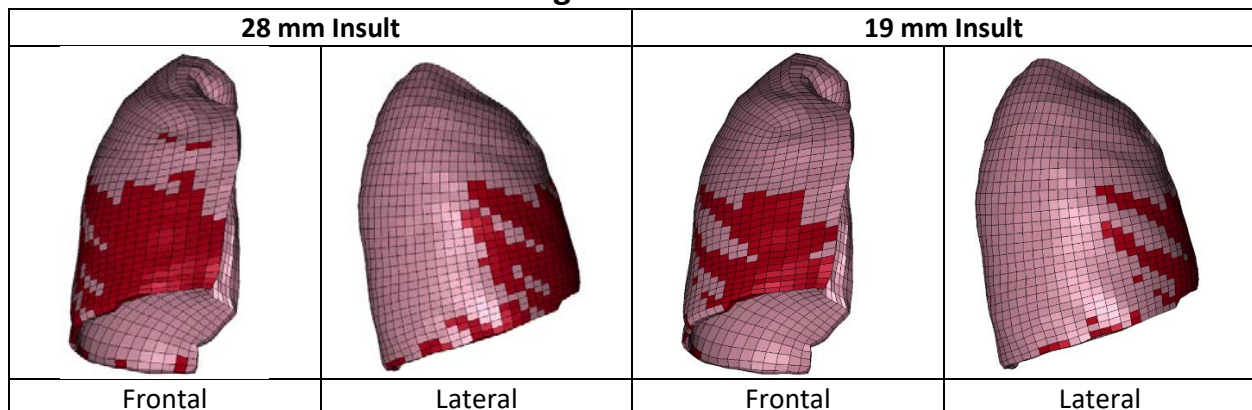
Fig 9.3.1.1 – Images of the right lung of the GHBMC with failed elements shaded red (See Table 9.3.1.2). Depicted are both frontal and lateral views of both levels of BABT insult from (Sondén et al., 2009)

9.3.2 Sensitivity studies

The sensitivity of impactor location onto the GHBMC with respect to lung damage and PC volume was investigated. Although the paper by Shen et al. included an exact location of impact on the right lung, (Shen et al., 2008b) the cylindrical impactor location was varied to examine applicability in instances where impact location is uncertain or unknown. The resulting PC volume measures can be seen in Table 9.3.2.1, with the average PC volume of all locations seen in the bottom of the table. The standardized boundary conditions for the simulations including the GHBMC within this research allows for rib element erosion if the boney failure is reached. To discover if the absence of rib element erosion significantly alters the volume of PC found in the model, separate location tests were run with the Shen et al. impactor with boney failure turned off. Including or excluding rib element erosion did not significantly affect PC volume results, as seen by Table 9.3.2.1. Therefore, lung damage and PC volume results can be considered independent from the GHBMC's rib element erosion criteria.

To ensure that the results of the location sensitivity study were not specific to impactor type, the BABT impactor was also varied by impact location in accordance with the 28 mm insult tests performed by Sonden et al. (Sondén et al., 2009) The PC volumes as they relate to location of impact can be seen in Table 9.3.2.2. Since rib element erosion in the GHBMC was not shown to affect PC volume, the boney failure sensitivity study was not performed for this set of location tests.

9.4 DISCUSSION

This research produces the only damage model of lungs to contain accurate failure criteria from mechanical testing of a human surrogate that can be translated into an appropriate PC risk for BABT. The

Table 9.3.2.1

Location	PC Vol.	Without Rib Erosion
Top	11.7%	11.6%
Middle	9.4%	9.4%
Lateral	7%	7%
Medial	5.25%	5.3%
Bottom	5%	5%
Average:	7.9% ± 3%	

Table 9.3.2.1 – Location sensitivity results for (Shen et al., 2008b). "Bottom" refers to the RLL

Table 9.3.2.2

Location	PC Vol.
Top	36.5%
Middle	33.1%
Lateral	38.5%
Medial	13.7%
Bottom	21.6%
Average:	28.7% ± 10.6%

Table 9.3.2.2 – Location sensitivity results for (Sondén et al., 2009). "Bottom" refers to RLL

results of this research indicate that structural failure of lung tissue, referred to as lung damage, correlates directly with PC volume at an hour after injury. This is especially evident in the BABT runs where PC volume calculated from the FE model falls within the standard deviation of the PC volume indicated from the paper. (Sondén et al., 2009) To transfer from physical lung tissue failure to PC volume, no scaling factor or function is needed when examining an hour after initial injury. There is a small discrepancy in the Shen et al. tests; the PC volumes output from the model do not match up exactly with the mean reported in the paper. However, the reported mean volume of PC lacked any error calculation or any form of range, which leaves room for ambiguity (e.g., rounding techniques allow the FE results to match the paper). (Shen et al., 2008b)

The lung damage to PC correlation was validated by matching experimental tests with different initial impact energies and impactor shapes. Likewise, those results were tested for applicability in regards to different thoracic impact locations over the right lung. Interestingly, the location that resulted in the greatest volume of PC was not the same for the BABT impactor as it was for the cylindrical impactor. This could be an effect of the shape of the BABT impactor's profile, or could possibly indicate that the impact location on the right lung is not a great contributing factor in the overall PC volume. The location of minimum PC volume was the same for both cases – the medial impact location. This is most likely due to the protection the sternum offers and the overall stability of the ribcage. The GHBMC with updated lung material and failure criteria proves capable of similar lung injury response in differing thoracic impact locations. This shows that localized thoracic insults can be properly modeled in respect to pulmonary response without any anomalous effects.

All testing was completed with focus on the right lung. Insult locations on the torso that exhibit bilateral lung contusions require an experimental basis for confirmation of prediction from a human body model. Further, live-porcine experimental testing with impact locations about the left lung would be beneficial to determine left lung PC prediction in a human body model. There is also the unanswered question of if PC can be caused by impacts not directly over the lung area, e.g., upper abdominal region. As of yet, there is no experimental basis by which to verify any response gained by the GHBMC in these areas of study. Future live-porcine testing should also focus on reporting PC volumes, as most studies only indicate that lung injury occurred and do not quantify. (Drobin et al., 2007; Gryth et al., 2007)

In summary, a relationship was found between structural lung damage and PC volume. This is the first study to ever connect physiological lung contusion with mechanical damage. While this research focuses in the area of BABT, the correlation between lung damage and PC an hour after injury can be

utilized for a variety of impacts. Future studies can use the results described here as a basis to explore

this relationship and validate injury criteria for a range of insults and PC progression.

CHAPTER 10: Investigation into the Relationship of PC and SaO$_2$

***See NOTICE after Chapter 5

To determine methods for predicting PC in BABT events, the case of connecting blood oxygen saturation to levels of PC found through FE calculations in Chapter 9 is explored. This is an investigation into another path towards utilizing the model to predict volumes of PC.

10.1 MOTIVATION

In order to be of use in a clinical atmosphere, the connection of lung damage with a physiological reading easily accessible within hospital would be groundbreaking. In this way, the missed and underdiagnosed cases of PC would be lessened, and medical professionals could gain a better understanding of patient needs and morbidity mitigation. Of course, this is reliant upon the information available within the literature. Throughout live-porcine BABT testing, arterial oxygen saturation (SaO$_2$) has been one of the most consistent recorded readings. When compared to controls, SaO$_2$ has obvious and predictable changes over time in pigs later diagnosed with PC. (Arborelius et al., 2004; Drobin et al., 2007; Gryth et al., 2007; Rocksén et al., 2020; Sondén et al., 2009) Further, SaO$_2$ can be related to PaO$_2$ through the oxyhemoglobin dissociation curve and has some relation to readings from a pulse oximeter, which may be easily useable in-field for BABT cases. Through these relationships, SaO$_2$ can be used as a predictor of PC, particularly to find a threshold between moderate and severe (>20%) PC, and the need for intubation (PaO$_2$ = 60 mmHg; SaO$_2$ = 90%).

Within the live-porcine BABT studies, the porcine specimens were monitored for two hours after impact with readings approximately every 30 minutes. (Arborelius et al., 2004; Drobin et al., 2007; Gryth et al., 2007; Rocksén et al., 2012) Time points need to be evaluated based on both trends within the experimental data, and reasonable times in which a patient of BABT may receive medical care or be admitted to hospital. The time point of an hour (60 minutes) was chosen to compare to volumes of PC found in other studies, so that a direct correlation could be made with the output of PC volume from the FE model. (Shen et al., 2008b; Sondén et al., 2009) This time point is also reasonable for in-field military personnel to receive first aid or other medical assessment. (Carr et al., 2016) The other time point investigated within this chapter is 30 minutes after impact, due to the trend in SaO$_2$ data. The mean specimen response in all studies indicates that the lowest reading in oxygen saturation occurs near half an hour after initial injury, and then steadily rises in cases of surviving specimens. Since 30 minutes is a reasonable time for other wearers of body armor such as law enforcement or security personnel to receive

medical care, the time is also included in the investigation. The goal of this chapter is see if a relationship can be found between SaO_2 and measures of PC from damage found in Chapter 9 through the GHBMC, since the vast majority of live-porcine BABT testing includes physiological readings, but no experimentally found volume of PC. There is also investigative insight into SaO_2's possible correlations with PaO_2, the need for supplemental oxygen, and the severity threshold of PC.

10.2 METHODS

Utilizing the clay to BABT impactor relationship found in Chapter 8, impact boundary conditions were determined for the live-porcine BABT testing through the reported depth in clay from the deformation of body armor. This information gained regarding the impact conditions can be seen in Table 10.2.1 for all studies of BABT testing that include SaO_2 readings.   From the impact conditions, the GHBMC is utilized to represent the specimens during impact. The FE simulations are set up likewise to the methods of Chapter 6 and 9. The impact location is on the thorax above the RLL of the right lung, and the velocity of the BABT impactor is varied to represent the different experimental energies listed in Table 10.2.1. After the BABT simulation, elemental lung data from the GHBMC is processed to obtain a volume of lung damage from the BABT impact. From Chapter 9, it is assumed that the volume of lung damage output from the model is comparable to the mean volume of PC seen in the specimens at an hour after impact.

After data has been collected from all BABT simulations, the volume of PC, gained through the FE model, for each case is compared to the readings for oxygen saturation. As mentioned above, two time points in the post-impact observation of the specimens are considered for investigation: SaO_2 at 30

Table 10.2.1

Study	Disp. in Clay (mm)	Calculated Energy (J)	Impactor Vel. (m/s)
Sonden 2009	28	166	38
Sondon 2009	19	98.6	29.5
Gryth 2007	34	236	45.6
Gryth 2007	40	335	54.3
Arborelius 2004	23	124.4	33
Drobin 2007	28	166	38
Gryth 2008	28	166	38
Rocksen 2012	42	376	57.5
Rocksen 2020	28 - 30	180	40

Table 10.2.1 – Test matrix for runs connecting BABT studies with PC and SaO_2. Displacement in clay is a measure for the specific armor used in the study, energy refers to calculated energy at impact (Chap. 8), and impactor velocity refers to the BABT impactor (Chap. 8)

minutes and at 60 minutes, as a mean value among tested specimens. All BABT studies report physiological readings as the mean among specimens save for one (Gryth et al., 2007). In this case, the mean among specimens undergoing the same impact conditions was calculated, and error was taken as the standard deviation. Only specimens that survived for the whole of the observation period were counted within the mean. (Gryth et al., 2007) It should be noted that the readings in the study (Rocksén et al., 2012) include specimens that died before sacrifice at the end of the two hour monitoring period.

10.3 RESULTS AND STATISTICAL ANALYSIS

Simulations on the GHBMC were run recreating the conditions of the live-porcine testing to determine a resulting volume of PC. That volume of PC can be seen in Table 10.3.1 along with the reported values of oxygen saturation levels in the impacted specimens at 30 minutes and 60 minutes after impact. Table 10.3.1 does not contain the error ranges for SaO_2 or PC. Error for PC comes from Chapter 8, and error for SaO_2 comes directly from the error reported in the studies for the specific time points. A scatter plot showing the PC and SaO_2 data for each time point can be seen in Figure 10.3.1 along with error bars. This plot is shown in SaO_2 versus PC to help determine a relationship between the two quantities.

Even with the uncertainty observed through the error bars in Figure 10.3.1, the data should be treated as relevant since the large error on each data point stems from the low number of studies. Therefore, a statistical analysis was performed on the data in which the individual data points were weighted by the number of specimens included in each study. This way, the mean from the study of 12 experimental specimens held more weight in overall trend then the study with 4 experimental specimens. Both linear and nonlinear correlation methods were attempted, and it was found that the relationship between PC and SaO_2 was linear (Figure 10.3.2) so a Pearson correlation (Appx. B.3) was used to determine statistical significance, where a correlation of -1 means that all data is perfectly in-line (for a negative slope). The analysis found that the relationship was significant for both time points, and specific values can be seen in Table 10.3.2.

In some medical instances, such as determining the necessity of supplemental oxygen, PaO_2 (partial pressure of oxygen) readings may be a better option to determine patient outcome. PaO_2 is related to SaO_2 through the oxyhemoglobin dissociation curve (Figure 10.3.3), so data can be easily converted. Using the same statistical methods as the SaO_2 readings described above, PaO_2 is compared to PC using a weighted Pearson correlation. The results, seen in Figure 10.3.4 and Table 10.3.3, indicate that there is also a significant linear relationship between PaO_2 and PC for both time points.

A determined relationship between PC and oxygenation readings allows for the investigation into certain threshold values. Values that would be important into the prediction of PC and patient outcome are the thresholds in SaO_2 and PaO_2 that might indicate the necessity of supplemental oxygen (90% and 60 mmHg respectively), and the threshold of PC for which cases are labeled severe (20%). To find if there is any significance at these thresholds, a t test was performed on each set of data. It was found that the thresholds held no statistical significance (p values > 0.5), mainly due to lack of data. There was not enough data from the literature concerning values above the thresholds for SaO_2 and PaO_2, and values below the 20% PC volume threshold.

Table 10.3.1

Study	N	PC Vol. (FE) (%)	SaO_2 – 30 min (%)	SaO_2 – 60 min (%)
Sonden 2009	10	21.6	85	91
Sondon 2009	5	13.3	92.5	94
Gryth 2007	4	29.4	84.5	84
Gryth 2007	4	36.9	71	78
Arborelius 2004	10	16.7	86.5	92
Drobin 2007	8	21.6	91.5	93
Gryth 2008	11	21.6	86	91.5
Rocksen 2012	12	39.9	50	60
Rocksen 2020	7	23	87	93

Table 10.3.1 – Results for the simulations recreating the studies seen to the left. N refers to the number of specimens that underwent BABT impacts, PC volume is an output of the model, and SaO_2 readings are listed as reported by the studies for times of 30 minutes and 60 minutes after impact

Figure 10.3.1
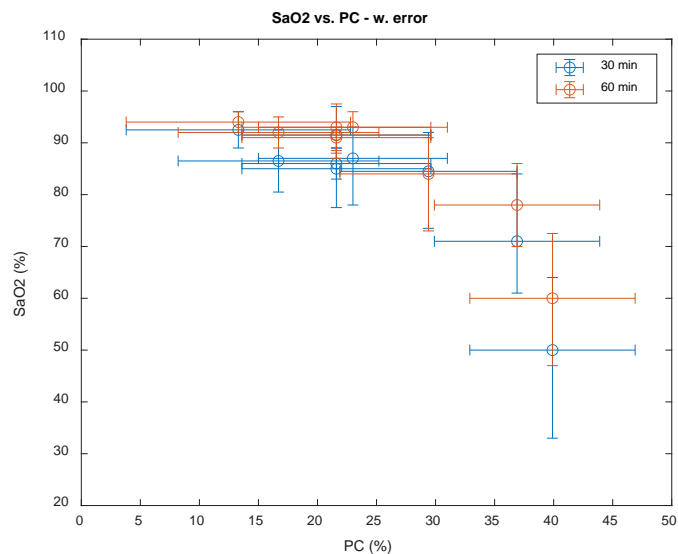
Fig 10.3.1 – Plot of SaO_2 values versus model PC volume outputs with error. Values obtained at 30 minutes are colored blue, and 60 minutes orange

Figure 10.3.2

SaO2 vs. PC
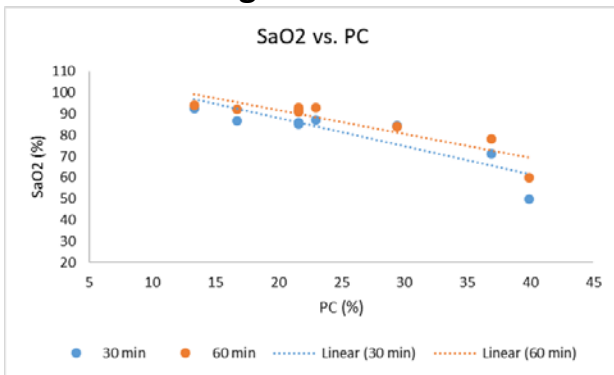
Fig 10.3.2 – Plot of SaO$_2$ versus PC were 30 min values are in blue and 60 min in orange, showing linear trendlines for each

Table 10.3.2

	Correlation	Std. Error	P Value
30 min	-0.91217	0.187	0.03
60 min	-0.9268	0.175	0.0272

Table 10.3.2 – Values for the statistical correlation between SaO$_2$ and PC. Correlation refers to the Pearson correlation

Figure 10.3.3

Oxyhemoglobin Dissociation Curve
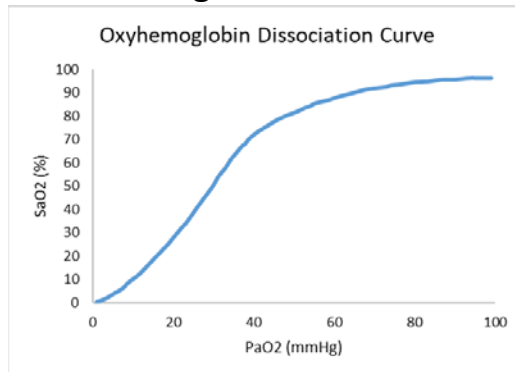
Fig 10.3.3 – The oxyhemoglobin dissociation curve that shows the relationship between SaO$_2$ and PaO$_2$

Figure 10.3.4

PaO2 vs. PC

Table 10.3.3

	Correlation	Std. Error	P Value
30 min	-0.92277	0.180	0.0272
60 min	-0.9622	0.150	0.016

Fig 10.3.4 – Plot of PaO_2 versus PC were 30 min values are in blue and 60 min in orange, showing linear trendlines for each

Table 10.3.3 – Values for the statistical correlation between PaO_2 and PC. Correlation refers to the Pearson correlation

10.4 DISCUSSION

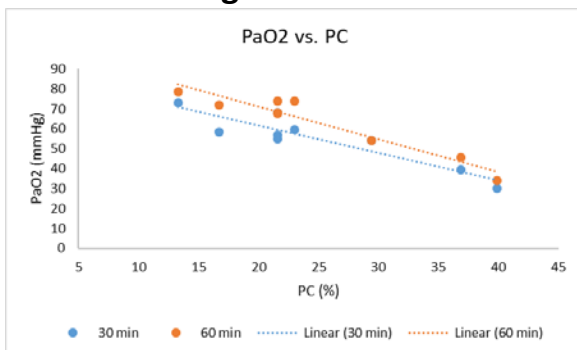There are many BABT studies on live porcine specimens that do not include information on lung injury or any measures of PC. Instead, the focus is on vital readings during a two hour time period after impact. (Arborelius et al., 2004; Drobin et al., 2007; Gryth et al., 2007, 2008; Rocksén et al., 2012, 2020) This chapter helped to make these studies useful in the area of PC prediction by using simulations to connect the studies with a PC volume. Figures containing the images of the GHBMC lung with failed elements indicated for all simulations of the live-porcine testing are located in Appx. B.3. By relating these studies with lung damage through the GHBMC, the physiological readings can have some connection to input conditions from the impact itself. This allows the studies to be included as data points for future BABT work.

The results of this chapter cumulate in a significant trend between SaO_2 or PaO_2 and PC. This has never been definitively shown, and has great impact not only in biomechanics, but in the medical field as well. Knowing that PC causes a dip in oxygen saturation 30 minutes to an hour after injury can possibly lead to better mitigation techniques and more consistent diagnoses of PC. For the field of injury biomechanics, mechanical failure of a tissue can be linked to a physiological symptom. These correlations, of course, require more data to be appropriately established. Within this current research and the availability of studies described in literature, there is enough data to establish a trend, but not enough to develop correlations regarding specific values of, for instance, PaO_2 for a certain volume of PC. The presence of a significant relationship between the readings and PC indicates that with more data, it should be entirely possible to determine thresholds such as the SaO_2 reading at an hour after injury that indicates severe PC. Future work in the area of live-porcine BABT testing should focus on non-injurious impacts, and impacts that would create moderate PC (<20%), since this is where the current data is most lacking. The severe PC threshold range should also be explored in more detail by slightly varying hits that are predicted to produce 20% volume of contusion. By exploring the PC severity threshold, this allows more information on the spread of data between specimens for oxygenation readings. The comparisons found within this chapter are a great start to PC prediction in BABT via physiological readings, but more research is needed to further explore this relationship.

CHAPTER 11: Conclusions

***See NOTICE after Chapter 5

11.1 SUMMARY

Pulmonary contusion (PC) is an injury of the lungs that is difficult to diagnose and can cause later morbidity and mortality. (Ganie et al., 2013; P. R. Miller et al., 2001) PC is especially a concern for the wearers of body armor, since most injuries that occur in-field are blunt thoracic impacts in the form of behind armor blunt trauma (BABT). (Cannon, 2001) In order to mitigate blunt injuries to the lungs, the biomechanical response of lung tissue along with a failure threshold must first be understood. The studies regarding the characterization of lung tissue within the current literature present a challenge, since material models for lung are based in either canine or murine data for which no scaling has been presented for comparison to human. (Stitzel et al., 2005; Vawter et al., 1979) For cases of lung injury, no failure threshold or function for lung tissue has been addressed, so the yield point of lung parenchyma remains unknown to the literature. For cases of BABT, there presents an even bigger challenge for lung injury prediction in that there is no established verification method for modeling BABT events with human body models such as the GHBMC. Further, PC has not been connected to any kind of lung tissue failure metric used in human body simulations, so a method for predicting PC in a human surrogate, especially for BABT, does not exist.

The objective of this dissertation was to create a model for lung tissue that includes a damage threshold, and then utilize the model to predict volume of PC in the case of BABT. This has been achieved through the completion of three aims: the development of a validated lung material model, the modeling of lung damage in BABT, and the determination of a method for predicting PC volume as an output from the model.

The development of a validated material model for lung was a crucial step for accurate modeling of the response of lung tissue during a thoracic impact. To achieve this goal, small-sample testing of lung parenchyma was carried out in quasi-static shear and step-hold shear to gain a dataset for the characterization of the mechanical properties. This data was used to fit parameters of a Hill Foam model, specifically derived for the shear case, paired with a quasi-linear viscoelastic model to account for the relaxation of the material. The fitted parameters, along with experimentally found material parameters, were placed into material cards for finite element (FE) analysis. The small-sample experimentation was replicated to ensure that model response was within a standard deviation of experimental response. For

validation of this material model, step-hold indentation tests were conducted experimentally and the response matched with the FE material model.

Once a lung material model was established, a methodology was employed to model lung damage in BABT events through the use of the GHBMC. Comparative testing was done with a whole body PMHS and the whole body GHBMC. This experimental testing and subsequent simulations recreated BABT events using an impactor, and data collected from sensors on the PMHS were compared to the output of the model. To gain an understanding of the volume of lung damage that results from thoracic impacts, a threshold for failure in lung tissue was determined for implementation into the FE model. Small sample shear testing to failure was conducted, and a strain threshold was achieved. This strain threshold was applied to the lung elements of the GHBMC, and a percentage of damage in the lungs was calculated based on total lung volume. At this point the GHBMC was validated for BABT loading and included a method of calculating lung damage volume, yet could not replicate the BABT experiments found in literature due to a discrepancy in input conditions. To quantify the initial impact energy of the BABT event, live-porcine studies report a depth into clay resulting from the deformation of the body armor whereas the FE simulations translate the deformation of the body armor into a BABT impactor. Consequently, a relationship was found between the displacements into clay from the testing in the literature and the BABT impactor initial velocity so that the GHBMC received the same impact to the body as the live-porcine specimens. With this relationship established, lung damage in BABT events can be properly modeled using the GHBMC.

A resulting lung damage volume gave information on the amount of mechanical lung failure, but insight into the physiological symptom of PC still needed to be attained. Thus, methods for the prediction of PC in BABT were determined. Two studies involving live-porcine thoracic impacts but with different test setups and impact conditions were simulated using the GHBMC. These studies report a measure of PC which was used to correlate PC volume to damage volume as output by the FE model. The results indicated that PC volume could be reasonably assumed to match damage volume at an hour after impact. This allowed the GHBMC to be able to predict PC volume at one hour for any given live-porcine BABT testing. Since a correlation was established between damage volume, as output by the GHMBC, and PC volume, the relationship between the physiological reading of SaO_2 and PC was investigated. This was achieved by using the GHBMC to simulate live-porcine studies that reported SaO_2, but did not necessarily report PC or any other injury level. PC volume was gained from the GHBMC, and an overall trend was found between simulated PC severity (as a volumetric measure) and reported SaO_2 levels. However, not enough data was present within the literature to be capable of predicting the exact level of PC from any

physiological reading. However, the results here do show that including additional data could make this method of predicting PC from physiological readings in BABT events a viable solution.

11.2 MAJOR CONTRIBUTIONS

Throughout the development of a lung material model, the simulation of BABT loading scenarios, and the investigation into PC volume prediction methods, knowledge was gained in the area of lung biomechanics for which previous gaps existed within the literature. These major contributions are described below:

- This work is the only lung-component testing to be done on a large mammal surrogate for comparison to human. The material model fitted from this testing is the only proposed finite element material model for lung that is not based experimentally in either canine or murine lung data.

- This lung material model is developed with shear sample testing and is the only material model for lung validated using a separate experimental configuration. Therefore, it can be utilized within a variety of modeled scenarios including motor vehicle crashes and other thoracic impacts.

- The failure threshold included in this work is the first method of quantifying lung damage using actual lung tissue. The current research has determined a threshold in strain for which the structure of lung tissue reaches its failure point. Since this failure point is based on the dynamic shearing within lung tissue, this failure threshold is relevant for any damage sub-blast within the lung. This provides an advancement in modeling possibilities since lung damage volume can be achieved for any insult relating to the lungs.

- A methodology for modeling BABT impacts with the GHBMC was created. This was accomplished through developing a relationship between armor deformation measures and the BABT impactor used in the model. The relationship allows for the GHBMC to recreate experimental tests on different hard armors so long as they were approved using the NIJ clay standard.

- This work is the first to establish a correlation between lung tissue failure and PC volume. Achieved through matched pair experimental testing and simulations, a lung damage volume output from the FE model is correlated to PC volume at an hour after impact.

- Included within this research is the first evidence of a possibly predictive trend between arterial oxygen saturation and PC volume at both time points of 30 minutes and one hour after initial

impact. Since PC can be connected with the amount of lung tissue damage, this is the first evidence of an association between a physical occurrence in lung parenchyma and a physiological symptom.

These major contributions include the most accurate lung model to date and allow for the modeling and prediction of lung damage in all thoracic impact scenarios sub-blast. Further, for the case of BABT, it has been shown that this lung model can be applied to achieve prediction of PC volume based in mechanical tissue failure. With more data, this can be further expanded upon for future PC prediction in other injurious cases and connection to other symptoms.

11.3 ASSUMPTIONS AND LIMITATIONS

As in any scientific work, there exists both assumptions that allow for the furthering of current research with empirical data, and limitations to the conclusions attained. One of these limitations is the use of fresh porcine lung tissue in the place of human lung tissue. This is considered a limitation rather than an assumption due to the evidence in the literature of porcine lung and human lung interchangeability and the preliminary correlation included within this work of lung response between species. (Hozain et al., 2020; Judge et al., 2014; Tenney & Remmers, 1963) It is hypothesized that with more human lung data, porcine lung can be shown to be a 1:1 surrogate for human lung. Although, within this work exists the long-standing assumption in the field of injury biomechanics that cadaveric tissue represents live-human tissue, and the same assumption is being made with cadaveric porcine tissue representing live-porcine tissue. Fresh porcine lung was obtained to limit the differing factors between in- and ex-vivo tissues. However, especially in the case of the lung, certain boundary conditions cannot be replicated. This includes the pressure differences present in each alveolar space throughout the lung during inhalation versus exhalation. All lung tissue was tested in an equilibrium environment – during neither inhalation nor exhalation, but rather an equalized pressure between the two in which the structure of lung remains in a relaxed state. This limits the validity of the material model and the failure threshold in that values may be represented differently at the lung's volumetric extremes.

While the use of porcine lung tissue has limitations, there also exists an assumption in this work concerning porcine anatomy in general. That assumption is live-porcine BABT data being directly transferred and recreated using a human body model. This assumes that injuries resulting from the live-porcine experimental testing coincide with human kinematics as represented by the FE model.

Discrepancies have been found in chest compression levels between the species, (Prat, Rongieras, de Freminville, et al., 2012; Viano & Warner, 1976) but it remains unclear on how chest compression measures affect severity of PC volume. Factors that can also affect transferability of results include the differences in bipedalism versus quadrupedalism, ribcage and other bone structures, organ placement within the thorax, and live subjects versus a static model. Regardless of the limitations, this comparison is necessary as a starting point to progress the connection of PC with lung biomechanics, and this path forward is restricted by the current availability within the literature.

The connection of PC to any kind of kinematic data is extremely important, yet there are limitations surrounding that connection that are important to acknowledge. First, the PC volume prediction portion of the human body model was only investigated for usability in BABT-like events. The lung material model and failure threshold are relevant for any blunt thoracic trauma, but PC measures were correlated specifically for BABT. For use in situations such as motor vehicle crashes, the damage volume measures should be validated with PC volumes for that specific insult. Second, the PC volume correlation is only valid for an hour after impact. PC has been known to change drastically with time and peak a day later, (Cohn & DuBose, 2010) so it is hypothesized that looking at any PC volume after this time point will not result in a 1:1 correlation with damage volume. This also relates to SaO_2 measures in that the maximum dip in readings occurs before the one-hour time point, and studies show that at two hours and beyond readings may equalize. (Arborelius et al., 2004; Drobin et al., 2007) Finally, variability in biological responses of specimens and patients can be large. This measure of PC volume resultant of the model is meant to be a mean response, and a mean response as calculated by a limited number of studies. For an individual specimen, PC volume and SaO_2 can be dependent upon specific biological makeup, and for human patients, can be affected by medications, prior medical histories, presence of other injuries, age, and many more factors. This research is not meant to be a direct diagnostic technique, but rather a step forward in the advancement of PC prediction and mitigation.

The biggest limitation in the prediction of PC for use in BABT loadings is the lack of data regarding PC, BABT, and lung response in general in the literature. More human lung tissue testing could verify the surrogacy of porcine lung tissue. A greater number of live-porcine studies is also needed in order to verify specimen responses and statistical correlations. In a clinical aspect, PC must be observed and reported so that incidence and injury mechanism can be more easily understood. The following section contains more information on exactly which areas of research need to be fortified to achieve a better prediction measure for PC.

11.4 FUTURE WORK

This dissertation provides major contributions to the field of lung biomechanics, and works to fill holes previously seen within the literature. Throughout the research conducted in this work, the necessity of future research became evident by either the lack of relatable and/or comparable data, or in order to continue the progression along the current path. Areas of future work are described below:

- There should be a push to increase field data related to PC. Observed cases in hospital should be reported, so that for all incidences of PC a better idea can be gained on the progression of the injury and symptoms in different forms of blunt thoracic trauma. This can include retrospective studies, so the outcome of patients is known. Particularly for cases of BABT, more in-field information should be made available to better understand the issue of injury mitigation.

- The relation of rib fracture to PC severity, if existing, should be addressed. Specific studies or experiments solely focusing on the possible connection between rib fracture number and PC severity should be performed. Whether the breaking of ribs dissipates energy in relation to the lung and therefore alleviates PC volumes, or if the fracture of ribs causes greater force in relation to the lung and therefore worsens PC volume levels needs to be answered.

- In regards to porcine lung as a human surrogate, or any other choice for lung surrogacy, more testing on human lung tissue must be performed. Particularly in the case of porcine lung tissue, a greater number of human lung specimens (N) is needed to confirm that no scaling factor is required. A repository of human lung tissue data would also make it possible to evaluate any other human lung surrogate.

- More live testing should be performed with large animal surrogates to report PC levels. Testing should include a variety of test setups and impact scenarios so that the results can be validated among studies. Longer observation periods after testing, perhaps a day or two days after impact, should be considered so that injury progression is understood. All large animal testing involving thoracic trauma should report PC levels, along with the method used to determine injury (i.e. X-ray, CT, necropsy) so that comparisons between studies can be made.

- To use physiological readings as predictors for PC volume, a wider impact severity range needs to be addressed to be statistically relevant. In order to determine the SaO_2 level that indicates severe (>20%) PC, or at what volume of PC an hour after impact causes PaO_2 levels to indicate the

necessity for supplemental oxygen, more data points surrounding these thresholds are necessary. Non-injurious data, in regards to PC and other lung injuries, should be collected to develop a threshold for the onset of PC and to ensure the physiological readings are a product of injury and not just impact.
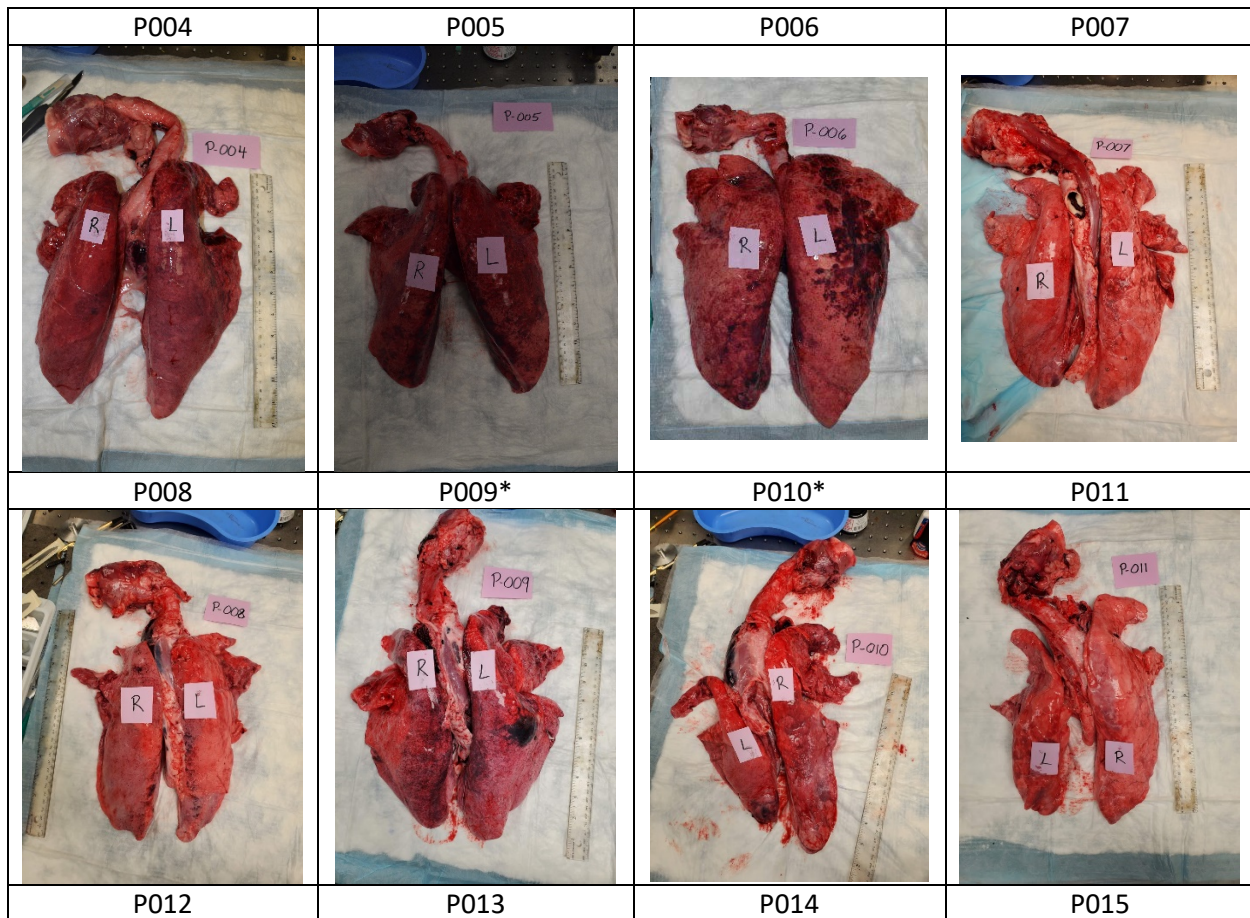
The future work listed above is, of course, not an extensive list concerning the furthering of the current research questions. Any future work concerning the advancement in knowledge of the biomechanical properties and injurious mechanisms of lung tissue would be extremely welcome in the field. There are many avenues not yet explored in the realm of blunt lung injury. The research contained in this dissertation advances the detection and understanding of lung injury significantly, yet it is only the beginning for PC prediction in any blunt trauma scenario.

APPENDIX A: Material Modeling of Lung

A.1 EXPERIMENTAL TESTING

A.1.1 Specimen Images

Below are the images of all whole lung specimens. The specimen number (e.g. P007, H707) is listed above the image of the lung, with 'P' indicating a porcine specimen, and 'H' a PMHS. The specimen number is also indicated by a label in the images, and 'R' and 'L' labels indicate right and left lungs. A special note: for all porcine lungs P004 up until P010 the right and left lung labels are switched. An asterisk after the specimen number indicates that the lung in question had an abnormality or deformed lobe that was not used in any testing.

P004	P005	P006	P007
P008	P009*	P010*	P011
P012	P013	P014	P015

P016	P017	P018	P019
P022	P023	P024	P025
P026*	H707	H984	H1002

A.1.2 Sample Measurements

Below is a table of individual samples and their dimensions for each of the specimens. Each new specimen is denoted by the heading 'P0XX' or 'HXXX.' All samples are listed under the specimen heading: SHS refers to step-hold shear, SHC step-hold compression (indentation), QSS quasi-static shear, and FS failure in shear. The 'LX' or 'RX' references the left or right lung, and the sample number from that lung. The second row of the table contains the titles 'thickness' and 'other,' and the labels should be assumed to extend throughout the whole table. Thickness refers to the measurement between shearing plates for the shear samples, and the height of the cylinder for the compression samples. 'Other' in the case of shear refers to the length and width dimensions (e.g. 7x9 = length of 7, width of 9), and refers to diameter in the compression samples. All measurements are in millimeters.

	P004				P005	
	thickness	*other*			*thickness*	*other*
SHS L1	6	11x9		SHS L1	6	8x10
SHS R1	8	10x10		SHS L2	7	8x8
SHS R2	6.5	7x8		SHS R1	6	9x8.5
SHC L1	8.5	31		SHC L1	10	34
SHC L2	8	28		SHC R1	12	31
SHC R1	9.5	31		SHC R2	9	34
QSS L1	8.5	11x9		QSS L1	7	9x9
QSS L2	7	13x9		QSS R1	8	10x9
QSS R1	7	12x12		QSS R2	8	8.5x9
	P006				P007	
SHS L1	5	7x5		SHS L1	6	8x7
SHS L2	7	10x8		SHS R1	5.5	7x9
SHS R1	6	8x7		SHS R2	6	6.5x8
SHC L1	8	38		SHC L1	12	33
SHC L2	9	34		SHC L2	9	35
SHC R1	10	36		SHC R1	12	36
QSS L1	7	8x8		QSS L1	7	7x5
QSS L2	7	9x7		QSS L2	6	6x6
QSS R1	6	8x9		QSS R1	6.5	6x7
	P008				P009	
SHS L1	6.5	8.5x8		SHS L1	6	6x9
SHS L2	5.5	9.5x8		SHS L2	6	10x10
SHS R1	6	8x8		SHS R1	7	8x7.5
SHC L1	6	36		SHC L1	7	30

SHC R1	11	37
SHC R2	8	38
QSS L1	6.5	7x8
QSS R1	6	9x10
QSS R2	7	6.5x8
	P010	
SHS L1	5.5	7x7
SHS L2	5.5	7x6.5
SHC L1	7	32
QSS L1	6.5	7x5
QSS L2	6	7x7.5
	P012	
SHS L1	9	10x6
SHS R1	6	6x6
SHS R2	7	9x6
SHC L1	10.5	34
SHC L2	12	31
SHC R1	10	31
QSS L1	7.5	7x6.5
QSS L2	8	6x6
QSS R1	7	6x8.5
	P014	
SHS L1	6	10x9
SHS L2	6	6.5x7
SHS R1	6	7x7
SHS R2	5	8.5x7
SHC L1	9	35
SHC L2	14	34
SHC R1	8.5	35
SHC R2	7.5	32
	P016	
SHS L1	6	10x9
SHS R1	6.5	10x10
SHS R2	6	8x6
SHC L1	9	34
SHC R1	11	36
SHC R2	9	31
FS L2	5.5	6.5x7

SHC R1	9	35
SHC R2	13.5	36
QSS L1	6.5	6.5x9
QSS R1	7	10.5x7.5
QSS R2	7	7x9
	P011	
SHS L1	8	8x8.5
SHS L2	7.5	5x7
SHS R1	5.5	6x6.5
SHC L1	9	33
SHC R1	8.5	35
SHC R2	11	30
QSS L1	8	8x7.5
QSS R1	5.5	7x6
QSS R2	5.5	7x7
	P013	
SHS L1	7.5	5x8.5
SHS L2	8	6.5x6.5
SHS R1	7.5	7x6.5
SHC L1	7	35
SHC R1	6.5	35
SHC R2	10	31
QSS L1	7	7x6.5
QSS R1	6.5	7.5x8
QSS R2	9.5	9x7.5
	P015	
SHS L1	8.5	7.5x10
SHS L2	7.5	8x8
SHS R1	8	8.5x9
SHC L1	5.5	32
SHC L2	8	32
SHC R1	8	35
	P017	
SHS L1	5.5	10x10
SHS R1	7	10x10
SHS R2	4.5	7x7
SHC L1	7	32
SHC R1	8	37
SHC R2	8	31
FS L2	4.5	8x7

FS L3	5.5	7x7.5
FS R3	4	4x10
P018		
SHS L1	6	7x7
SHS L2	5	7x8
SHS R1	7	8x6
SHC L1	8.5	35
SHC L2	11	33
SHC R1	10	35
FS L3	4	6x6
FS R2	5	7x8
FS R3	5	6x9
P021		
FS L1	6	7x6
FS L2	5.5	10x9
FS R1	5	7.5x7
FS R2	6	7x8
P023		
SHS L1	6.5	7x6
SHS L2	7	8x10
SHS R1	9	8x6
SHS R2	6	6x8
P025		
SHS L1	7	8x7
SHS L2	6	6x8.5
SHS R1	5	6.5x8.5
SHS R2	5.5	8x7.5
H707		
SHS R1	4.5	10x8
SHS R2	5.5	8x7
SHS R3	6	10x7
SHS R4	6	10x10

FS L3	6	11x8
FS L4	4.5	8.5x6.5
FS R3	5	11x10
P019		
FS L1	5	7.5x7
FS L2	5.5	10x7
FS R1	5	6.5x5
FS R2	5.5	11x7
P022		
SHS L1	7	7x7
SHS L2	7	6.5x5
SHS R1	5.5	7x9
SHS R2	8.5	6x4.5
FS L3	8.5	6.5x3
FS L4	9.5	7x4.5
FS R3	6	6.5x4.5
FS R4	6	8.5x7
P024		
SHS L1	6.5	8x7
SHS L2	7	7x7
SHS R1	8.5	10x8.5
SHS R2	6.5	7x5.5
P026		
SHS L1	6.5	7x7
SHS L2	6	7x6.5
SHS R1	6	7x8
SHS R2	7	7.5x7.5
H984		
SHS L1	9	14x9
SHS L2	8.5	12x14
SHS L3	7	9x10
SHS L4	7.5	12x13
SHS R1	7	11x11
SHS R2	6.5	10x9
SHS R3	7.5	13x12
SHS R4	7.5	15x9

	H1002					
SHS L1	5	10x7				
SHS R1	6	8x9				
SHS R2	5	10x7				
QSS L1	5	6x12				
QSS L2	5	11x8				
QSS R1	4.5	10x9				

A.1.3 Reduction of Noise in Small Sample Testing

A.1.3.1 Test Setup

The Bose machine functions on an isolation table, but the Bose machine itself creates vibrations that can be seen on data traces. The first step in reducing this noise is to determine an offset platform on which to place the stage that holds the sample fixtures. Below is an example of the noise seen with different platform options; 'air' means that the Bose actuator is only moving through air with no other contact. The final option (quadrant IV of the figure) was the option used for all testing. An image of the full test setup can be seen at the bottom of the section.
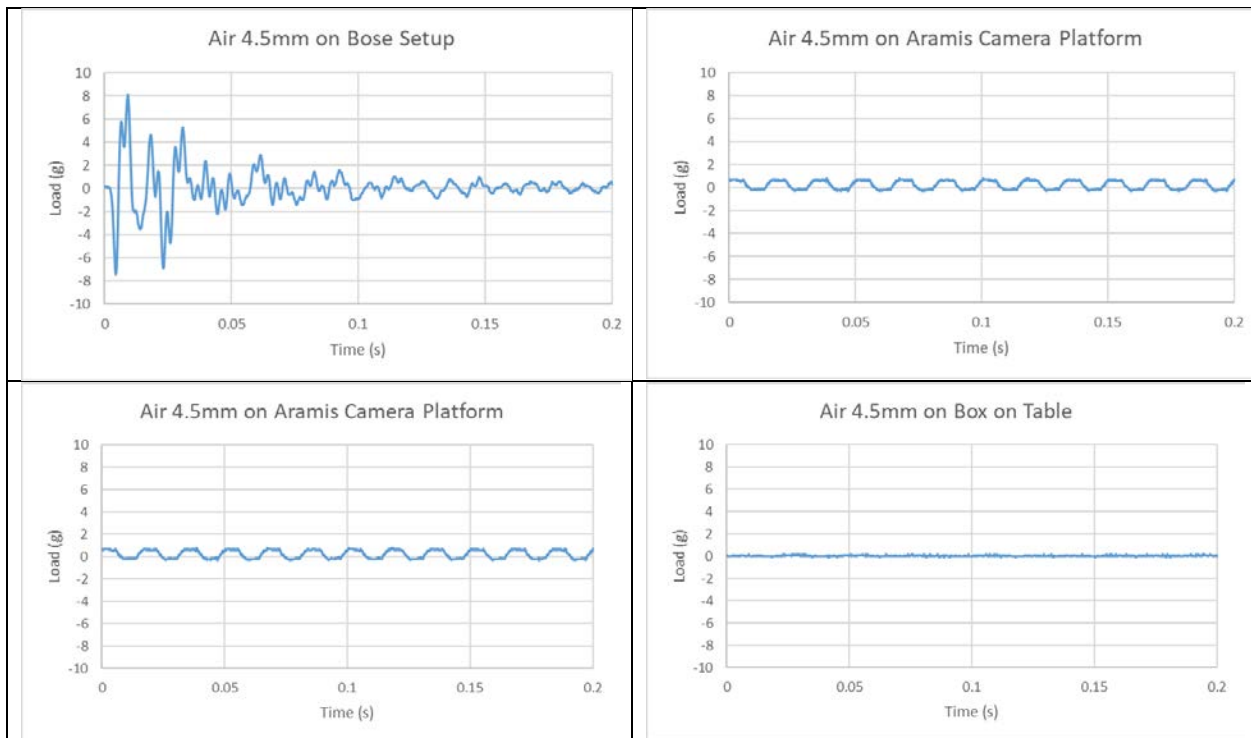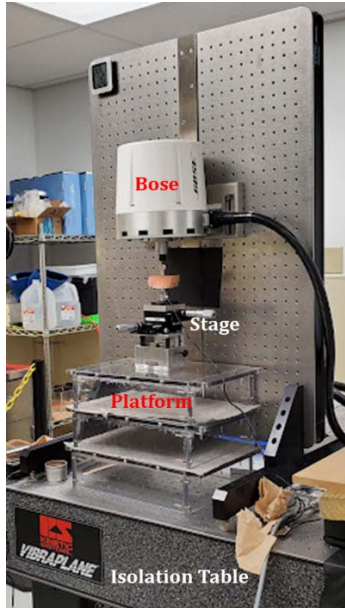
A.1.3.2 Mass Compensation

Even with a noise-cancelling platform, noise was still evident in the data traces from the vibrations of the test fixtures themselves. Therefore, an accelerometer was included on top of the load cell so the acceleration trace could be used in mass compensation. The mass-compensated force was equal to the raw force output subtracted by the accelerometer trace multiplied by half the mass of the fixtures and load cell (20g for compression, 30g for shear). The result of the mass compensation can be seen by the example below, where the blue trace is the original raw data, and the orange trace is the mass compensated data.

Example of Mass Compensation - P023
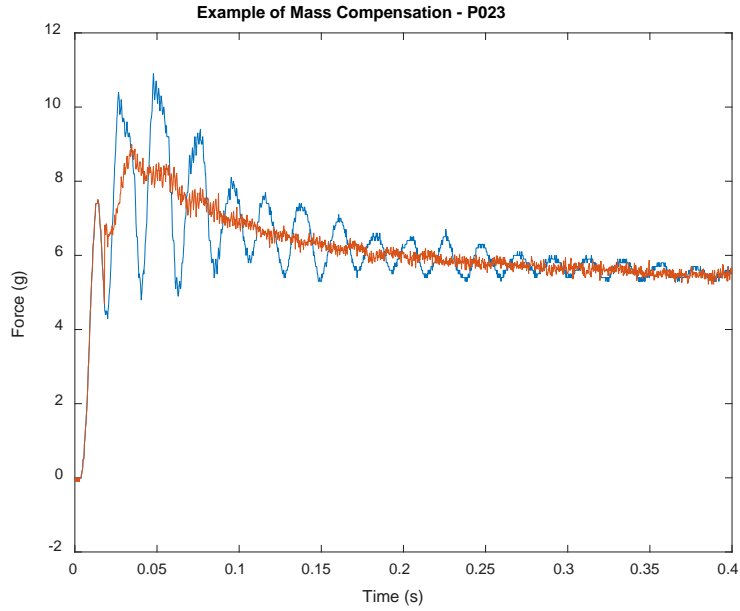
A.1.3.3 Fast Fourier Transform

The final step in noise reduction is filtering. A Fast Fourier Transform (FFT) was performed on the mass compensated data to find the frequency to properly filter the data. An example FFT can be seen below; the frequency 150 Hz was chosen for a low-pass filter.

P005 L2 Shear FFT
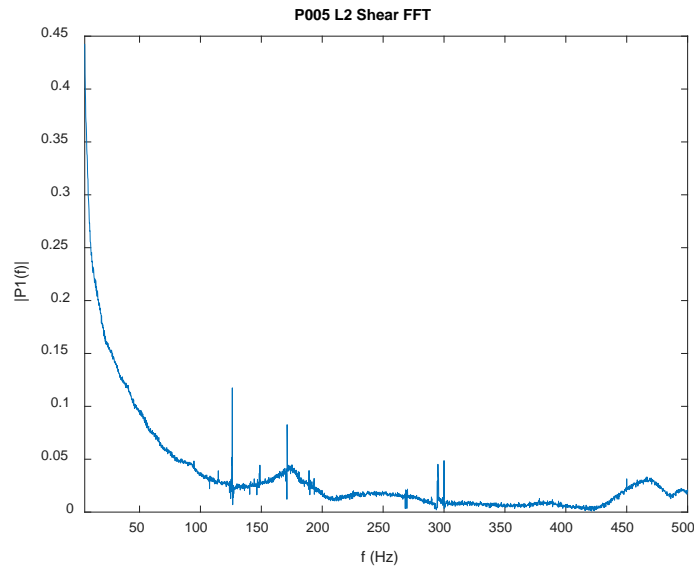
A.1.4 Specimen and Sample Force vs Time

A.1.4.1 Quasi-Static Shear

The below figure includes all samples plotted with respect to specimen number. Each plot is the samples for a specific specimen labelled in the title. Quasi-static plots are in force versus time, and differences in sample dimensions are unaccounted for; see A.1.2 for corresponding sample measurements.   For specimens that have less than 3 sample curves: the absence of sample curves are due to misfires or noise abnormalities.
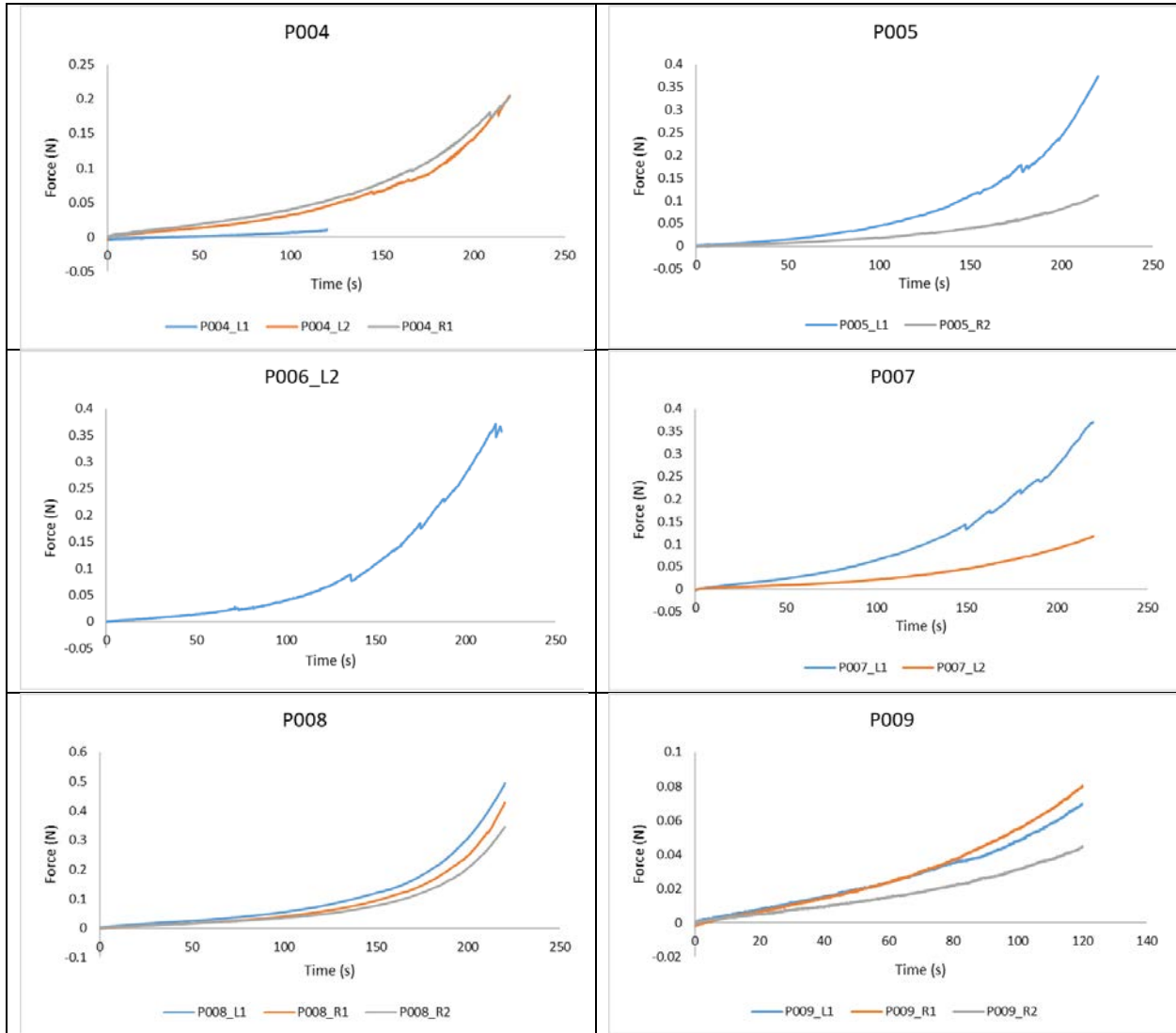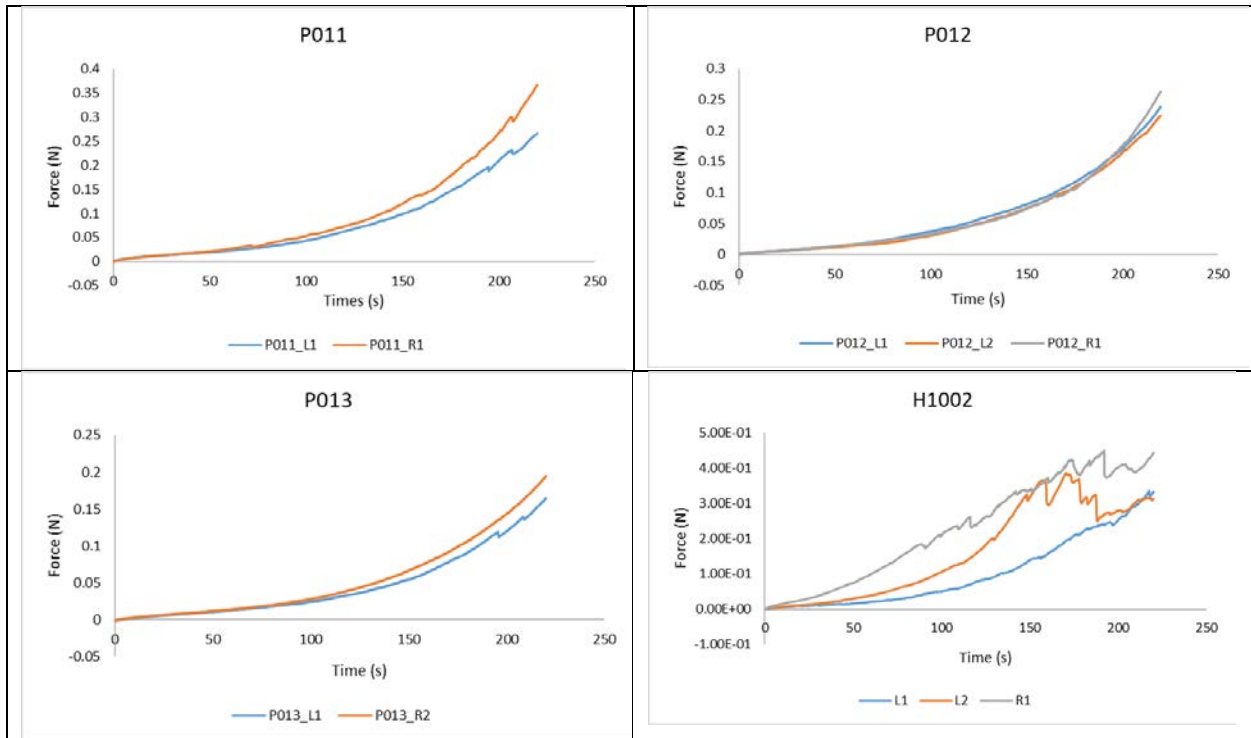
A.1.4.2 Step-Hold Shear

The below figure includes all samples plotted with respect to specimen number. Each plot is the samples for a specific specimen labelled in the title. Step-hold shear plots are in force versus log time, and differences in sample dimensions are unaccounted for; see A.1.2 for corresponding sample measurements. For specimens that have less than 3 sample curves: the absence of sample curves are due to misfires or noise abnormalities.

P016

P017

P018

P023

P024

H707

H984

H1002
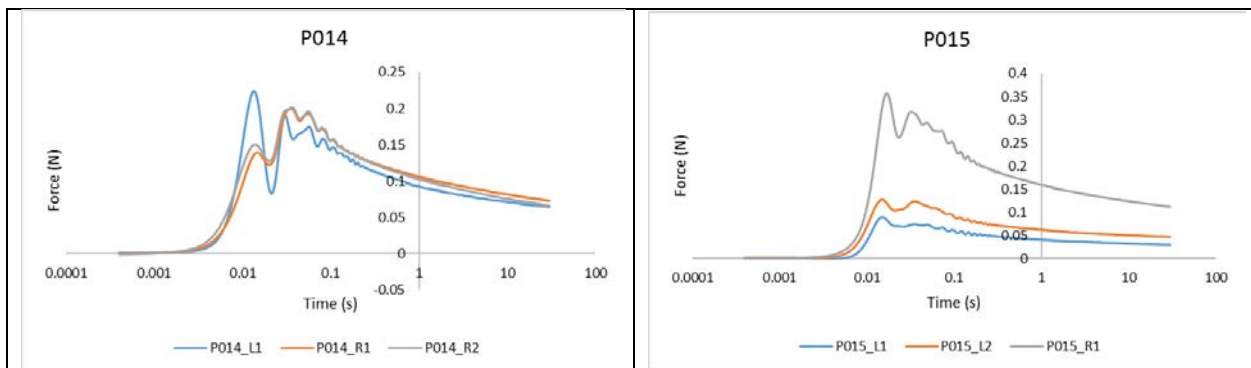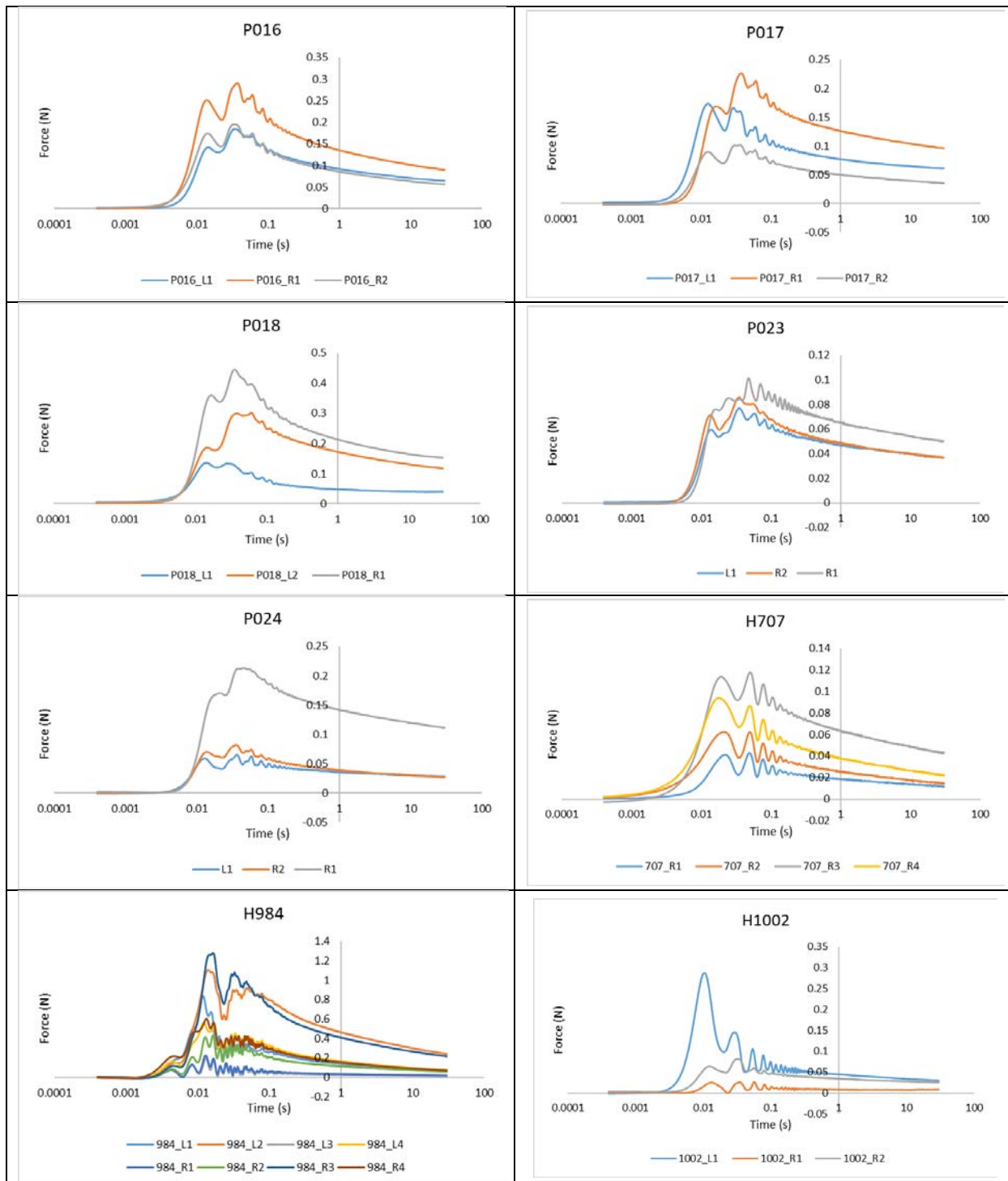
A.1.4.3 Step-Hold Indentation

A.1.4.3.1 All Samples at 0.35 Strain

127

The below figure includes all samples plotted with respect to specimen number. Each plot is the samples for a specific specimen labelled in the title. Step-hold indentation plots are in force versus log time, and differences in sample dimensions are unaccounted for; see A.1.2 for corresponding sample measurements. For specimens that have less than 3 sample curves: the absence of sample curves are due to misfires or noise abnormalities. Only the strain of 0.35 is plotted per sample, see below section for specimen averages for all strains.

Below are plots of the specimen averages for each step-hold strain (0.1, 0.2, 0.35, 0.45). Samples were averaged by specimen, and the specific specimens can be seen in each plot's legend. Plots are in force versus log time.
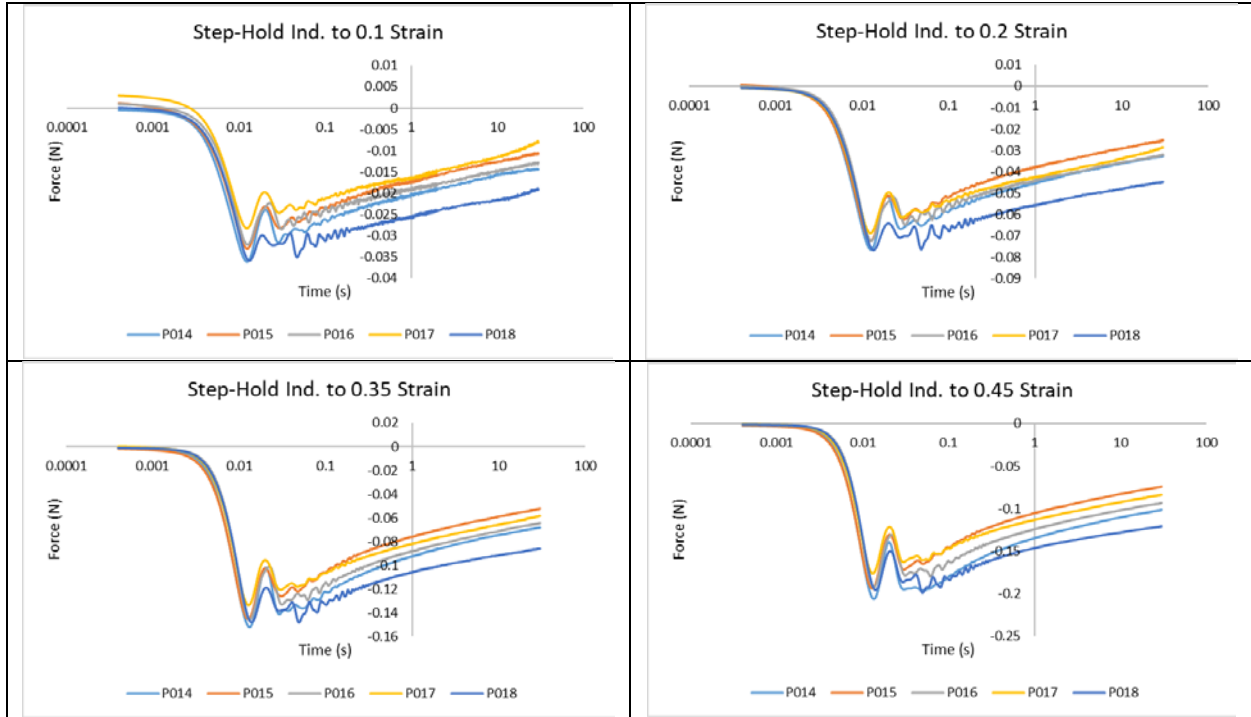
A.1.5 Linear Mixed Model Results

A linear mixed model was run using the program R to determine N (specimen number) and n (sample number) such that the 95% confidence interval was less than 20% of the mean. Below is a table of the information gained through the model. For quasi-static shear (QSS), step-hold shear – ramp portion (SHSramp), step-hold shear – relaxation portion (SHSrelax), and failure in shear (FS), there is listed N, n, the standard deviation (SD), standard error (SE), and the 2.5% and 97.5% intercepts (CI 2.5%, CI 97.5%). Note: the step-hold shear only shows N=5 because from this information it was concluded that two more specimens would meet criteria. The failure shear is in Lagrangian strain, not true strain. All others are in Lagrangian stress.

	N	n	SD	SE	CI 2.5%	CI 97.5%
QSS	10	23	0.1779	0.09625	0.5786	0.9749

SHSramp	5	15	0.5532	0.3688	1.6078	3.1940
SHSrelax	5	15	0.0052	0.0098	0.3189	0.3618
FS	5	7	0.0609	0.0526	1.3910	1.6169

A.1.6 Density Measures

Densities were calculated individually for each sample, and then the sample densities averaged per specimen to reach a mean specimen density. Below is a table of each specimen's mean density as well as a mean density for porcine and human, and their respective standard deviations.

Porcine Specimen	Mean Density (g/cm^3)	Human Specimen	Mean Density (g/cm^3)
P004	0. 481	H1002	0.414
P005	0. 472	H707	1.023
P006	0. 587	H984	0.823
P007	0. 542		
P008	0. 496		
P009	0. 553	**Porcine Average**	**Human Average**
P010	0. 494	0.5350	0.753
P011	0. 588	**SD**	**SD**
P012	0. 422	0.07	0.311
P013	0. 572		
P014	0. 416		
P015	0. 68		
P016	0. 513		
P017	0. 52		
P018	0. 462		
P023	0. 558		
P024	0. 739		

A.2 FE SIMULATIONS FOR A MATERIAL MODEL

Below is listed the k file code meant for solving in LS-DYNA for the material model for lung found in Chapter 5.

*MAT_HILL_FOAM_TITLE

Shear Hill

$#   mid   ro   k   n   nu   lcid fittype   lcsr

15.35000E-79.00100E-4   0.45   0.1   0   1   0

$#   c1   c2   c3   c4   c5   c6   c7   c8

6.68000E-71.32000E-7   0.0   0.0   0.0   0.0   0.0   0.0

$#   b1   b2   b3   b4   b5   b6   b7   b8

    4.0   7.0   0.0   0.0   0.0   0.0   0.0   0.0

$#   r   m

    0.0   0.0

*HOURGLASS

$#   hgid   ihq   qm   ibq   q1   q2   qb/vdc   qw

    1   5   0.1   0   1.5   0.06   0.1   0.1

*MAT_ADD_INELASTICITY

$#   mid   nielinks   unused   unused   unused   aopt   macf   beta

    1   4   0.0   0.0   0.0

$#   xp   yp   zp   a1   a2   a3

$#   v1   v2   v3   d1   d2   d3

$# nielaws   weight

    1 0.0883633

$#   law   model

    6   1

$#   p1   p2   p3   p4   p5   p6   p7   p8

    0.1   0.0   0.0   0.0   0.0   0.0   0.0   0.0

$# nielaws   weight

    1 0.365548

$# law model

   6   1

$# p1   p2   p3   p4   p5   p6   p7   p8

  0.01   0.0   0.0   0.0   0.0   0.0   0.0   0.0

$# nielaws   weight

   1 0.119346

$# law model

   6   1

$# p1   p2   p3   p4   p5   p6   p7   p8

  0.001   0.0   0.0   0.0   0.0   0.0   0.0   0.0

$# nielaws   weight

   1 0.0963434

$# law model

   6   1

$# p1   p2   p3   p4   p5   p6   p7   p8

1.00000E-4   0.0   0.0   0.0   0.0   0.0   0.0   0.0

APPENDIX B: Pulmonary Damage in BABT

B.1 DAMAGE THRESHOLD

Below are the plots of each small sample that failed in shear. The plots are in force in grams versus Lagrangian strain, and each plot is titled with the specimen number and the specific sample. The yield point in engineering strain of these samples was used to establish the failure threshold of lung tissue in true strain.

P022 L2
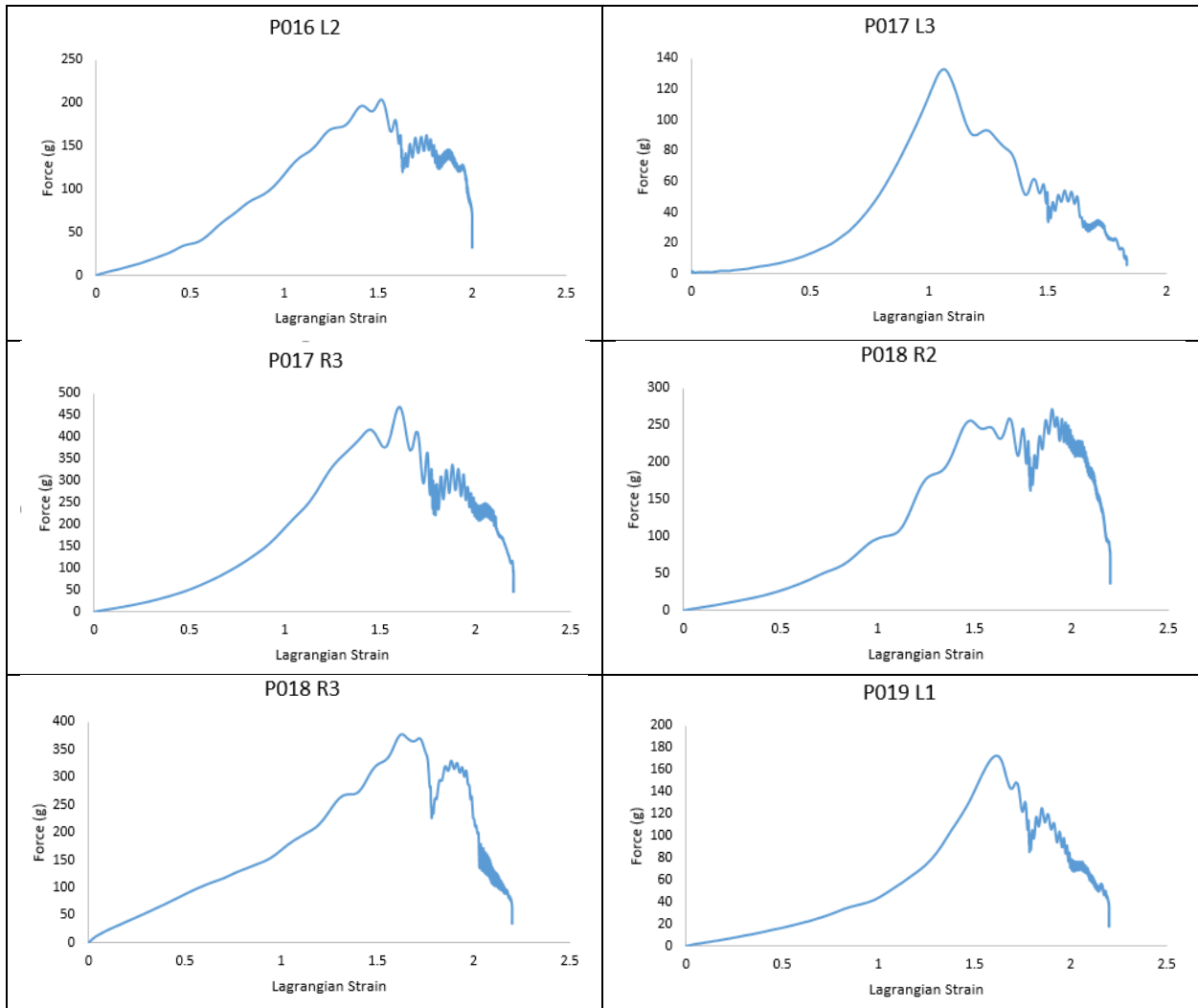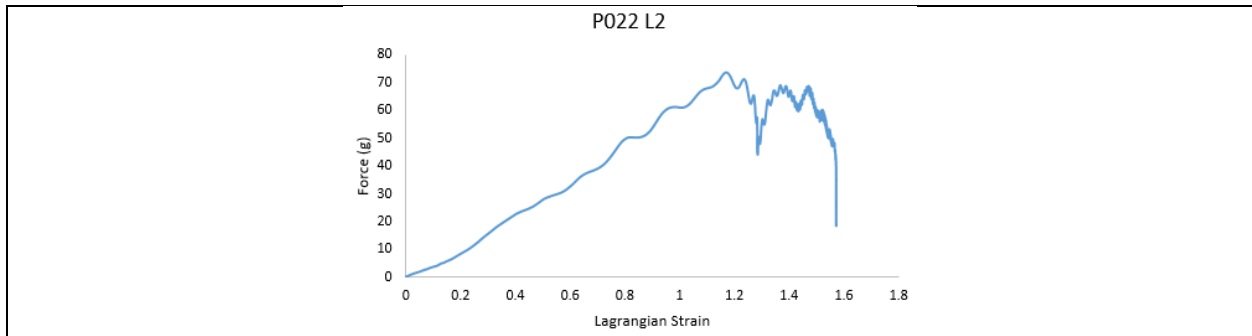
B.2 EXPERIMENTAL BABT SIMULATIONS

B.2.1 Clay Testing

B.2.1.1 Clay Fixture

Below is an image of the clay fixture used for clay impact testing. The fixture consists of a wooden box with dimensions according to the NIJ standard for impact with a 4 inch-diameter impactor. (U.S. Department of Justice, 2008) As seen in the corner of the image, temperature was measured also in accordance with the standard. The clay was heated to near liquid and then smoothed on the top so that no air pockets existed in the block and the impact surface was level.
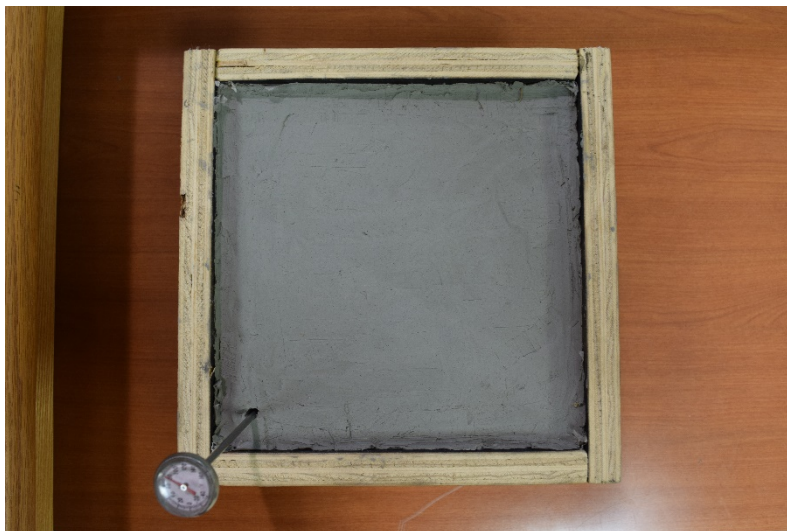
B.2.1.2 DRAGun Setup

The below images show the clay fixture set up at the launch-end of the DRAGun. This way, the impactor is contained and is allowed a controlled free flight.
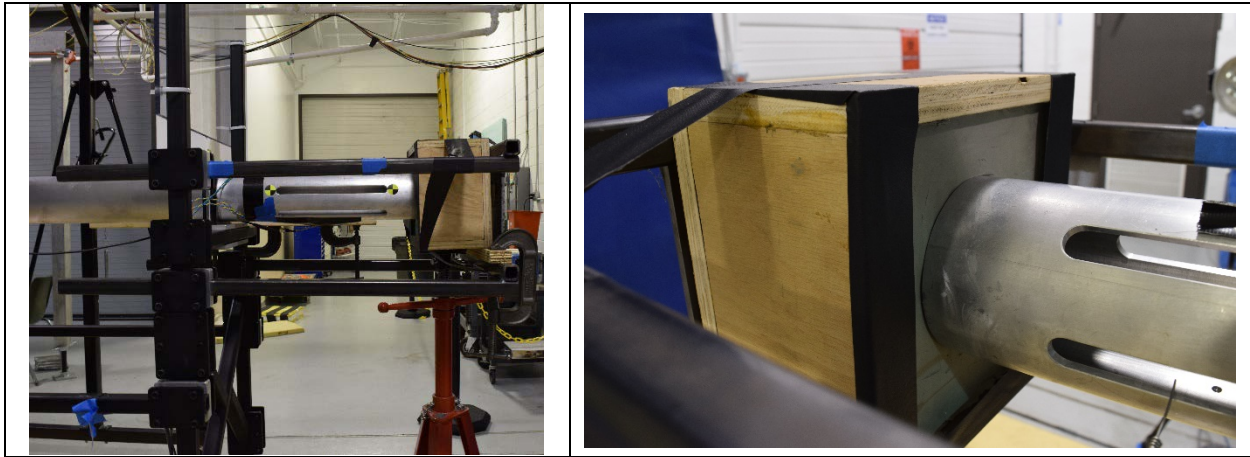
B.2.1.3 Method of Clay Displacement Measurement

B.2.1.3.1 Smoothing the Clay

After impact into clay from the BABT impactor, the clay displacement must be measured according to the standard. This is first done by smoothing the side of the impact location to be level with the outside area of the clay. This is shown in the below image by placing a metal plate to ensure that the surface is flat.

B.2.1.3.2 Marking Displacement

The next step in the measurement of clay displacement is to mark the depth of the impact crater with a straight instrument. An Allen wrench is used here to mark displacement.

B.2.1.3.3 Final Measurement

Finally, the marked depth is measured to achieve the displacement from the impact into clay.
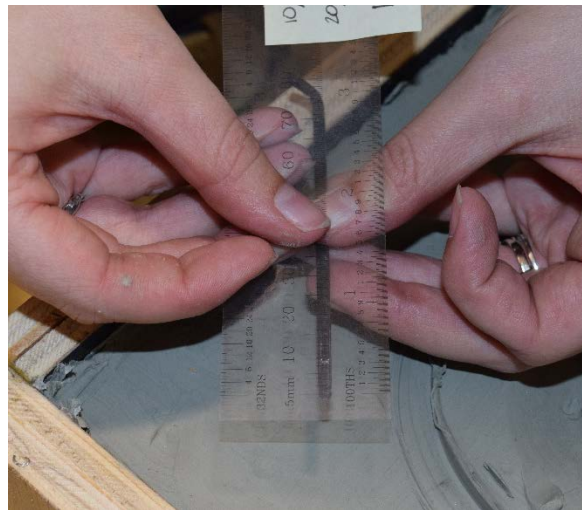
B.2.1.4 Impact Images

Below are images of different impacts into the clay. The top left and right images are from the ball drop calibration of the clay temperature – the top left is the ball dropped onto the clay, and the top right is the impression from the ball drop. The bottom left and right images are from low and high speed hits with the BABT impactor – the bottom left is an image of a low speed hit, and the bottom right is an image of a high speed hit.
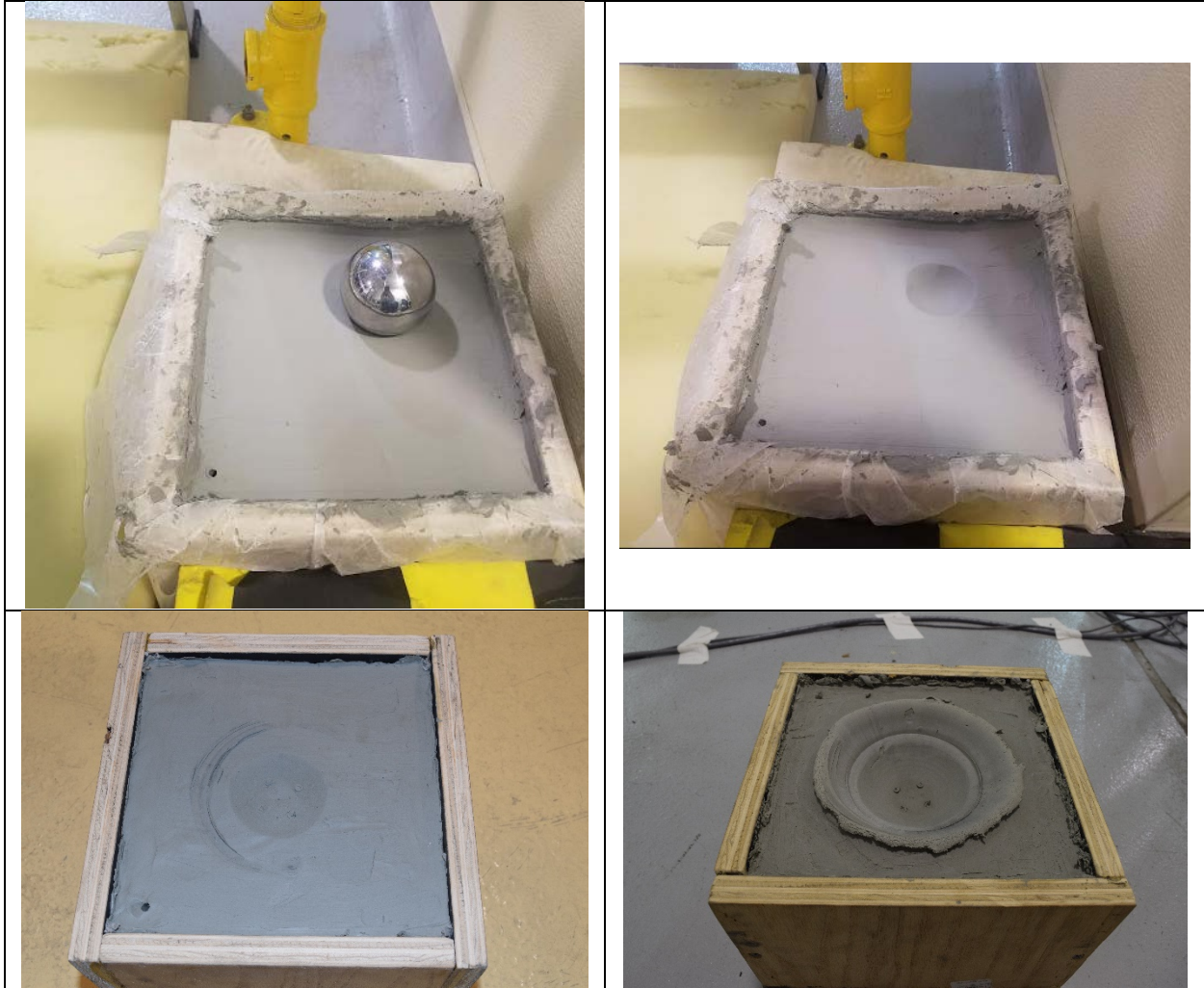
B.2.2 PMHS Testing

      B.2.2.1 DRAGun Setup

Below are images regarding the PMHS setup at the launch-end of the DRAGun. The images here are with an ATD in the place of the PMHS, and show gantry position and the harness supporting the specimen.
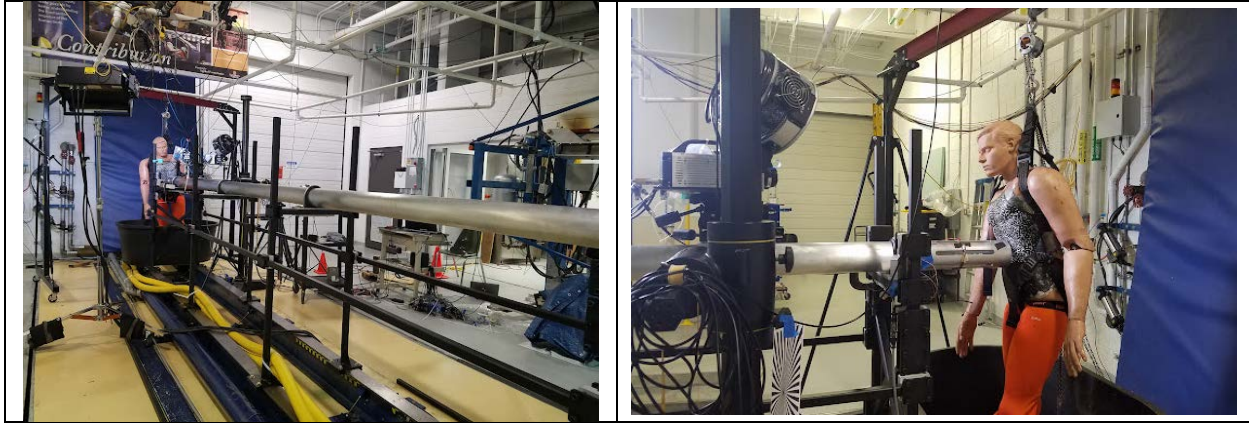
B.2.2.2 Anthropomorphic Data for PMHS

The following table contains both the anthropomorphic measures of specimen 826 and, for comparison, the USA 50th percentile male. The leftmost column indicates the type of measurement being performed, and all measurements are in centimeters.

Measurement	USA 50th (cm)	UVA PMHS 826 (cm)
Standing Height	168.67	172
Shoulder Height	146.33	149
Waist Height	108.38	106
Seated Height	92.96	96.5
Head Length	19.86	18
Head Breadth	15.57	16.4
Head to Chin Height	23.24	21.8
Neck Circumference	37.95	41.5
Shoulder Breadth	46.2	34
Chest Depth	23.32	20.5
Chest Breadth	32.89	36.4
Waist Depth	21.51	28
Waist Breadth	28.22	39.5
Buttock Depth	23.19	18
Hip Breadth	35.43	58.5
Shoulder to Elbow Length	37.54	39.8
Forearm Hand Length	48.69	29
Biceps Circumference	32.92	28
Elbow Circumference	31.42	25.5
Forearm Circumference	29.08	25
Wrist Circumference	17.86	19.5
Knee Height	53.14	42.5
Thigh Circumference	50.52	58
Upper Leg Circumference	37.24	49
Knee Circumference	36.2	42.5

Calf Circumference	33.32	35.6
Ankle Circumference	21.06	29.5
Ankle Height	6.91	8
Foot Breadth	9.35	8.6
Foot Length	25.4	24.3

B.2.2.3 PMHS Instrumentation

Below are three figures showing the instrumentation placement on the PMHS. The left figure shows the placement of the spinal accelerometers which have 6 degrees of freedom, the center figure shows the placement of the 20 strain gauges and the uniaxial sternal accelerometer (mount), and the right figure shows the paths of the pressure transducers.
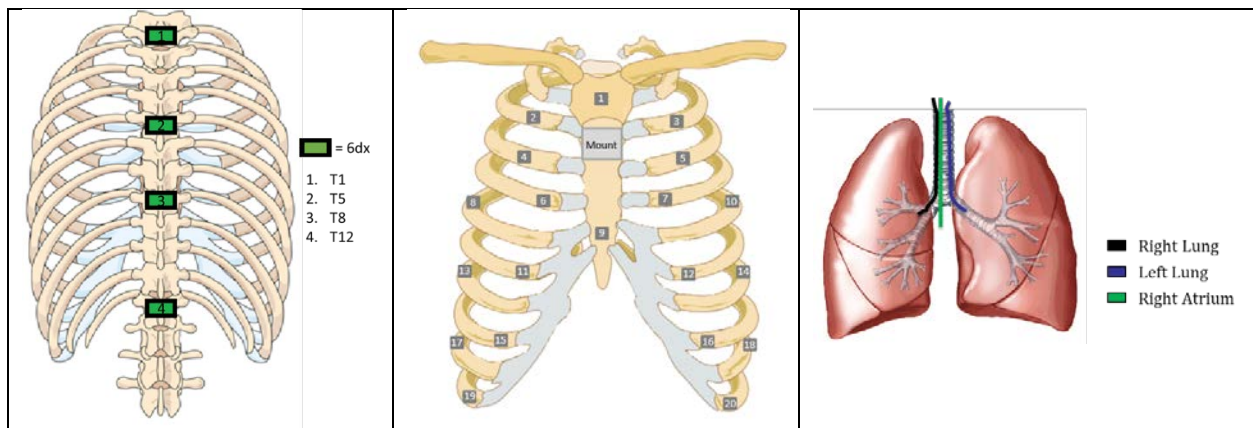
B.2.2.4 PMHS Sensor Results

B.2.2.4.1 Impactor and Sternal Accelerations

The accelerometers inside the impactor and mounted on the PMHS sternum were uniaxial accelerometers in the x-direction. The plots of each can be seen below, with the impactor accelerometer on the left and the sternal accelerometer on the right. All three tests are shown on each graph, with Test 1 in blue, Test 2 in black, and Test 3 in red. Peak accelerations for each test are listed on the graphs.

Accelerometer Inside Impactor / Sternal Acceleration

Peaks (Accelerometer Inside Impactor):
Test 01: 1338 g
Test 02: 1118 g
Test 03: 6843 g

Peaks (Sternal Acceleration):
Test 01: -87g
Test 02: 90 g
Test 03: -328 g
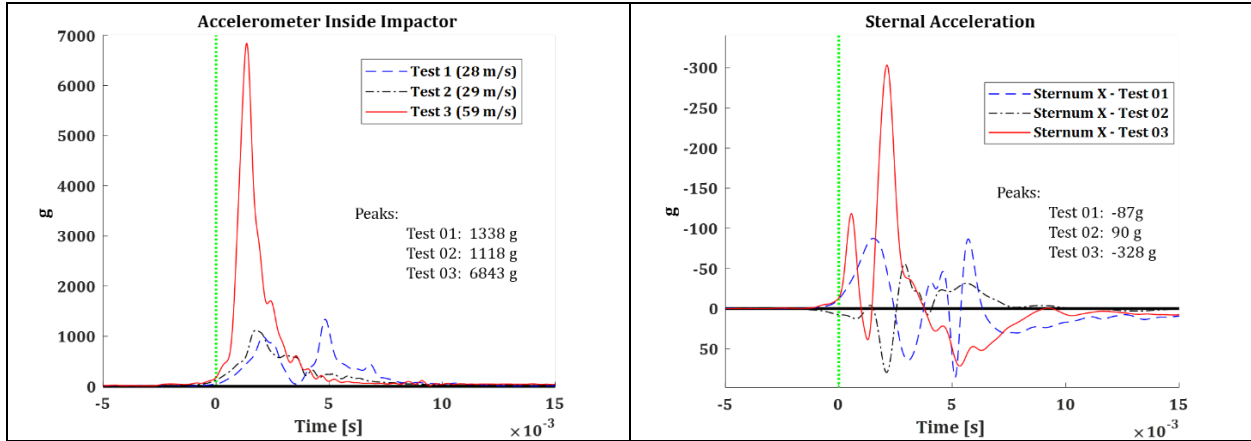
B.2.2.4.2 Translational Spinal Accelerations (X)

While the spinal accelerometers recorded data in all six directions, only two directions were particularly useful for the specific test setup. For the translational accelerations the x-direction contained the most information, and is therefore shown below. The first set of figures breaks down what is happening during Test 2. The color-coded regions on the graph refer to the color-coded schematics showing direction of acceleration for each spinal mount with an arrow. In both the graph and the arrows, T1 is represented with green, T5 with red, T8 with black, and T12 with blue.
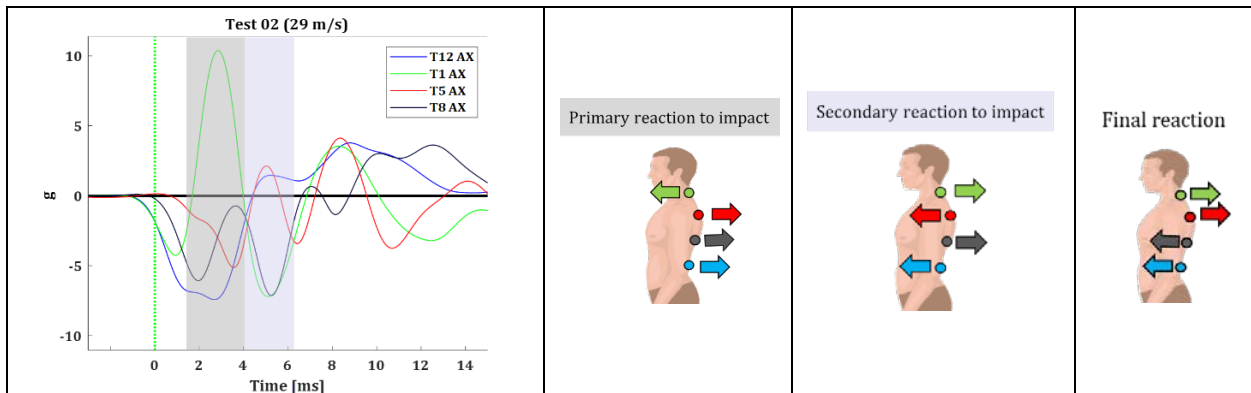
This second set of figures shows the translational X data for all the spinal accelerometers for the other two tests. In these cases, T1 is red, T5 is green.
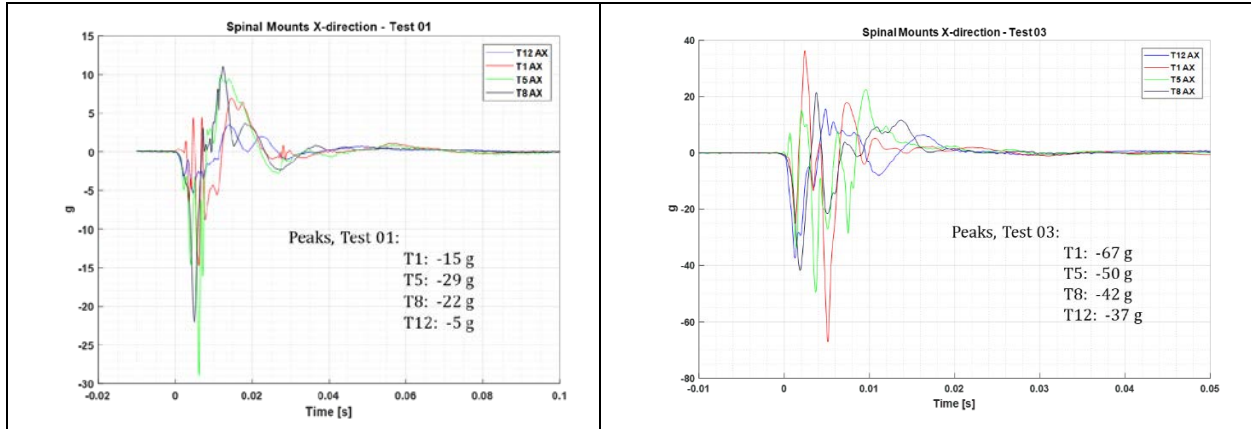
B.2.2.4.3 Rotational Spinal Acceleration (RY)

As described in the previous subsection, for the particular test setup the RY-direction of all the rotational directions contained the most useful information from the spinal accelerometers. Likewise to the Test 2 translational X figures, as an example a breakdown of the Test 1 RY spinal acceleration data is shown in the first set of figures below. After a 2ms delay until the spine sees any rotational acceleration, the graph is color-coded to refer to the schematics showing the direction of acceleration by use of arrows. In both the graph and the schematics, T1 is represented by green, T5 by red, T8 by black, and T12 by blue.
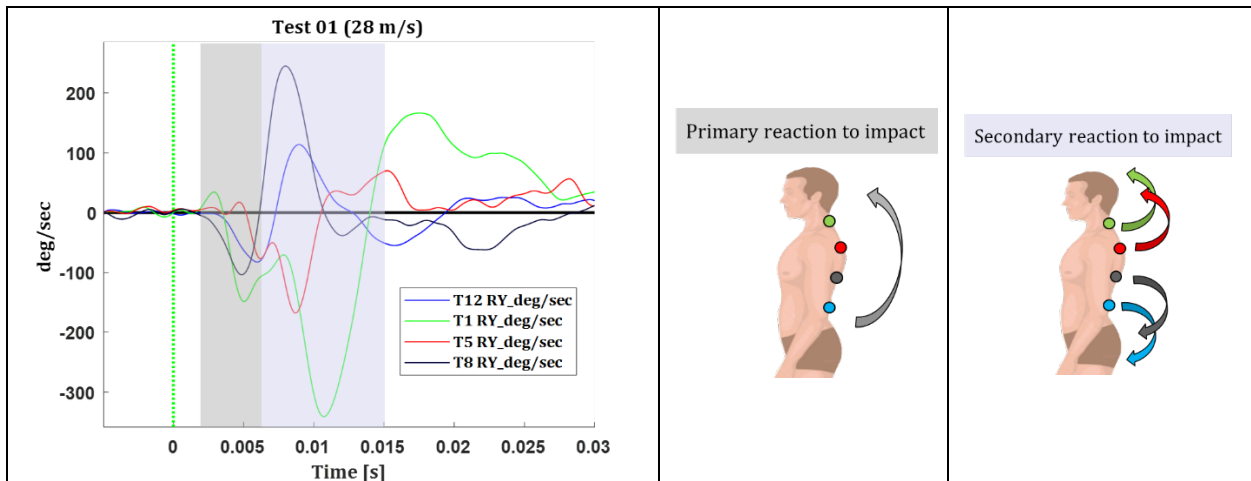
This second set of figures shows the rotational y-direction data for the spinal accelerometers in the other two tests. The color coding for the individual accelerometers is the same as mentioned above.
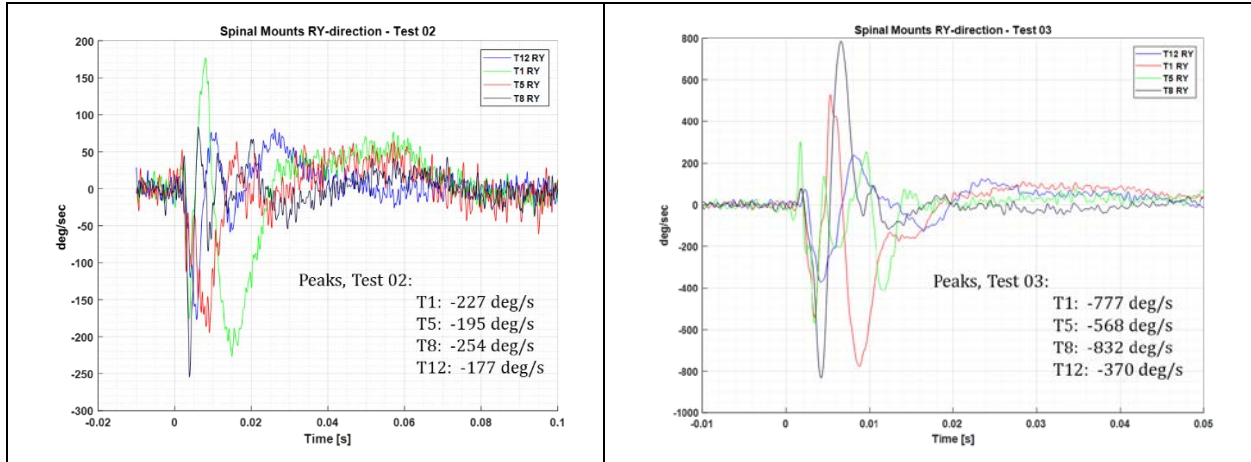
B.2.2.4.4 Pressure Transducers

Below are plots indicating the pressure transducer results for each test. The top left plot is for Test 1, the top right for Test 2 and the bottom for Test 3. In all plots, the pressure in the right atrium is indicated by a blue line, the left lung by black, and the right lung by red.
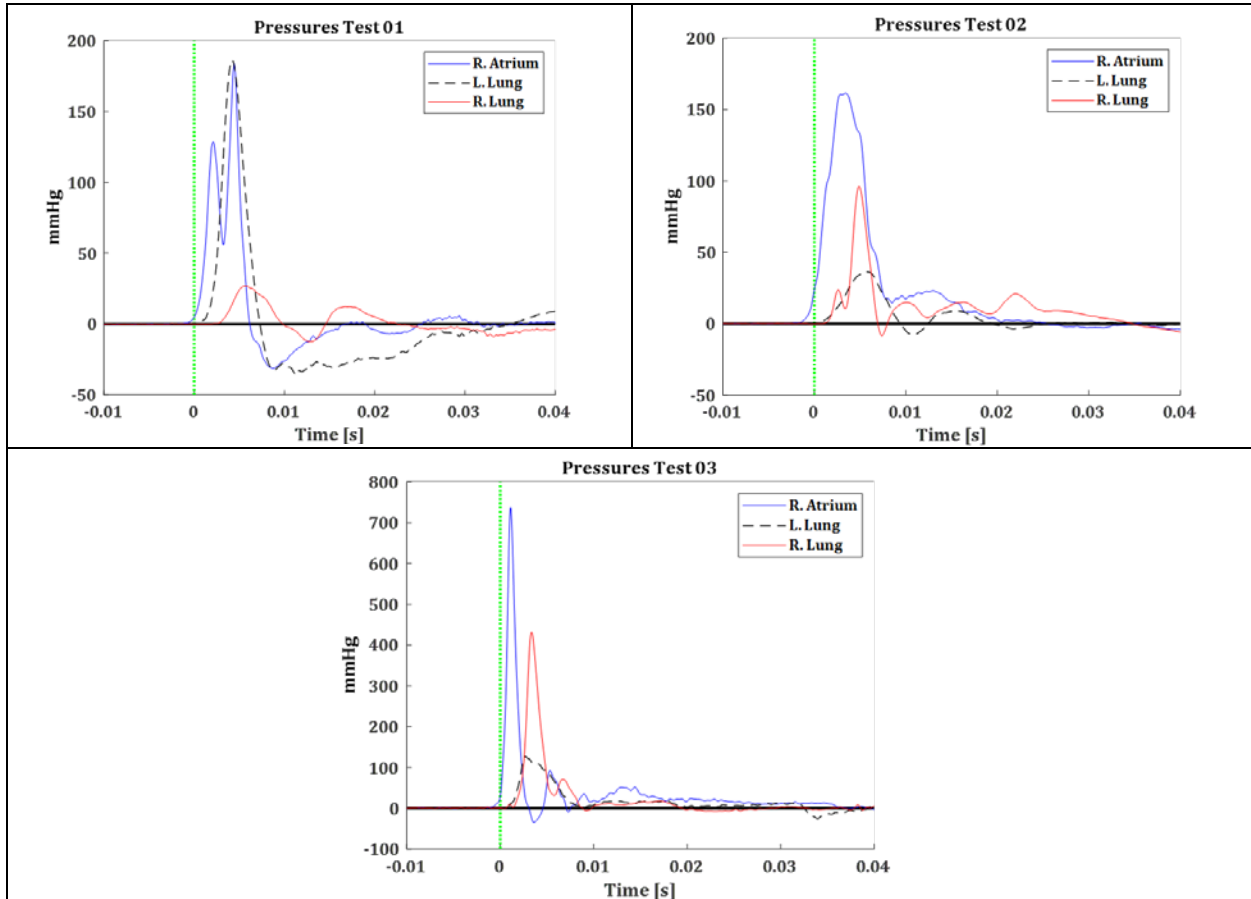
B.2.2.4.5 Strain Gauges

There were 20 strain gauges placed on the ribs of the PMHS as shown in B.2.2.3. The results of the strain gauges for each test are shown below.

Strain Gauges - Test 03
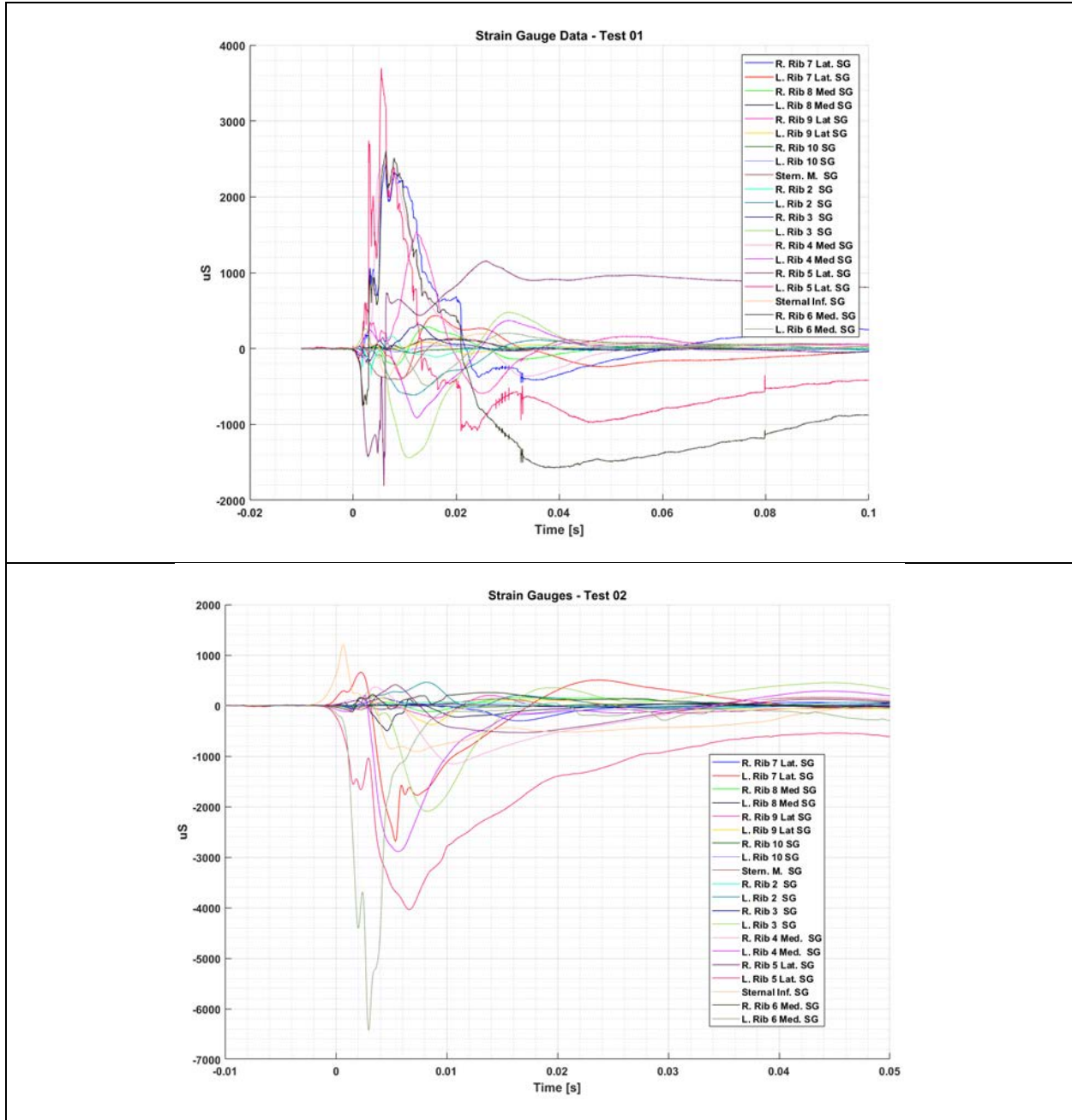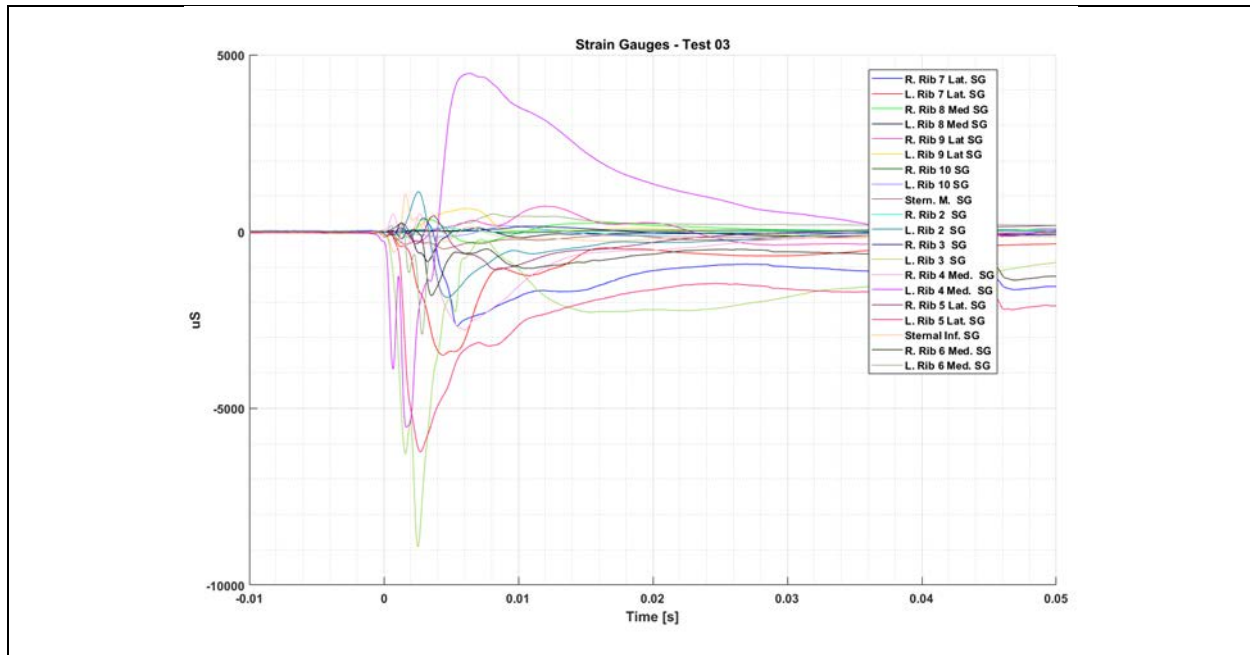
B.2.2.5 CT Results

B.2.2.5.1 Radiologist Report

Below is a summary of the radiologist report regarding the post-test CT scan of the PMHS:

▶ *CHEST:*
- Lungs/Pleura: Expected postmortem appearance.
- Mediastinum: Expected postmortem appearance.
- Heart: Expected post normal appearance
- Bones: Minimally displaced fractures of the left anterior fourth and fifth ribs. Minimally displaced fracture of the anterior left sixth rib at the costochondral cartilage.
- Extrathoracic Soft tissues: Multiple leads are positioned adjacent to multiple anterior ribs bilaterally.

▶ *CERVICAL SPINE:*
- No spine fractures are evident. Multilevel discogenic degenerative changes worst at C5-C6 and C6-C7.

▶ *THORACIC SPINE:*
- No spine fractures are evident. Fixation hardware at the T1, T5, T8/T9, and T12 levels. Mild multilevel degenerative changes

B.2.2.5.2 Pre- and Post-Test CT

Below are segmented images of the anterior and posterior views of the ribcage for the PMHS. The top two images are pre-test anterior and posterior views respectively, and the bottom two images are post-test anterior and posterior views.
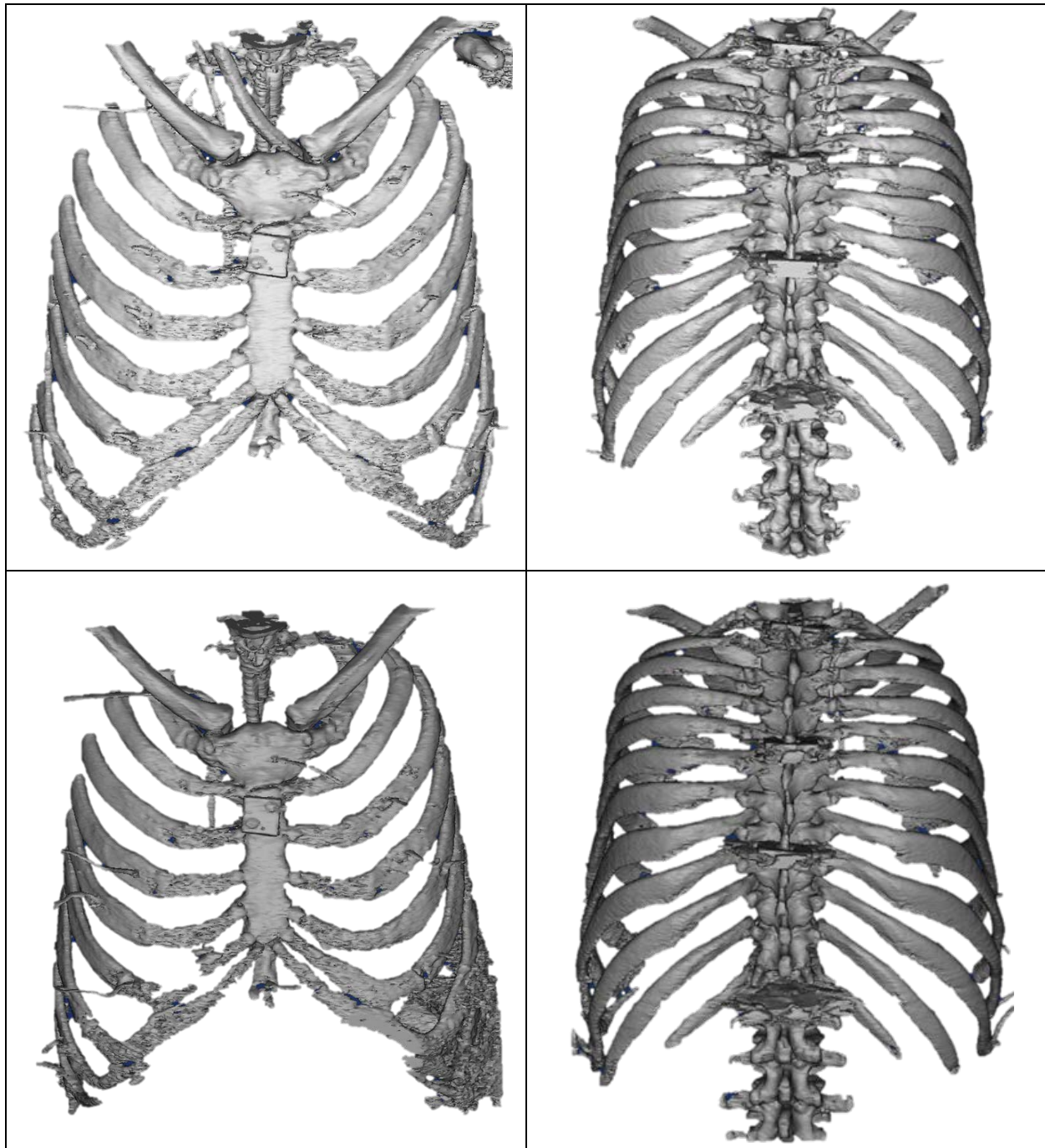
B.3 FE SIMULATIONS FOR INJURY PREDICTION

B.3.1 Python Script for Model Damage Volume

Below is the python script that was used to read the strain data binary output from LS-DYNA. Note – for true strain to be written to the output in LS-DYNA, STRFLG=1 in *DATABASE_EXTEBT_BINARY. This script finds the principal strains, the maximum principal strain, and then finds the volume of damage. The volume of damage is found by listing all the elements that met or exceeded the given strain threshold, and then finding the volume of those elements. Damage volume is output as failed volume over total lung volume.

{ "cells": [

 { "cell_type": "code",

  "execution_count": 1,

  "id": "cceec5f1",

  "metadata": {},

  "outputs": [],

  "source": ["import matplotlib.pyplot as plt\n",

  "from scipy import signal\n",

  "import numpy as np\n",

  "\n",

  "from lasso.dyna import Binout"   ] },

 { "cell_type": "code",

  "execution_count": 2,

  "id": "b80ff860",

  "metadata": {},

"outputs": [],

 "source": [

 "file2load='.\\\\\\\binout0006' #Enter the path of the file to load\n",

 "file2saveas='.\\\\\\\Clay_28_SD.csv' #Enter the path/name of the file to save as\n",

 "thresh=0.96 #Enter the strain threshold"   ] },

{   "cell_type": "code",

 "execution_count": 3,

 "id": "e276aac2",

 "metadata": {},

 "outputs": [],

 "source": [

 "binout = Binout(file2load) #load file and read in data\n",

 "strains=binout.read(\"elout\",\"solid_hist\",\"strain\")\n",

 "time=binout.read(\"elout\",\"solid_hist\",\"time\")\n",

 "eleids=np.arange(4253305,4260172,1)"   ] },

{   "cell_type": "code",

 "execution_count": 4,

 "id": "2bf9b382",

 "metadata": {},

 "outputs": [],

 "source": [

 "num_elements=6867\n",

 "ele_maxval=[]\n",

```
"ele_maxtime=[]\n",

"ele_maxeigvec=[]\n",

"\n",

"ele_threshval=[]\n",

"ele_threshtime=[]\n",

"ele_thresheigvec=[]\n",

"\n",

"for k in range(num_elements):\n",

"    eigvals=[]\n",

"    eigvecs=[]\n",

"    for t in range(501):\n",

"        d=np.diag(strains[t][6*k:6*k+3])\n",

"        d[0,1]=strains[t][6*k+3]\n",

"        d[1,2]=strains[t][6*k+4]\n",

"        d[0,2]=strains[t][6*k+5]\n",

"        strain_mat=np.tril(d.T)+np.triu(d,1)\n",

"        eigsys=np.linalg.eig(strain_mat)\n",

"        maxeigval=np.max(np.abs(eigsys[0]))\n",

"        maxvalloc=np.where(maxeigval==np.abs(eigsys[0]))[0][0]\n",

"        eigvals.append(eigsys[0][maxvalloc])\n",

"        eigvecs.append(eigsys[1][maxvalloc])\n",

"        \n",

"    threshloc=np.where(np.abs(np.asarray(eigvals))>=thresh)\n",
```

```
    "    if np.size(threshloc)==0:\n",

    "        ele_threshtime.append(0)\n",

    "        ele_threshval.append(0)\n",

    "        ele_thresheigvec.append(np.array([0,0,0]))\n",

    "    else:\n",

    "        ele_threshtime.append(time[threshloc[0][0]])\n",

    "        ele_threshval.append(eigvals[threshloc[0][0]])\n",

    "        ele_thresheigvec.append(eigvecs[threshloc[0][0]])\n",

    "    \n",

    "    maxloc=np.where(np.max(np.abs(eigvals))==np.abs(eigvals))[0][0]\n",

    "    ele_maxval.append(eigvals[maxloc])\n",

    "    ele_maxtime.append(time[maxloc])\n",

    "    ele_maxeigvec.append(eigvecs[maxloc])\n",

    "\n",

    "    \n",

    "maxvec_x=np.asarray(ele_maxeigvec).T[0]\n",

    "maxvec_y=np.asarray(ele_maxeigvec).T[1]\n",

    "maxvec_z=np.asarray(ele_maxeigvec).T[2]\n",

    "\n",

    "thvec_x=np.asarray(ele_thresheigvec).T[0]\n",

    "thvec_y=np.asarray(ele_thresheigvec).T[1]\n",

    "thvec_z=np.asarray(ele_thresheigvec).T[2]"   ]
    },
```

{ "cell_type": "code",

 "execution_count": 5,

 "id": "993f4225",

 "metadata": {},

 "outputs": [],

 "source": [

  "labels='Ele

ID,Maxval,Max_evec_x,Max_evec_y,Max_evec_z,Maxtime,Threshval,Thresh_evec_x,Thresh_evec_y,Thr

esh_evec_z,Threshtime'\n",

"data=np.asarray([eleids,np.asarray(ele_maxval),maxvec_x,maxvec_y,maxvec_z,np.asarray(ele_maxtim

e),np.asarray(ele_threshval),thvec_x,thvec_y,thvec_z,np.asarray(ele_threshtime)])\n",

  "np.savetxt(file2saveas, data.transpose(), delimiter=\",\",header=labels)"] },

{ "cell_type": "code",

 "execution_count": 6,

 "id": "7b25dc33",

 "metadata": {},

 "outputs": [

 {   "name": "stdout",

  "output_type": "stream",

  "text": [

   "Frac above threshold: 0.21479539828163682\n"   ] }],

 "source": [

 "print('Frac above threshold: ',len(np.nonzero(ele_threshval)[0])/len(ele_threshval))"] },

{   "cell_type": "code",

 "execution_count": 7,

 "id": "1233c348",

 "metadata": {},

 "outputs": [

 {   "name": "stdout",

  "output_type": "stream",

  "text": [

   "Largest   10   max   strains   [2.33701581 2.36363511 2.40892835 2.42477202 2.44480243
2.46152664\n",

    " 2.51268438 2.51590097 2.51828083 2.55373053]\n"   ]   }],

 "source": [

  "print('Largest 10 max strains ',np.sort(np.abs(ele_maxval))[-10:])"   ] }],

 "metadata": {

 "kernelspec": {

  "display_name": "Python 3 (ipykernel)",

  "language": "python",

  "name": "python3" },

 "language_info": {

  "codemirror_mode": {

   "name": "ipython",

   "version": 3   },

  "file_extension": ".py",

    "mimetype": "text/x-python",

    "name": "python",

    "nbconvert_exporter": "python",

    "pygments_lexer": "ipython3",

    "version": "3.9.12" } },

  "nbformat": 4,

  "nbformat_minor": 5}

B.3.2 X-Ray to PC Volume

      B.3.2.1 Surface Areas of Lung Specimens

To translate a surface area of PC as seen by X-ray into a volume of PC, the first step was to create a database of porcine lung surface areas. This allows for a mean determination of whole lung surface area to compare with the surface area of PC. The surface area was determined through images of right lungs of previously photographed porcine specimens. A software was used to map out the perimeter of the right lung, and read out an overall area (SketchandCalc©), as seen in the below image.
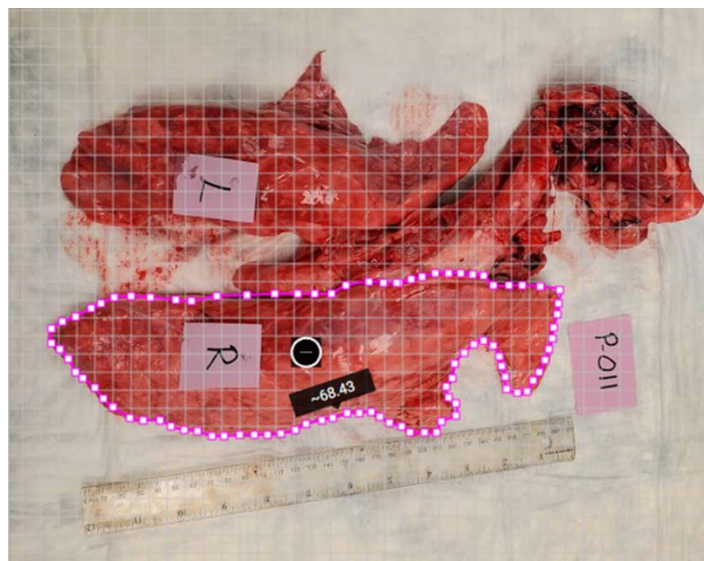
The resulting surface areas of all measured right lungs is shown in the table below. Some specimens are not included due to the images having no ruler or other scaling method. The mean value of right lung surface area was 219.5 cm^2.

Specimen:	P004	P007	P008	P009	P010	P011	P012
SA (cm^2):	225.8	186.1	189.9	209.3	190.8	166.7	158.4
Specimen:	P013	P016	P017	P018	P020	P021	P022
SA (cm^2):	170.2	253.5	257.5	227.3	256.2	310.7	270.9

B.3.2.2 Method of Determining Volume

Once a comparative mean surface area of porcine lung has been achieved, PC volume based on whole lung volume can be calculated using the study by Prat et al. This study contains an image of a sliced lung with PC (shown below). (Prat et al., 2010) Using the same area calculating software, the area of PC for each whole slice was obtained. This was compared to an 'X-ray' measurement: the length of PC seen from the outer membrane of each slice was measured and then converted into a surface area since all slices were of thickness 1 cm. This provided a basis of surface area compared to a volume from which to determine PC volumes.
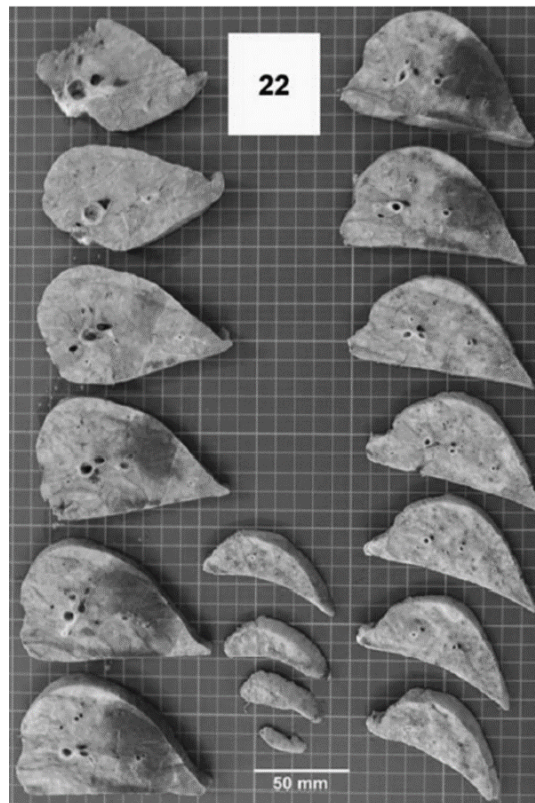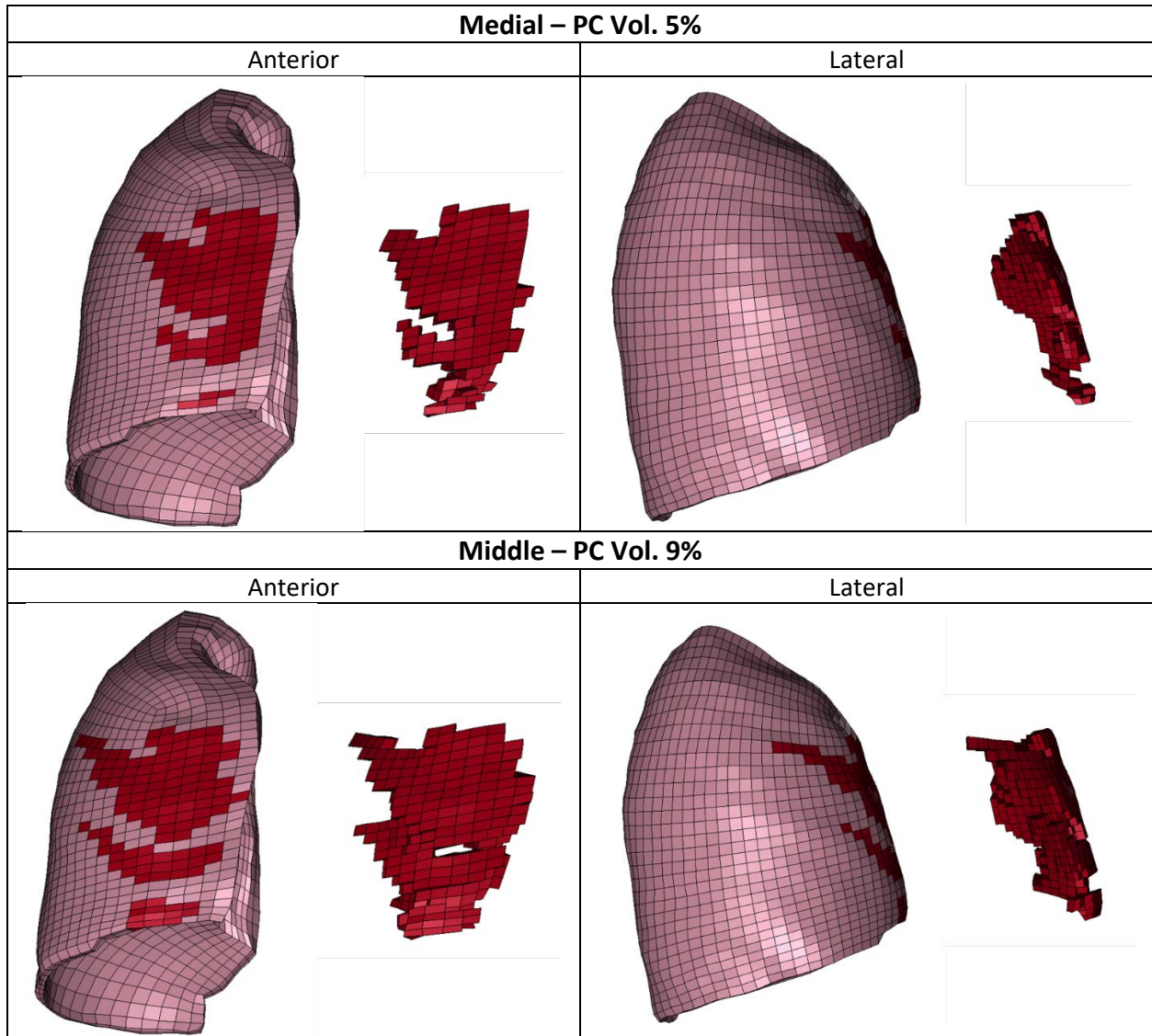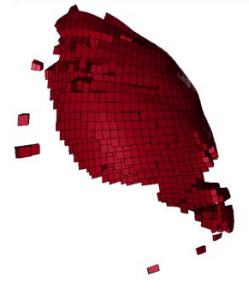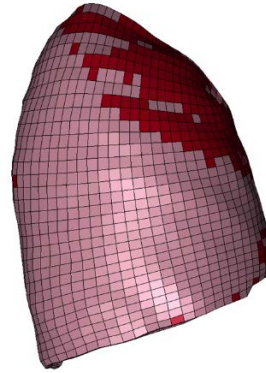
B.3.3 FE Model PC Volumes

B.3.3.1 Cylinder Location Study

Below are the results of the Shen et al. location sensitivity study as images of the FE right lung. (Shen et al., 2008b) In all images, pink elements indicate that those elements did not reach the failure threshold, and red elements indicate that those elements reached and/or surpassed the failure threshold. Above each set of images is the location indicator (Top, Lateral, Medial, Middle) and the volume of PC calculated from the model. Both anterior and lateral views of the lung are shown, and to the left of the lung image is an image of only the failed elements.

Shen et al. Cylinder Location Sensitivity Study	
Top – PC Vol. 12%	
Anterior	Lateral
Lateral – PC Vol. 7%	
Anterior	Lateral

Medial – PC Vol. 5%	
Anterior	Lateral

| Middle – PC Vol. 9%	
Anterior	Lateral
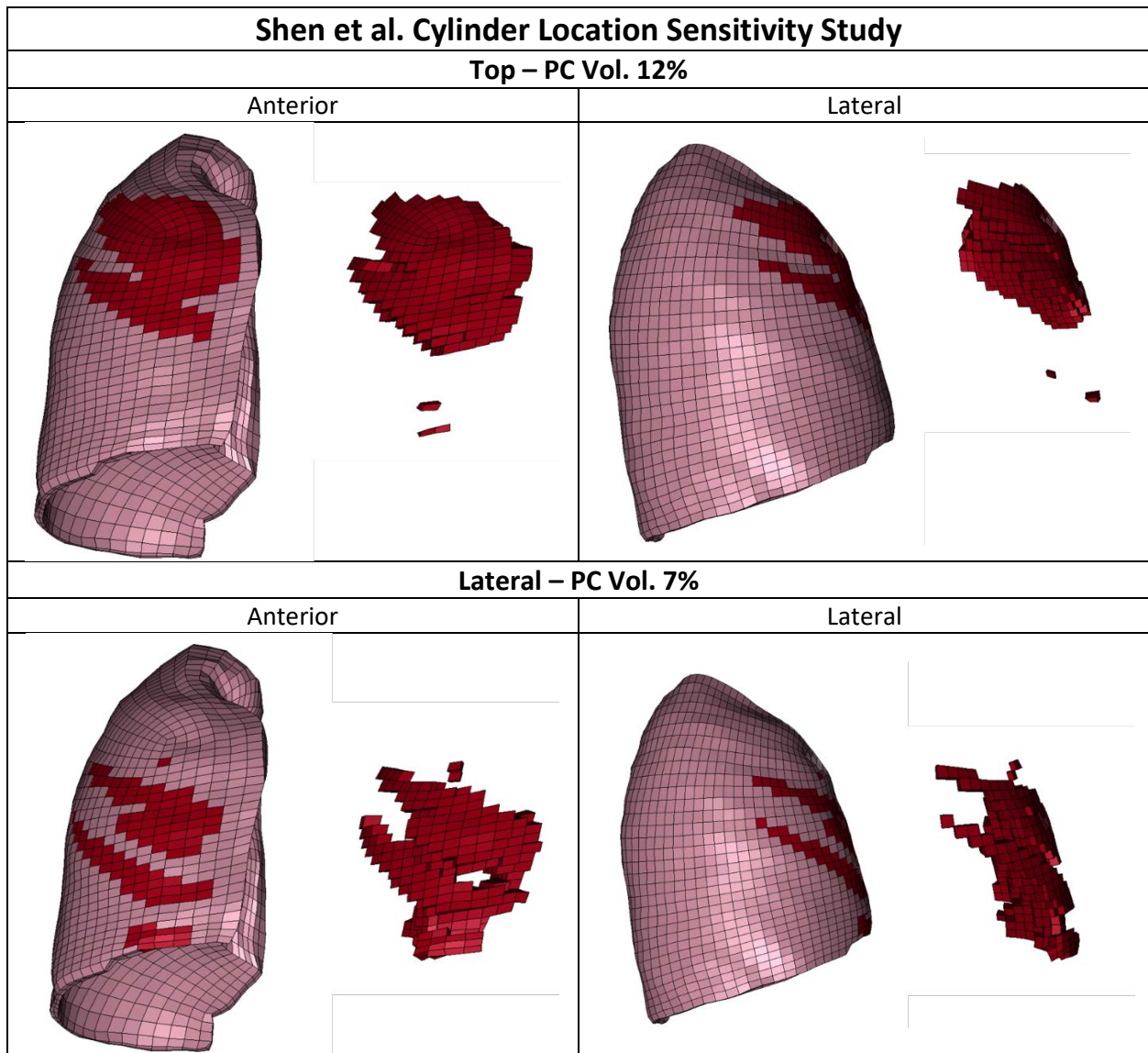
B.3.3.2 Clay 28mm Location Study

Below are the results of the Sonden et al. 28 mm into clay location sensitivity study as images of the FE right lung. (Sondén et al., 2009) In all images, pink elements indicate that those elements did not reach the failure threshold, and red elements indicate that those elements reached and/or surpassed the failure threshold.   Above each set of images is the location indicator (Top, Lateral, Medial, Middle) and the volume of PC calculated from the model. Both anterior and lateral views of the lung are shown, and to the left of the lung image is an image of only the failed elements.

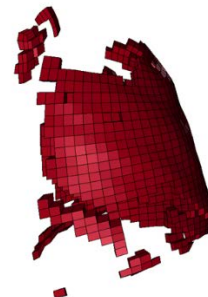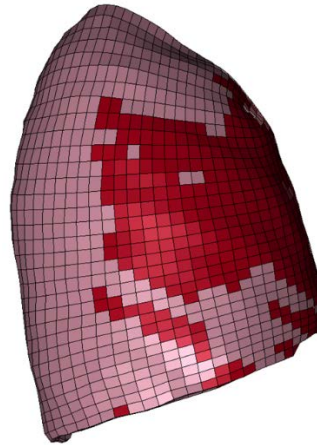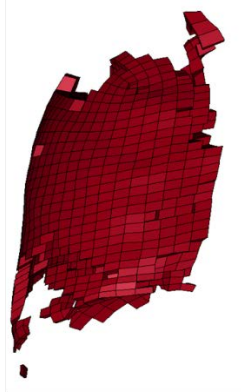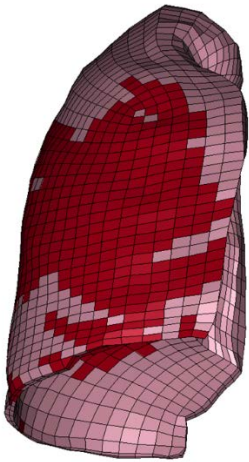**Sonden et al. BABT – Clay 28mm Location Sensitivity Study**

Top – PC Vol. 36.5%	
Anterior	Lateral
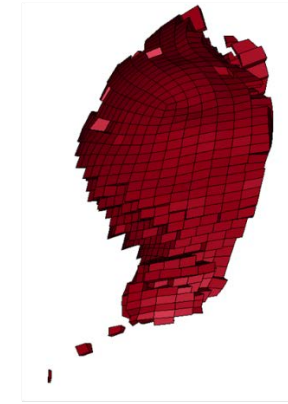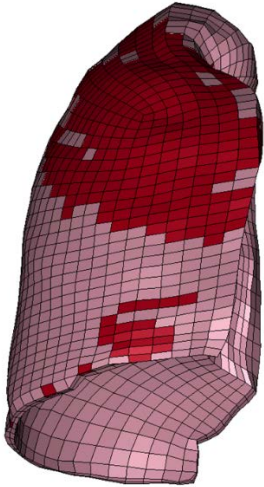
Lateral – PC Vol. 38.5%	
Anterior	Lateral

Medial – PC Vol. 13.7%	
Anterior	Lateral

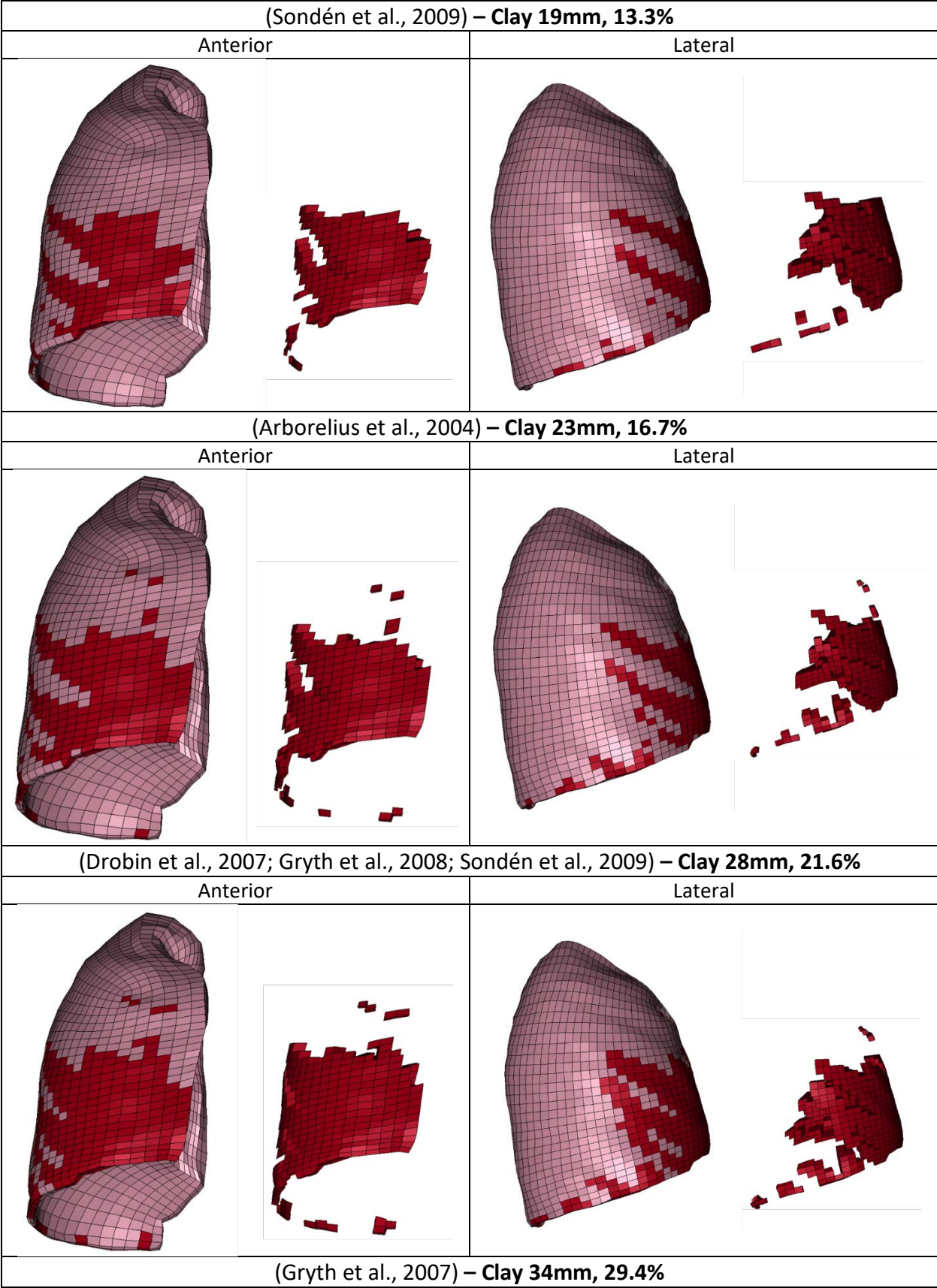| Middle – PC Vol. 33.1%	
Anterior	Lateral
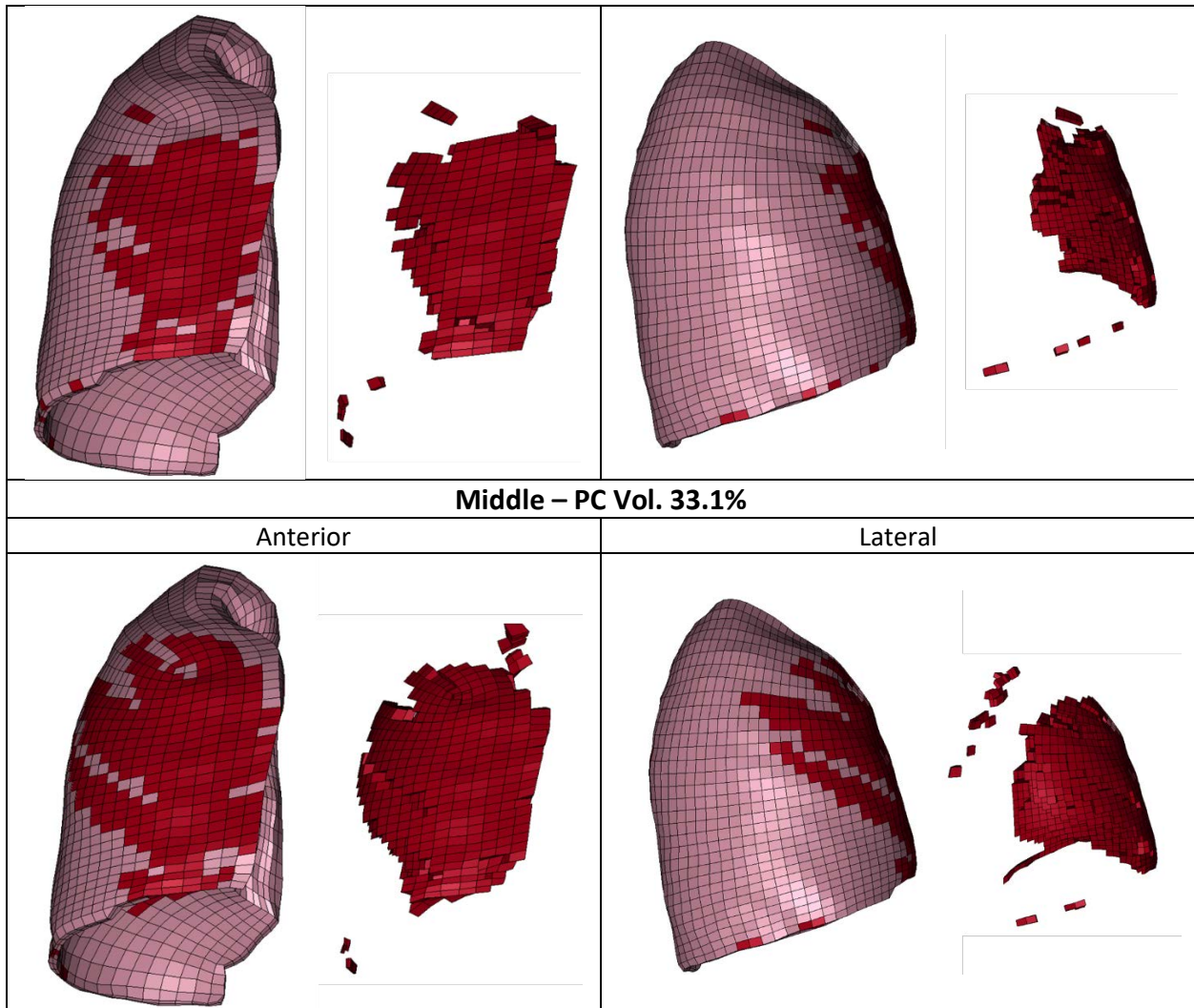
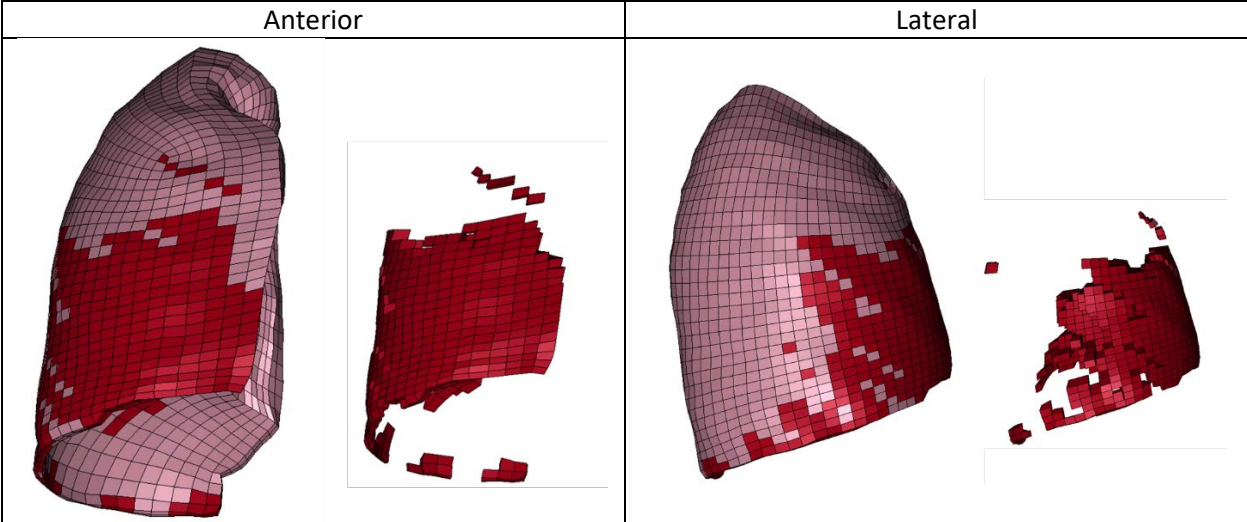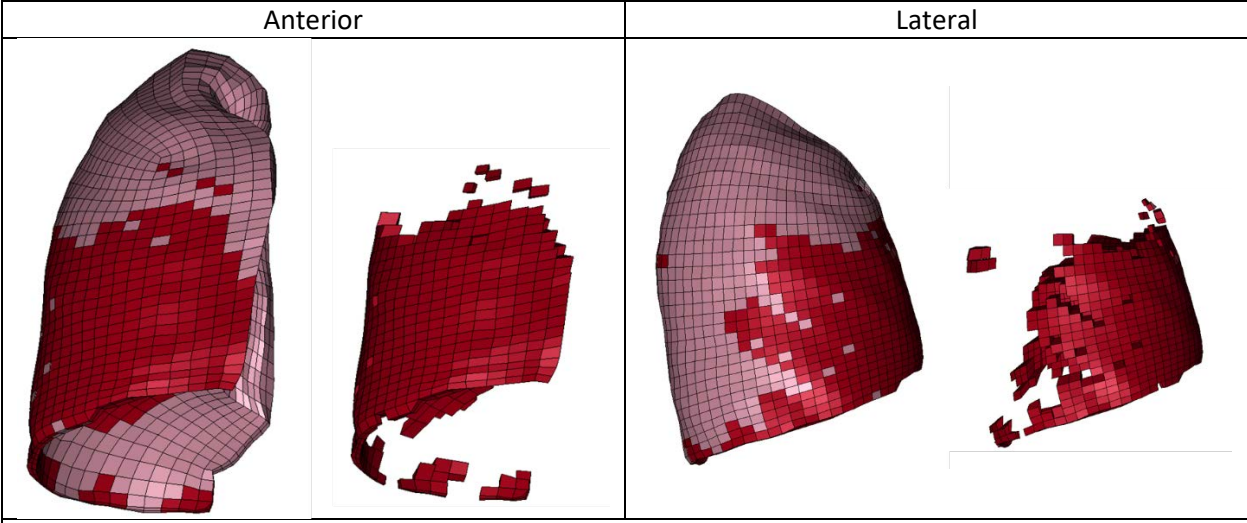### B.3.3.3 BABT FE PC Volumes

Likewise to the previous sections, the below figures contain images of the GHBMC right lung. These images of PC found in the FE model have the corresponding study and clay displacement value listed above – the PC volume in each case is the listed percent. The images contain the anterior view of the right lung on the left, and the lateral view on the right, with failed elements shown in red.

(Sondén et al., 2009) – **Clay 19mm, 13.3%**	
Anterior	Lateral

(Arborelius et al., 2004) – **Clay 23mm, 16.7%**	
Anterior	Lateral

(Drobin et al., 2007; Gryth et al., 2008; Sondén et al., 2009) – **Clay 28mm, 21.6%**	
Anterior	Lateral

| (Gryth et al., 2007) – **Clay 34mm, 29.4%** ||

Anterior	Lateral
(Gryth et al., 2007) – **Clay 40mm, 36.9%**	
Anterior	Lateral
(Rocksén et al., 2012) – **Clay 42mm, 39.9%**	
Anterior	Lateral
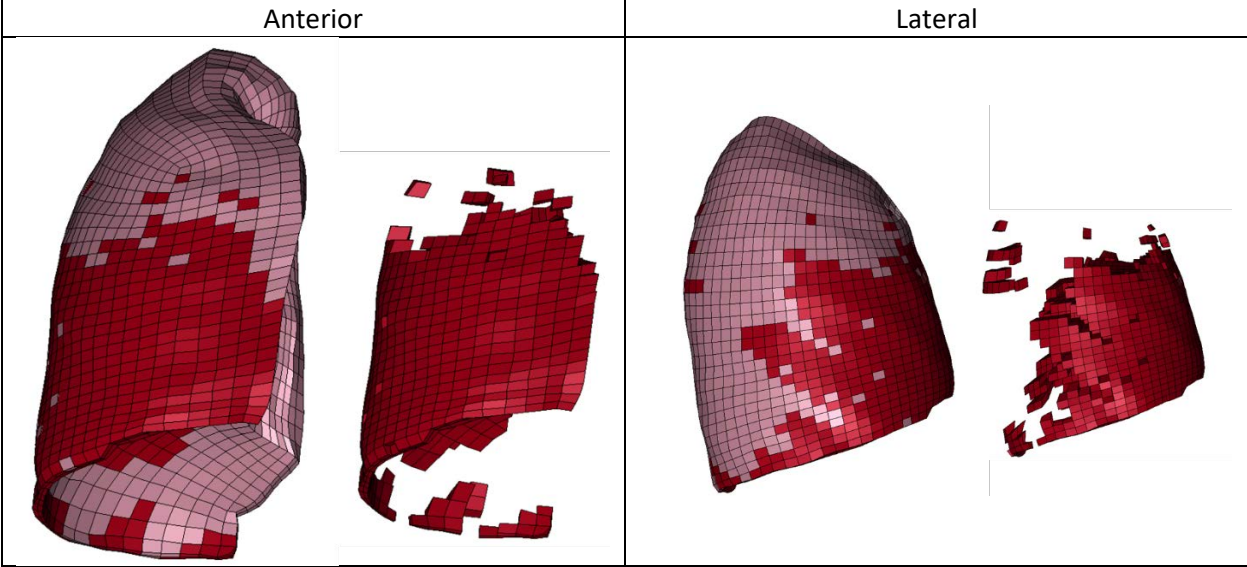
B.3.4 R Script for Pearson Correlation

The Pearson correlation coefficient is a measure of linear correlation between two datasets. The equation for two datasets, X and Y, is given by:

$$r = \frac{cov(X,Y)}{\sigma_X \sigma_Y}$$

where 'cov' refers to the covariance, and the σ's are standard deviations. For the data in Chapter 10, weighting was required due to different studies having different specimen numbers. Therefore, the R code below was used to weight the data.

```
#SaO2 vs PC

plot(SaO2_30_Avg ~ PC,data=D)

cor.test(D$SaO2_30_Avg,D$PC,method="pearson") #<-note limitation in using pearson corr.

# cor.test(D$SaO2_30_Avg,D$PC,method="kendall")


#SaO2 vs PC

plot(SaO2_60_Avg ~ PC,data=D)

cor.test(D$SaO2_60_Avg,D$PC,method="pearson") #<-note limitation in using pearson corr.


#PaO2 vs PC

cor.test(D$PaO2_30_Avg,D$PC)


################################################################################

library(weights)
```

```
set.seed(101119852)

w<-D$N/sum(D$N)   #weights are prop to sample size

wtd.cor(D$SaO2_30_Avg, D$PC, w,bootn=5000,

     bootse=TRUE,bootp = TRUE) #weighted Pearson correl.



set.seed(101119852)

wtd.cor(D$SaO2_60_Avg, D$PC, w,bootn=5000,

     bootse=TRUE,bootp = TRUE) #weighted Pearson correl.



set.seed(101119852)

wtd.cor(D$PaO2_30_Avg, D$PC, w,bootn=5000,

     bootse=TRUE,bootp = TRUE) #weighted Pearson correl.



set.seed(101119852)

wtd.cor(D$PaO2_60_Avg, D$PC, w,bootn=5000,

     bootse=TRUE,bootp = TRUE) #weighted Pearson correl.



#################### weighted t test ###########

one<-D[which(D$PC < 20),6]*w[which(D$PC < 20)] #<-applies weights

two<-D[which(D$PC > 20),6]*w[which(D$PC < 20)]

t.test(one,two)  #<-regular t test on weighted quantities; only pvalue is interpretable



one<-D[which(D$PaO2_60_Avg < 60),3]*w[which(D$PaO2_60_Avg < 60)] #<-applies weights
```

two<-D[which(D$PaO2_60_Avg > 60),3]*w[which(D$PaO2_60_Avg > 60)]

t.test(one,two) #<-regular t test on weighted quantities; only pvalue is interpretable

REFERENCES

Automatic citation updates are disabled. To see the bibliography, click Refresh in the Zotero tab.